Functional Consequences of Dendritic Inhibition in the Hippocampus

Matthew Lovett-Barron

Submitted in partial fulfillment of the
requirements for the degree of
Doctor of Philosophy
under the Executive Committee
of the Graduate School of Arts and Sciences

COLUMBIA UNIVERSITY
2014

Abstract

Functional Consequences of Dendritic Inhibition in the Hippocampus

Matthew Lovett-Barron

The ability to store and recall memories is an essential function of nervous systems, and at the core of subjective human experience. As such, neuropsychiatric conditions that impair our memory capacity are devastating. Learning and memory in mammals have long been known to depend on the hippocampus, which has motivated widespread research efforts that converge on two broad themes: determining how different cell types in the hippocampus interact to generate neural activity patterns (structure), and determining how neural activity patterns implement learning and memory (function). Central to both these pursuits are pyramidal cells (PCs) in CA1, the primary hippocampal output, which transform excitatory synaptic inputs into the action potential output patterns that encode information about locations or events relevant for memory. CA1 PCs are embedded in a network of diverse inhibitory (GABA-releasing) interneurons, which may play unique roles in sculpting the activity patterns of PCs that implement memory functions. As a consequence, investigating the functional impact of defined GABAergic interneurons can provide an experimental entry point for linking neural circuit structure to defined computations and behavioral functions in the hippocampal memory system. In this thesis I have applied a panel of novel methodologies to the mouse hippocampus *in vitro* and *in vivo* to link structure to function and behavior, and determine 1) how hippocampal inhibitory cell types shape

distinct patterns of PC activity, and 2) how these inhibitory cell types contribute to the encoding of contextual fear memories.

To first establish the means by which interneuron subtypes contribute to PC activity patterns, I used optogenetic techniques to activate spatiotemporally distributed synaptic excitation to CA1 *in vitro*, and recorded from PCs to quantify the frequency of output spikes relative to input levels. I subsequently used a dual viral and transgenic approach to combine this technique with selective pharmacogenetic inactivation of identified interneurons during synaptic excitation. I found that inactivating somatostatin-expressing (Som+) dendrite-targeting interneurons increased the gain of PC input-output transformations by causing more output spikes, while inactivating parvalbumin-expressing (Pvalb+) soma-targeting interneurons did not. Inactivating Som+ inhibitory interneurons allowed the dendrites of PCs to generate local NMDA receptor-mediated electrogenesis in response to synaptic input, resulting in high frequency bursts of output spikes. This discovery suggests neuronal coding via hippocampal burst spiking output can be regulated by Som+ dendrite-targeting interneurons in CA1.

Specific types of neural codes are believed to have different functional roles. Neural coding with burst spikes is known to support hippocampal contributions to classical contextual fear conditioning (CFC). In CFC the hippocampus encodes the multisensory context as a conditioned stimulus (CS), whose burst spiking output is paired with the aversive unconditioned stimulus (US) in the amygdala, allowing for fear memory recall upon future exposure to the CS. To investigate the contribution of Som+ interneurons to this behavior, I designed a CFC task for head-fixed mice, allowing for optical recording and manipulation of activity in defined CA1 cell types during learning.

Pharmacogenetic inactivation of CA1 Som+ interneurons, but not Pvalb+ interneurons, prevented the encoding of CFC. 2-photon Ca^{2+} imaging revealed that during CFC the US activated CA1 Som+ interneurons via cholinergic input from the medial septum, driving inhibition to the PC distal dendrites that receive coincident excitatory input from the entorhinal cortex. Inactivating Som+ interneurons increases PC population activity, and suppressing dendritic inhibition during the US alone is sufficient to prevent fear learning. These results suggest sensory features of the US reach CA1 PCs through entorhinal inputs, and thus require active inhibitory filtering by Som+ interneurons to ensure hippocampal output exclusively encodes the CS during CFC.

In conclusion, I found that Som+ interneurons in CA1 are an effective regulator of PC burst spiking because they inhibit dendritic electrogenesis. This function is used by the hippocampus to prevent the US from influencing the burst spike output of PCs that encode the CS, ensuring successful CFC. This work bridges the gap between cells, circuits, and behavior, and provides mechanistic insight into one of our most essential cognitive functions – the ability to learn and remember.

Table of Contents

List of Figures

Acknowledgments

I owe a great debt to all of the people who have helped me and supported me over the years, both scientifically and personally.

I would first like to thank my thesis advisor Attila Losonzcy, who has been a tremendous mentor over my years in his lab. I was particularly fortunate to be the first person to join Attila's lab, which has afforded me the invaluable experience of watching how he established and grew his lab, won grants, and expanded his scientific focus. My achievements in his lab are a testament to his skills as a scientist and teacher, and I could not be more grateful for his mentorship. I also hope to never be his competitor.

In addition to Attila, I benefited a great deal from the mentorship and guidance of my thesis committee: Steve Siegelbaum, Josh Gordon, and Randy Bruno, and my outside examiner György Buzsáki, whose work has been a source of inspiration. I would also like to thank the program directors for guidance and support: Carol Mason, Ken Miller, and Darcy Kelley. I would not be at Columbia without the support of my mentors at Queen's University: Cella Olmstead, Eric Dumont, and Scott Hayton.

I am grateful for my talented colleagues in the Losonczy Lab, including Gergely Turi, Thomas Reardon, Nathan Danielson, Jeff Zaremba, Joseph Tsai, Angel Castro, Mohsin Ahmed, Rachel Field, Anna Sarfaty, Alyson Lowell, and others. I am particularly grateful for the contributions of Patrick Kaifosh, who has been my close collaborator on the establishment of *in vivo* imaging in the lab, and whose intelligence and creativity have allowed the Losonczy lab to achieve a great deal. I also thank our collaborators Mazen Kheirbek, René Hen, Walter Fischler, Scott Sternson, and Boris Zemelman.

I could not have achieved any of this without the support of my friends and family. I thank my friends here at Columbia, particularly Christine Constantinople, Tim Machado, and Brian DePasquale, and other friends in New York and Toronto. I would like to thank my family, particularly my parents Rod and Maureen, who have always supported me and were the first to show me the mysteries and promises of studying the mind and brain. Finally I want to thank my partner Sarah Pike, who has often had more faith in me than I did, and has always supported my dreams and ambitions. I could not have achieved any of this without her love and support.

Chapter 1 - Introduction

The Hippocampus and Memory

Organisms must adapt their behaviors to survive in constantly changing environments. Single experiences are often sufficient to change an organism's behavior for the rest of its life. Although many organisms can adapt to environmental changes, this capacity is greatly enhanced in animals with nervous systems, which can flexibly alter neural processing of environmental stimuli to change future behavior (Swanson, 2003), whose products are referred to as 'learning and memory'. The neural substrates that allow for certain salient experiences to be stored as memories have been extensively studied throughout the animal kingdom, resulting in knowledge of the molecular, structural, and physiological steps required for neurons to implement the intertwined processes of learning and remembering. These efforts are helping to illuminate the mechanisms by which humans and other animals accumulate information over their lives. These mechanisms allow for adaptive behavior in all animals, but also the sense of personal history in humans. Because of the importance of memories for our subjective experiences of the world and our lives, disorders of learning and memory such as Alzheimer's disease and Post-traumatic Stress Disorder are often devastating. Studies of the neural mechanisms of memory may allow for the development of effective therapeutics for treating such diseases.

In humans, these efforts have focused on the hippocampus and associated medial temporal lobe structures as the seat of episodic memory storage. This was motivated by the early findings from the patient Henry Molaison (H.M.), who had much of his medial temporal lobes removed to treat severe epilepsy, including bilateral hippocampus and entorhinal cortex. After this surgery H.M. could remember past

experiences, but suffered from severe anterograde amnesia – he could not form new explicit, or 'declarative', memories (Scoville & Milner, 1957). In contrast, implicit or 'procedural' memory was left intact.

While H.M. displayed broad deficits in declarative memory, in healthy people this type of memory can be further dissociated into episodic and semantic types of declarative memory. Episodic memories are memories of specific experiences in one's life, whereas semantic memory refers to factual memories that are not necessarily associated with personal experience (Tulving, 1972; Squire 1992). Both of these functions, and particularly episodic memory, believed to require a functioning hippocampus and associated medial temporal lobe structures (Vargha-Khadem et al., 1997; Squire & Zola, 1998; Tulving & Markowitsch, 1998). Although Tulving initially stated that episodic memory was unique to humans, requiring conscious experience (1972), recall of past experiences has been demonstrated in animals such as non-human primates (Hampton, 2001; Schwartz & Evans, 2001), rodents (Eichenbaum & Fortin, 2003), and birds (Clayton & Dickinson, 1998), among others (Hampton & Schwartz, 2004), suggesting episodic-like memory systems in non-human animals amenable to experimental analysis.

This specificity of H.M.'s deficits motivated a series of studies in animals to re-create more restricted lesions to the hippocampus and medial temporal lobe, revealing that the hippocampus is indeed important for forming episodic memories (Squire, 1992; Maren, 2001; Nadel et al., 2003; Fanselow & Poulos, 2005). Hippocampal lesions in rodents have been associated with deficits in a variety of learning and memory tasks, including spatial learning (Moser et al. 1993; Moser et al., 1995; Broadbent et al., 2004),

trace eyeblink conditioning (Kim et al., 1995; McEchron & Disterhoft, 1999; Weiss et al., 1999), contextual fear conditioning and discrimination (Kim & Fanselow, 1992; Philips & LeDoux, 1992; Maren & Fanselow, 1997; Frankland et al., 1998; Frankland et al., 2004; Goshen et al., 2011), and tasks requiring working memory and/or recognition memory (Stevens & Cowey, 1973; Aggleton et al., 1986; Hock & Bunsey, 1998; Potvin et al., 2006), among others. Despite these results, the variable nature of lesion methods and their efficacy make it difficult to come to definitive conclusions about the neural substrates of memory from these experiments alone (Frankland et al., 1998; Anagnostaras et al., 2001; Rudy et al., 2004; Fanselow, 2010; Goshen et al., 2011). Nevertheless, this broad approach has led to a more nuanced understanding of how the hippocampus and related brain regions interact to form memories, and the neurotransmitter systems involved.

Macro-anatomy of the hippocampus

While the focus on the hippocampus as the seat of memory was advanced since Scoville and Milner's discoveries in the 1950s, the hippocampus has been studied from an anatomical perspective for more than a century – with the laminar structure observed in humans and other animals by cellular stains performed by Golgi, Cajal, and de Nó, among others (Andersen et al., 2007). Extensive anatomical study has since revealed the primary excitatory circuits that comprise the hippocampus and its connected regions. The anatomy alone suggests a dominant flow of excitation from entorhinal cortical regions through the hippocampus and back to the cortex again – comprising

trisynaptic, disynaptic, and monosynaptic excitatory loops (Amaral & Witter, 1989; Amaral, 1999; Andersen et al., 2007; Carr & Frank, 2012; **Fig 1.1**).

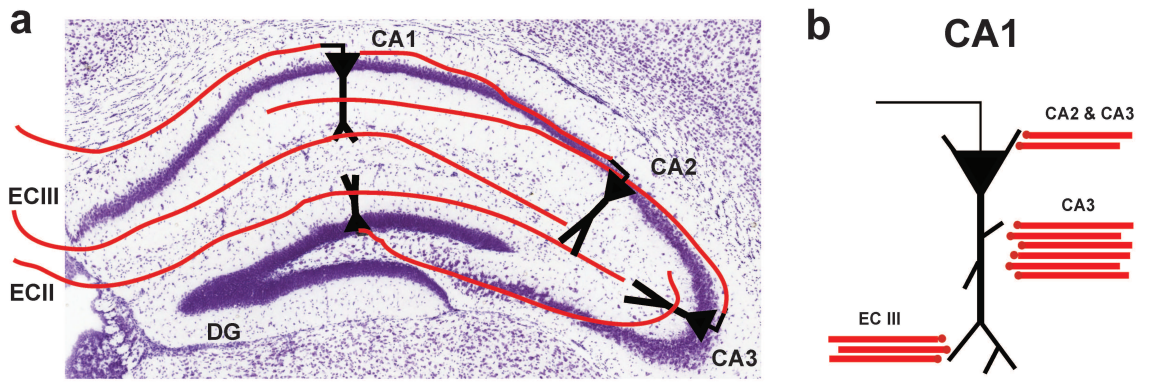

Figure 1.1 – Hippocampal excitatory circuits. **a)** Simplified schematic of major excitatory pathways in the dorsal hippocampus, overlayed on a coronal section with Nissl stain of cell bodies (Allen Brain atlas). **b)** Schematic of subcellular locations of major excitatory inputs to CA1 PCs.

The primary flow of excitatory activity is from the superficial layers of the entorhinal cortex to granule cells in the dentate gyrus, whose output goes to pyramidal cells (PCs) in CA3, whose output goes to PCs in CA1, and out again to the deep layers of the entorhinal cortex (trisynaptic pathway), often via the subiculum. Superimposed on this loop are the monosynaptic pathway from superficial entorhinal cortex directly to CA1 PCs, and the less-studied disynaptic pathway from superficial entorhinal cortex to CA1 PCs via CA2 (Chevaleyre & Siegelbaum, 2010). This organization has suggested that highly-processed sensory information about the environment is relayed by the entorhinal cortex into the hippocampus, where it is transformed in a manner conducive to memory storage and abstracted representations of space (Amaral & Witter 1989; Amaral, 1999; Andersen et al., 2007; Carr & Frank, 2012). While this simplified model suggests a closed loop, PCs send major outputs to other regions, including the lateral

septum, the subiculum, mammillary bodies, and the prefrontal cortex, among other efferent targets (Swanson & Cowan, 1975; Risold & Swanson, 1996).

Anatomical studies in rodents have also demonstrated that the hippocampus receives long-range inputs from diverse subcortical areas, although the properties of these inputs have been studied less extensively than the dominant entorhinal-hippocampal excitatory loops. These afferent inputs include cholinergic and GABAergic neurons in the medial septum and diagonal band of broca (Swanson & Cowan, 1975; Freund & Antal, 1988; Toth et al., 1997), dopaminergic neurons in the ventral tegmental area (Pasquier & Reinoso-Suarez, 1978, Wyss et al., 1979; Verney et al., 1985), noradrenergic neurons in the locus coeruleus (Pasquier & Reinoso-Suarez, 1978; Wyss et al., 1979; Loughlin et al., 1986), serotonergic/glutamatergic neurons in the raphe nucleus (Pasquier & Reinoso-Suarez, 1978; Wyss et al., 1979; Varga et al., 2009), the supramammilary bodies (Pasquier & Reinoso-Suarez, 1978; Wyss et al., 1979), the thalamic reunions nucleus (Vertes et al., 2007), and the amygdala (Wyss et al., 1979; Felix-Ortiz et al., 2013). When considering anatomical evidence alone these inputs are often considered to be minor or 'modulatory' – a view enforced by the inability to selectively control these inputs *in vivo* or in brain slices using traditional stimulation methods. However, these allegedly 'minor' inputs may have outsize influence on certain neuronal processes *in vivo*. Studies employing optogenetic projection stimulation and *in vivo* recordings are beginning to elucidate their functions (eg. Dorsal raphé serotonergic projection – Varga et al., 2009; amygdala glutamatergic projection – Felix-Ortiz et al., 2013; septal GABAergic projection – Kaifosh et al., 2013). All of these examples of powerful physiological or behavioral effects via subcortical connectivity occur through

connectivity with local hippocampal interneurons, which in turn exert inhibitory effects on excitatory PCs. Subcortical influences over local inhibition may be particularly influential in hippocampal processing, and will be outlined in the main body of this thesis (particularly *Chapter 3*).

The hippocampus is not a unitary structure, but can be broadly segmented into dorsal and ventral structures. These structures differ in their gross anatomy and gene expression (Fanselow & Dong, 2010), afferent and efferent connectivity (Risold & Swanson, 1996; Fanselow & Dong, 2010), spatial coding properties (Kjelstrub et al., 2008; Royer et al., 2010), and relevance for learning and memory (Moser et al., 1993; Hock & Bunsey, 1998; Fanselow & Dong, 2010; Khierbek et al., 2013). These differences have led to the broad assertion that the dorsal hippocampus is involved in the performance of cognitive functions, such as the encoding of spatial and contextual information, whereas the ventral hippocampus is more involved in emotional and affective functions, such as the modulation of stress and anxiety (Moser & Moser, 1998; Fanselow & Dong, 2010). As a consequence, most studies of episodic memory focus on the dorsal hippocampus. The experiments reported in this thesis (*Chapters 2* and *3*) will also be conducted in this region.

Knowledge of the hippocampal macro-anatomy has influenced conceptual models of the hippocampus and its potential role in memory. However, to understand how the hippocampus produces memory, researchers must be able to record the activity of hippocampal neurons during relevant behaviors, and determine the structure of the neural circuitry that implements these functions. Although these challenges have the same long-term goal – to understand how neural circuits implement memory

functions - the research programs that investigate these two broad topics have diverged.

Divergent Experimental Approaches to Investigate Hippocampal Function

Traditionally, neuroscientists investigating the hippocampus have studied either the microcircuit structure of the hippocampus, or the functional/behavioral correlates of hippocampal activity. There has been with little data to bridge the two worlds of anatomical and behavioral analysis, largely due to the techniques traditionally used in each field: physiological analysis of cell types defined by morphological or molecular criteria was only possible in brain slices (without behavioral relevance), and neuronal recording during behaviors was achieved with extracellular electrodes (without definitive knowledge of cell type). However, recent technical advances have presented opportunities to perform experiments that can link the two – allowing experimentalists the first opportunities to ask how neural circuit structure creates the physiological activity that drives behavior. Below I will briefly review the two separate programs of research and suggest approaches for linking these fields. The experiments reported in *Chapter 2* and *Chapter 3* of this thesis will provide an example of linking these two fields by examining how somatostatin-expressing dendrite-targeting interneurons in dorsal CA1 control the input-output function of CA1 PCs, and the encoding of environmental context during Pavlovian fear conditioning.

Relationships between hippocampal PC activity and memory function

Memories are stored in the brain through molecular and structural changes to neurons and synapses, most notably with long-term potentiation (LTP) of synaptic transmission. LTP was first described in the hippocampus (Bliss & Lomo, 1973), and had been extensively studied since (Malenka & Nicoll, 1999), leading to the dominant hypothesis that increases in synaptic efficacy between co-active neurons is the cellular substrate for neural network changes (Hebb, 1949) and memory formation (Bliss & Collingridge, 1993; Whitlock et al., 2006; Neves et al., 2008). Other mechanisms of neuronal changes such as structural plasticity (Holtmaat & Svoboda, 2009) and changes to membrane excitability (Zhang & Linden, 2003; Losonczy et al., 2008; Makara et al., 2009) also likely contribute. While these cellular processes and their molecular and genetic underpinnings have been closely examined, the activity of neurons in relevant brain regions during learning has been relatively neglected. This is historically due to a lack of methods to adequately investigate these neuronal dynamics during learning and remembering (Neves et al., 2008), including the inability to record from defined cell types over long periods of time. Neuronal activity during memory formation has been difficult to record and interpret, and therefore has not been exhaustively examined thus far. However, an understanding of the neural substrates of memory requires knowledge of how the activity of the participating neurons creates conditions conducive to the storage of memory through changes to specific synaptic weights.

Instead of directly studying learning and memory, most studies of hippocampal neuronal activity have been investigations of place cells in rodents during navigation.

Place cells are neurons in the hippocampus and associated regions that fire action potentials in restricted regions of physical space during navigation (a neuron's "place field"), which together are hypothesized to provide the animal with a cognitive map of space (O'Keefe & Dostrovsky, 1971; O'Keefe & Nadel, 1978; Wilson & McNaughton, 1993). In any given environment, a subset of hippocampal neurons can be defined as place cells, although this definition depends on the particular criteria used by the investigator and the method of recording neurons; current estimates using relatively unbiased recording methods suggest ~20-30% of spontaneously active PCs in CA1 have place cell properties (Harvey et al., 2009). This assessment does not include the large proportion of PCs that are silent in a given environment (Thompson & Best, 1989; Epsztein et al., 2011), leading to the assessment of ~15-20% active cells in recordings from both active and silent cells (Dombeck et al., 2010). While an individual neuron can be a place cell in multiple environments, representations of place can be distinguished at the population level, where distinct ensembles of neurons are active in each environment, and neurons have distinct place fields relative to environmental landmarks (O'Keefe & Conway, 1978; Wilson & McNaughton, 1993; Harris et al., 2003; Dombeck et al., 2010; Ziv et al., 2013). Place cells have also been observed in the human hippocampus, which were recorded in patients implanted with electrodes for treatment of epilepsy, while they navigating virtual environments (Ekstrom et al., 2003). Despite these estimates about the proportion of active place cells, the categorization of which cells carry spatial information depends on the criteria set by the experimenter. As a consequence, the neural sources the animal uses to establish their sense of place and navigational abilities is more difficult to discern.

Studying the activity of place cells and elucidating the mechanisms that generate their activity may be particularly useful for understanding the more elusive mechanisms of memory representation (Eichenbaum et al., 1999; Knierim et al., 2006; Colgin et al., 2008; Buzsáki & Moser, 2013). Specifically, Buzsáki and Moser (2013) propose that mechanisms underlying particular aspects of spatial navigation also underlie specific aspects of declarative memory: egocentric path integration-based navigation is analogous to episodic memory (because both are referenced subjectively), and allocentric map-based navigation is analogous to semantic memory (both are referenced objectively). This suggests that the path-integration system implemented by the place cells in the hippocampus and grid cells in the entorhinal cortex may have similar mechanistic properties as these systems in episodic memory. Using within-subjects design, some recent studies have found that the properties of externally generated place cells and internally generated neuronal activity related to memory are remarkably similar (Pastalkova et al., 2008; MacDonald et al., 2011). Studying the cellular and circuit mechanisms generating neuronal activity in these navigation tasks may give us hints into the general neuronal algorithms used by the hippocampus and entorhinal cortices for memory functions as well.

Neural spiking patterns

The extensive study of place cells has revealed unique modes of hippocampal firing activity that may convey different aspects of information relevant to spatial representations, including temporal codes, rate codes, burst codes, and ensemble codes (Huxter et al. 2003; Mehta et al., 2002; Leutgeb et al., 2004; Ahmed & Mehta,

2009; Buzsáki, 2010). These spiking patterns may therefore be critical to the implementation of hippocampal-dependent memory functions as well (Buzsáki & Moser, 2013).

One means by which neurons can convey information is through the timing of their spikes, often referred to as a temporal code. This notion is supported by the widespread observation of precisely timed rhythmic events in many brain regions recorded with extracellular electrodes. These emergent events are hypothesized to reflect underlying synaptic and spiking activity that may underlie a variety of functions. Rhythms believed to be important to hippocampal function include oscillations in the theta (~4-12 Hz), gamma (~30-120 Hz), and ripple (~150-200 Hz) bands. For instance, theta phase precession refers to the phenomenon by which the firing of a place cell shifts progressively forward in the phase of each extracellular theta cycle as the animal progressed through their place field during navigation (O'Keefe & Recce, 1993). In addition to theta, the precise spike timing of hippocampal neurons relative to other extracellular rhythms such as gamma (Buzsáki & Wang, 2012) and ripple events have been associated with the ability to perform certain short-term working memory tasks (Lisman & Idiart, 1995; Jadhav et al., 2012), which require the subject to bridge a temporal gap between stimulus and action. Some recent findings of hippocampal neurons that bridge discontiguous temporal events (eg. 'time cells', MacDonald et al., 2011) may be critical to understanding the contribution of temporal coding to hippocampal-dependent memory functions.

Another prominent form of neuronal coding is through firing rates. The frequency of neuronal spiking has long been recognized to carry information in nervous systems

(Adrian & Zotterman, 1926), and in certain systems is considered a more reliable means of neuronal communication compared to the timing of individual spikes. This view is prominent among those who study neocortex, where the utility of temporal coding for conveying information has been questioned by those who observe that the impact of a single spike, and thus its timing, is unlikely to be an effective means of coding in the brain due to divergent connectivity, neural noise, and the stochastic nature of neurotransmitter release, among other issues (Shadlen & Newsome, 1998; London et al, 2010). In the hippocampus, Ahmed and Mehta (2009) have argued that PC firing rates convey the essential information related to spatial coding in CA1, through interactions between synaptic integration of CA3 and entorhinal input rates, and local inhibitory circuits. This model of place cell generation predicts that if spatial information is generated by firing rates, then place cells should be driven by underlying membrane depolarization, rather than precise spike timing relative to rhythms like theta. This observation has been observed in whole-cell recordings from place cells in head-fixed mice navigating in virtual environments (Harvey et al., 2009) as well as freely-moving rats navigating in real environments (Epsztein et al., 2011; Lee et al., 2012a). However, evidence for one coding scheme does not imply the absence of another; rather, it is likely that neural networks may carry multiple forms of information simultaneously in several neural coding schemes, such as rate and temporal codes (eg. Mehta et al., 2002; Huxter et al., 2003).

Another form of neural coding is through the firing of spike bursts, defined as an epoch of high-frequency spiking instead of a single spike. Bursts of spikes cause reliable neurotransmitter release to downstream targets, and are thus viewed as a very

reliable means of information transmission in noisy systems such as the cortex and hippocampus (Lisman, 1997; Kepecs & Lisman, 2004). Many neuron types across the nervous systems of vertebrates and invertebrates use spike bursts to communicate, including the hippocampus (Kandel & Spencer, 1961), where rat CA1 PCs include approximately 20% of their spikes in bursts (Harris et al., 2001). The relation of burst spikes to single spikes may reflect different coding regimes, but may also reflect mechanisms for neuronal firing rate homeostasis (Buzsáki et al., 2002). These theories have not yet been studied extensively, due to experimental difficulties in dissociating single spikes from bursts. However, one recent study by Xu and colleagues (2012b) has been able to test the behavioral influence of ablating synaptic transmission triggered by single spikes, while leaving burst spiking-triggered synaptic transmission intact. The authors achieved this selectivity by using a virus to knock down the presynaptic Ca^{2+} sensor synaptotagmin-1 in infected neurons, which prevented neurotransmitter release via single spikes, but not burst spikes. By targeting this virus to the hippocampus, entorhinal cortex, or medial prefrontal cortex (mPFC), the authors investigated the effects of removing single spikes from these regions on the acquisition and recall of contextual fear conditioning (CFC). They found that while single spikes in the entorhinal cortex and mPFC are required for CFC, single spikes in the hippocampus were dispensable, suggesting hippocampal contributions to CFC are mediated by burst spiking. This may be a powerful approach for studying the use of distinct neural codes by different brain regions during specific behaviors, and the implications of these specific results will be discussed in the next section and during *Chapter 3* and *Chapter 4*.

Therefore, knowledge of neural coding in the hippocampus has largely benefitted from the well-established study of place cells and spatial coding. However, the implications of these coding schemes for implementing mnemonic functions, such as episodic memory formation and recall, are not as well studied (Buzsáki & Moser, 2013). A better understanding of the mechanisms underlying memory will require expanding hippocampal neural recording efforts to well defined memory tasks in animals models.

Relevance for memory

Spatial coding in the hippocampus may have relevance for particular forms of memory, but non-spatial associative conditioning is also known to depend on the hippocampus. One of the most effective approaches for studying learning and memory in animal models is the use of Pavlovian classical conditioning (Pavlov, 1927). Classical conditioning involves learning associations between a neutral stimulus (conditioned stimulus, CS) and a salient stimulus (unconditioned stimulus, US) that causes a physiological or behavioral response on its own (unconditioned response, UR). Conditioning is achieved by pairing these stimuli with each other by presenting them to the subject together, which will cause the subject to associate the CS with the US. After conditioning, the CS alone will be able to evoke a conditioned response (CR), which does not necessarily have to be the same as the UR. Classical conditioning can take many forms, and a variety of brain regions are capable of encoding the associative relationship between CS and US. In each of these cases, learning changes neural processing of the CS. The hippocampus can contribute to classical conditioning under two circumstances: when the CS-US pairing is separated by a stimulus-free 'trace'

interval, and when the CS is a multisensory environmental context (Maren, 2001; Fanselow & Poulos, 2005). The hippocampus is believed to bridge the temporally discontiguous events in the case of the former, and is believed to form a neural representation of context or place in the case of the latter. For experiments in rodents, these two forms of hippocampal-dependent classical conditioning are most commonly in the form of trace eyeblink conditioning, and contextual fear conditioning, respectively.

In trace eyeblink conditioning, the CS is usually a unimodal sensory cue such as a light or tone, and the US is an aversive shock or air-puff to the eyelid; the CS offset is separated from the US onset by a stimulus-free 'trace' period of ~500ms (although this varies among species and preparations). The UR and CR are both a blinking response – a conditioning of the muscles controlling the eyelid that is measured by recording video of the eye or the activity of the muscles. When an animal successfully learns trace eyeblink conditioning, they will blink in the CS and/or trace period, whereas before training they blink only upon onset of the US. Hippocampal neural recordings during this behavior were pioneered by Richard Thompson's lab, who investigated trace eyeblink conditioning in rabbits, rats, and mice by recording from CA1 over the course of learning (Thompson & Kim, 1996; McEchron & Disterhoft, 1999; Fanselow & Poulos, 2005). These research efforts have primarily used extracellular recording electrodes to record the firing rates of 'complex spike cells' (putative PCs, referring to their propensity to fire action potentials that appear as complex spike bursts in extracellular recordings) as well as 'theta cells' (putative interneurons, referring to the ~4-12 Hz theta oscillations observed in the firing rates of some interneurons). These efforts have found that the responses of complex cells to the CS (tone) show a variety of changes after pairing with

a US, including increased activity, decreased activity, and sustained activity into the stimulus-free trace period (Berger et al., 1976; Weiss et al., 1996; McEchron & Disterhoft, 1997). Despite these advances, single neurons have been recorded one-by-one and the molecular identity of neurons has yet to be reported. Thus, the neural coding strategies and circuit mechanisms by which the hippocampus stores and recalls trace memories remains elusive.

Another well-studied form of hippocampal-dependent classical conditioning is contextual fear conditioning (CFC). The hippocampus encodes specific multisensory environments or 'contexts' during learning, which is believed to provide the amygdala with a context CS to pair with an aversive US for associative plasticity and fear learning (Kim & Fanselow, 1992; Phillips & LeDoux 1992; Holland & Bouton, 1999; LeDoux, 2000; Anagnostaras 2001; Maren, 2001; Fanselow & Poulos, 2005; Fanselow, 2010; Maren et al., 2013). As discussed above, mice display deficits in CFC upon ablation of hippocampal spiking, but not upon ablation of single spikes, suggesting hippocampal encoding of the CS occurs through the burst spike output of the hippocampus (Xu et al., 2012b).

While there have not been any electrophysiological recordings of hippocampal neurons during the acquisition of this task, researchers have been able to broadly map the spatial distribution of cells activated during memory acquisition and/or recall by labeling neurons that express activity-dependent genes or proteins. These studies indicate that fear conditioning makes dorsal CA1 ensembles more sparse (Naloor et al., 2012), and causes a partial re-organization of cells active during the CS after training (Vazdarjanova & Guzowski, 2004; Sheth et al., 2008). Some groups have used

transgenic strategies to express neuronal activators (optogenetic or pharmacogenetic tools) in these activity-dependent ensembles to causally demonstrate that synthetic activation of the training ensemble in the dentate gyrus of the hippocampus can re-activate the fear memory, as if it were recalling the training context (Liu et al., 2012). Further evidence that these hippocampal ensembles represent the CS comes from studies that have found under some conditions these synthetically re-activated training ensembles can be merged with naturally activated training ensembles to create 'hybrid' or 'false' memories (Garner et al, 2012; Ramirez et al, 2013).

While hippocampal cells have not been recorded during the moment of fear conditioning, two studies have used electrophysiological recordings of place cell properties of rats navigating in an environment before and after fear conditioning in that environment, demonstrating that place cells can be altered upon learning (Moita et al., 2004; Wang et al., 2012). These efforts have revealed that hippocampal representations of place will 'remap' upon fear conditioning, such that the subsets of place cells that represents the training environment, or certain place fields in the environment, can change upon exposure to a fearful stimulus in that environment (Moita et al., 2004), and that some of these new spatial representations are further stabilized (Wang et al., 2012). Remapping may reflect the NMDA receptor-mediated synaptic plasticity occurring in the hippocampus during CFC (Quinn et al., 2005), which may be a mechanism for learning-related shifts in synaptic weights (Colgin et al., 2008). Therefore, CFC is known to involve the long-term reorganization of CS-coding ensembles, which may show enhanced stability and greater sparsity after learning.

Nevertheless, the spiking properties of defined hippocampal cell types during the conditioning phase of CFC remain unexplored.

In conclusion, the activity of hippocampal neurons can vary substantially depending on the task the animal is engaged in, or the relevant parameters of neuronal activity being investigated, such as spike timing, spike rate, spike bursting, or ensemble identity. Despite the heterogeneity of PC activity and the cognitive functions associated with them, a common feature of hippocampal dynamics is its selectivity. Only a small subset of hippocampal principal neurons are active in any given situation (eg. the 15-20% of CA1 PCs that are place cells; Dombeck et al., 2010), and when neurons are active, they are active only under specific circumstances (eg. a neuron's place field). This is referred to a 'sparse activity', a term that encompasses the aforementioned properties of population sparsity and single-cell sparsity, respectively (Ahmed & Mehta, 2009). Theorists have long hypothesized that this sparse activity allows for the expanded memory capacity afforded by the hippocampus (Marr, 1971), as more sparse codes can be represented by a finite population of neurons than dense codes that include many neurons, by reducing overlap and potential interference of distinct representations such as memories (Marr, 1971; Olshausen & Field, 2004; Silva et al., 2009). The sparse and selective firing of hippocampal neurons may be critical to their functions in memory storage and retrieval. However, hippocampal neurons receive thousands of excitatory inputs, only a small proportion of which are required to drive a neuron to spike under *in vitro* conditions. Therefore, the hippocampus must possess local circuit mechanisms that enforce the sparse and selective activity of the hippocampal output neurons, CA1 PCs. Linking defined circuit elements to

hippocampal spiking patterns and memory functions is still an unmet goal in neuroscience. The identification of these circuits is a primary aim of this thesis, and is required for a full understanding of how the physical circuitry of the hippocampus generates the neural activity that allows for learning and memory functions.

Relationships between local interneuron types and PC activity

Throughout the nervous system, discrete brain regions receive input from one or more presynaptic regions, and using the electrical properties of neurons and the connectivity amongst input and output neurons within the region, transform this synaptic input into an action potential output to be sent to downstream regions in the brain. Understanding this input-output transformation is critical to understanding how information from the outside world and internally generated activity is progressively processed by the nervous system towards generating actions and changing mental states or memory. Understanding this process is complicated by the neuronal connectivity within a region, including excitatory and inhibitory circuits, and the complexity of neuronal membrane excitability, such as the capacity for dendritic electrogenesis. These complications are particularly pronounced in the hippocampus and neocortex, but detailed descriptions of their input-output processing are nonetheless essential to understanding how these regions generate the activity observed during behavior, and the functions they generate, including perception, cognition, memory, and thought.

Amongst these regions, the CA1 subfield of the hippocampus may be more amenable to physiological characterization of neuronal input-output processing. CA1

contains a single layer of relatively homogenous PCs (but see Mizuseki et al., 2011) that have negligible recurrent connectivity (Knowles & Schwartzkronin, 1981). These PCs are all aligned within CA1: somata in *stratum pyramidale*, dendrites in *strata oriens, radiatum,* and *lacunosum-moleculare*, and axons passing through *oriens* en route to their output via the *alveus* (Spruston, 2008). As outlined above, CA1 PCs receive two primary excitatory input pathways: from CA3 to the proximal dendrites in *stratum oriens* and *radiatum*, and from entorhinal cortex (EC) to the distal dendrites in *stratum lacunosum-moleculare*. Proximal dendrites in *stratum oriens* also receive input from CA2 (Chevaleyre & Siegelbaum, 2010), which is not as well studied. PCs in CA1 and neocortex possess excitable dendrites, with active voltage-gated conductances that can modulate the effectiveness of input to drive output spikes (Magee, 2000; Spruston, 2008). These excitatory circuit properties are advantageous because they allow the study of single PC input-output transformations without the influence of other neurons to contaminate these measures via recurrent connectivity, and allow for targeted stimulation of excitatory input to spatially organized dendritic compartments. This contrasts with the neocortex, where there are several excitatory cell types that are intermingled among the six layers and are densely interconnected, causing any input to drive multiple cell types at several dendritic locations, which in turn can excite one another. CA1 allows for controlled input, especially in quiescent brain slices, that can be quantified by recording input currents from one PC without contamination by recurrent network excitation. Therefore CA1 is an ideal cortical circuit to study input-output transformations.

While CA1 is unique amongst hippocampal and cortical regions for its constrained excitatory circuitry, it shares with these regions the vast complexity and diversity of local inhibitory (GABA-releasing) interneurons (Freund & Buzsáki, 1996; Markram et al., 2004; Ascoli et al., 2008; DeFelipe et al., 2013). Recent estimates suggest at least 21 different inhibitory cell types within the rat CA1 alone (Klausberger & Somogyi, 2008). These GABAergic cell types can be uniquely defined based on a combination of molecular markers, morphology, physiological properties, input/output connectivity, and *in vivo* firing patterns (Freund & Buzsáki, 1996; Ascoli et al., 2008; Klausberger & Somogyi, 2008; DeFelipe et al., 2013). Similar to the advantages of studying excitation in CA1, the study of inhibitory interneuron interactions with PCs have also been facilitated by the unique properties of CA1. PCs are spread throughout the neocortex, which makes the connectivity from interneurons to PC ambiguous: if an inhibitory axon arborizes in layer II/III, this could be targeting the apical dendrites of layer V PCs or the somas of layer II/III PCs, or both. Conversely, the locations of inhibitory axons in CA1 correspond to known subcellular compartments of PCs - a simplicity that has allowed for the in-depth study of CA1 inhibitory interneurons, particularly in brain slices. In both neocortex and hippocampal regions, local inhibition from these diverse cell types plays a critical role in regulating and shaping the transformation of synaptic input into action potential output (Isaacson & Scanziani, 2011; **Fig 1.2a**).

With knowledge that there exist multiple interneuron types with unique anatomical positions, researchers have long theorized these cells may play unique functional roles in circuit function and resultant behaviors (Marr, 1971; Freund &

Buzsáki, 1996; Paulsen & Moser, 1998; Klausberger & Somogyi, 2008). One means by which inhibitory interneurons implement distinct circuit functions is their relative contributions to feed-forward or feed-back inhibition. Feed-forward inhibition can be achieved with both perisomatic-targeting interneurons (Buzsáki, 1984; Pouille & Scanziani, 2001) and dendrite-targeting interneurons (Alger & Nicoll, 1982; Klausberger, 2009), which is believed to provide a brief temporal window for monosynaptic excitatory integration before it is quenched by disynaptic inhibition. This organization encourages precisely timed action potentials (Pouille & Scanziani, 2001). Feed-forward inhibition therefore scales local excitation to the level of afferent excitation. In contrast, feed-back inhibition is a response to recurrent drive from local excitatory neurons, and thus scales local excitation to the level of efferent excitation. Similarly, feed-back inhibitory circuits include both perisomatic-targeting and dendrite-targeting interneurons (Sloviter, 1991; Isaacson & Scanziani, 2011). These cells can respond to distinct aspects of CA1 PC activity, where soma-targeting basket cells are activated by the

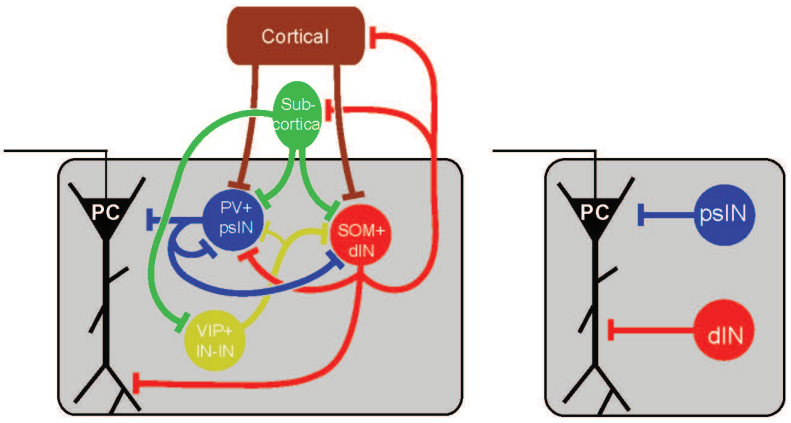

Figure 1.2 – Local inhibitory circuitry. **a)** Diagram of local inhibitory complexity present in hippocampal and neocortical circuits, including local and distant disinhibitory influences. **b)** Diagram of simplified models of local inhibitory circuitry – segregating interneuron types based on the subcellular compartment of PCs they inhibit, such as the perisomatic region (soma, proximal dendrites, and axon initial segment: psINs) or dendrites (basal, radial oblique, and distal tuft branches: dINs).

onset of PC spiking and distal dendrite-targeting OLM cells are activated by persistent spiking, indicating unique feed-back inhibitory circuits responsive to the timing and rate of efferent spikes, respectively (Pouille & Scanziani, 2004).

Inhibitory synapses contacting the soma and dendrites of CA1 PCs are believed to have distinct functional impacts on PCs, due to the different biophysical properties of the perisomatic and dendritic compartments. Somatic inhibition can control aspects of spike timing, such as spike timing relative to the theta oscillation (Cobb et al., 1995; Losonczy et al., 2010), whereas dendritic inhibition may be more effective at regulating local dendritic spiking (Miles et al., 1996; Larkum et al., 1999; Murayama et al., 2009; Palmer et al., 2012b), which is known to be regulated via voltage-gated NMDA receptors and Ca^{2+} channels (Collingridge et al., 1988; Losonczy & Magee, 2006; Dudman et al., 2007; Takahashi & Magee, 2009). Despite these predictions, prior to the initiation of the studies described in this thesis the impact of these cells on distributed synaptic integration and in the behaving animal had not been tested. Furthermore, the molecular identities of the inhibitory interneurons contributing to these functions had not been conclusively demonstrated.

Perisomatic inhibition of PCs arises from distinct cell types in CA1, specifically basket cells and axo-axonic cells, among others (Freund & Buzsáki, 1996; Klausberger & Somogyi, 2008). Similarly, the sources of dendritic inhibition to PCs correspond to distinct cell types, including oriens lacunosum-moleculare (OLM) cells, bistratified cells, ivy cells, neurogliaform cells, and stratum radiatum interneurons, among others (Freund & Buzsáki, 1996; Klausberger & Somogyi, 2008; Klausberger, 2009). Furthermore, some cell types can mediate inhibition across the membrane surface of PCs, such as

trilaminar cells (Freund & Buzsáki, 1996). Therefore these distinct cell types may serve as distinct molecular and genetic entry points to researchers aiming to investigate the basis of functions mediated by dendritic and somatic inhibition (**Fig 1.2b**). Therefore, although we know a great deal about the molecular, anatomical, and physiological diversity of inhibitory cell types, relatively little is known about the impact of these cells on PC spiking activity, neural coding, and behavior. We will discuss these issues below, and aim to address these concerns the experiments described in *Chapter 2* and *Chapter 3*.

Approaches for Linking Interneurons to PC Activity Patterns and Behavior

We know that PC firing patterns govern behavioral expression, and that subtypes of local inhibitory interneurons can differentially modulate these PC firing patterns. This implies that particular types of interneurons may have dissociable influences over behaviors that rely on these distinct firing patterns (Lovett-Barron & Losonczy, 2014). This structure-function relationship may be particularly useful for therapeutic purposes, by identifying genetically defined inhibitory cells that implement cognitive functions through modulation of known computations in PCs. Despite this promise, very little has been done thus far to link these two levels of analysis.

While inhibitory cell types have long been hypothesized to possess dissociable roles in controlling PC activity and resultant behavior, this has been traditionally difficult to test experimentally, as discussed in the previous section. However, research efforts in the last decade have yielded a remarkable array of tools to facilitate the recording

and manipulation of activity in defined inhibitory cell types in the hippocampus and neocortex of behaving animals. Central to these advances has been the development of genetically engineered mice that express cre recombinase in specific cell types defined by molecular identity (Luo et al., 2008; Taniguchi et al., 2011), which can be bred with other mice or combined with viral approaches to flexibly drive expression of genetically encoded fluorescent proteins and sensors or modulators of neural activity in cre-expressing cells. Defining cell types based on single molecular criteria is insufficient to capture individual cell classes, as cell types are more stringently defined by a combination of distinct features such as morphology, activity, and connectivity (Ascoli et al., 2008; DeFilipe et al., 2013). Nevertheless, molecular factors can broadly segment cell types, such as those that target the perisomatic region of PCs (eg. Parvalbumin-expressing, Pvalb+) versus those that target PC dendrites (eg. Somatostatin-expressing, Som+).

Methods for recording neural activity *in vivo* such as electrophysiology and fluorescence imaging typically do not provide definitive information about cell type. However, expression of fluorescent proteins in cells of interest allow them to be targeted with recording electrodes under visual guidance, or selected for fluorescence analysis during Ca^{2+} imaging. Alternatively, cell types can be labeled with a physiological tag in the form of optical activators or suppressors, allowing for identification of extracellularly recorded units (Lima et al., 2008). To selectively manipulate the activity of molecularly defined cell types, experimenters can express reversible modulators of electrical activity in neurons including optogenetic (Deisseroth, 2011; Fenno et al., 2011) and pharmacogenetic tools (Rogan & Roth, 2011; Magnus et al., 2011). Permanent

manipulations can also be targeted to cell types, such as deletions of excitatory receptors or expression of toxins (Luo et al., 2008), but these methods suffer from the possibility of adaptation or compensation over longer timescales.

Linking inhibition to function in the hippocampus

One approach to strictly define cell classes without genetic tools is to label recorded interneurons with dyes through recording electrodes then stain for proteins expressed by the recorded cell. This technique has been used in freely-moving rats to show that soma-targeting basket cells are more sensitive to behavioral state than dendrite-targeting Ivy cells (Lapray et al., 2012). This technique has also been used in awake head-fixed mice to show a stereotypical temporal ordering in spiking of basket cells and distal dendrite-targeting OLM cells and increased firing of OLM cells during sharp-wave ripples (Varga et al., 2012), which contrasts with reports in anaesthetized rats (Klausberger et al., 2003).

Whereas the above results show how the activities of defined interneurons are modulated in behaving mice, fewer experimenters have assessed their causal roles in behavioral performance. In pioneering early studies, knockout of excitatory AMPA (Fuchs et al., 2007) or NMDA receptors (NMDARs; Korotkova et al., 2010) in Pvalb+ cells were found to impair spatial working memory, although similar NMDAR knockouts (Carlen et al., 2012) found minimal impairment, instead reporting deficits in fear conditioning. These behavioral deficits are difficult to interpret because these receptor knockouts are not anatomically restricted, but are present in Pvalb+ cells throughout the hippocampus and neocortex, among other regions. In a more refined approach, Murray

and colleagues virally restricted tetanus toxin light chain to Pvalb+ interneurons in CA1, irreversibly blocking synaptic release (Murray et al., 2011). The authors found this manipulation selectively disrupted spatial working memory, while sparing performance in a spatial reference memory task. Whether separate classes of CA1 interneurons regulate other memory functions remains largely untested. A primary goal of this thesis is to test the behavioral role of another major interneuron class – Som+ dendrite-targeting interneurons.

Linking inhibition to function in the neocortex

Despite these advances in the hippocampus, direct links between inhibitory neuron contributions to behavior, and their precise role in the circuits that implement these behaviors, remain largely unknown. These relationships have been studied in greater detail in the neocortex. Due to the architectural and physiological similarities between neocortex and the hippocampus, we can learn a great deal about inhibitory interneuron function in neocortical regions. Furthermore, cortical circuits may be more favorable to neuronal recording and analysis, due to the superficial location in the brain, and the fact that externally driven sensory perception is more easily studied under experimental conditions than internally-driven memory phenomena.

Experiments conducted in visual cortex of anesthetized mice have reported the responses of Pvalb+, Som+, and vasoactive intestinal polypeptide-expressing (Vip+) interneurons in layers I and II/III to visual stimuli, finding broad orientation tuning for all inhibitory subtypes (Kerlin et al., 2010), although some groups have reported tuned firing of Som+ interneurons (Ma et al., 2010) or a subset of Pvalb+ interneurons

(Runyan et al., 2010; Runyan et al., 2013). In a recent study, Lee and colleagues (2012b) found that optical activation of Pvalb+ interneurons in visual cortex of anesthetized mice enhanced the orientation selectivity of PCs, whereas activation of Som+ or Vip+ interneurons did not. Accordingly, photoactivation of Pvalb+ interneurons in a head-fixed go/no-go task increases the ability of mice to discriminate between similar orientations. Although other recording studies in anesthetized mice found that exciting Pvalb+ interneurons did not affect PC orientation selectivity (Atallah et al., 2012; Wilson et al., 2012), there has yet to be any behavioral evidence to extend these findings. Beyond orientation tuning, Pvalb+ interneurons in primary visual cortex have been implicated in ocular dominance plasticity, a form of cortical plasticity occurring in juvenile mice in response to monocular deprivation. A recent study (Kuhlman et al., 2013) found that while layer II/III PCs increase their activity upon sensory deprivation, Pvalb+ interneurons in binocular visual cortex reduced their evoked activity, a result of pruned excitatory input. This insight allowed the authors to causally test the link between circuit function and behavior. Although typically not observed in adults, the authors could induce ocular dominance plasticity by chronically suppressing Pvalb+ interneuron activity during monocular deprivation in adult mice.

Roles for Pvalb+ interneurons have also been found in the primary sensory cortex responsible for processing other sensory modalities. Studying primary somatosensory barrel cortex, Sachidhanandam and colleagues (2013) used mice behaving in a whisker stimulus detection task, and found that detection correlated with delayed PC depolarization, both of which could be counteracted by optogenetic activation of Pvalb+ interneurons. In primary auditory cortex, Letzkus and colleagues

(2011) investigated the role of inhibitory cell types in the cortical processing of complex tones during auditory cortex-dependent fear conditioning, where the CS is a complex tone sweep and the US is a foot shock. The authors found that in anesthetized mice, foot shocks excite GABAergic interneurons in layer I of auditory cortex via basal forebrain cholinergic input. The authors found these layer I interneurons inhibited layer II/III Pvalb+ interneurons, resulting in enhanced net excitation of PCs. Using extracellular recordings in behaving mice during conditioning, the authors also reported that fast-spiking interneurons (presumed to be Pvalb+) were inhibited during foot shocks, whereas PCs were excited by the shock. The authors provided support for this model by photoactivating Pvalb+ interneurons during the US, and found that this manipulation prevented fear conditioning. Some recent work has suggested that these layer I interneurons mediating aversive stimulus-evoked disinhibition may be Vip+ (Pi et al., 2013), although these cells are believed to preferentially inhibit Som+ interneurons, rather than the Pvalb+ interneurons studied by Letzkus and colleagues (2011).

Although sensory perception implemented by the neocortical structures described above is very different from the computations performed in the hippocampus, some basic lessons can be learned from these studies in neocortex, such as the ability of interneurons to shape PC input processing and plasticity, the ability to sculpt the acuity of sensory receptive fields (Carandini & Ferster, 2000; Isaacson & Scanziani, 2011), and the capacity of disinhibitory circuits to influence circuit processing and behavior. These features may generalize to many different circuits where excitatory and inhibitory neurons are intermingled. Therefore, similar in-depth investigations of

inhibitory interneurons in the hippocampus of behaving animals may reveal how similar functions contribute to learning and memory.

Dissecting the Role of Inhibitory Interneurons in Memory Functions

The research reviewed above demonstrates the power of using transgenic or knock-in mice that label defined cell types to record and manipulate the activity of known subtypes of inhibitory interneurons in regions of neocortex during relevant

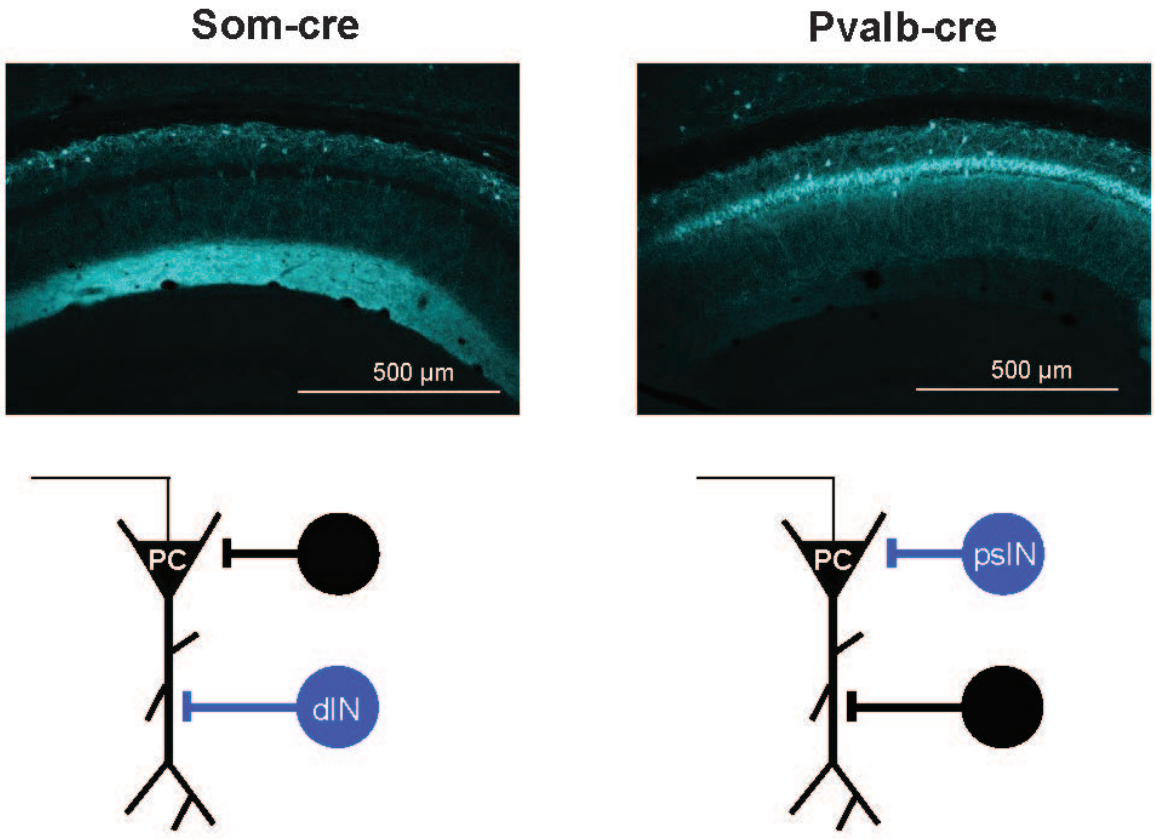

Figure 1.3 – Genetic targeting of dendrite- and soma- targeting interneurons in CA1. Genetic access to dendrite-targeting interneurons (Som+) and perisomatic-targeting interneurons (Pvalb+) in CA1 using the cre/loxP system and viral vectors. Top: confocal images of viral expression in *Som-cre* and *Pvalb-cre* mice. Bottom: Schematic of interneurons targeting of CA1 PC subcellular compartments.

behaviors. We aim to take a similar approach to the hippocampus, and determine how inhibitory interneurons control the activity patterns of PCs and the memory functions they implement. We will make use of cre recombinase knock-in mice that allow for viral expression of exogenous proteins in cre+ subtypes of inhibitory interneurons, corresponding to cells that inhibit the perisomatic or dendritic regions of PCs (Pvalb+ and Som+ interneurons, respectively; **Fig 1.3**)**.** As reviewed above, these mice have been used extensively in recent years (Luo et al., 2008; Taniguchi et al., 2011; Lovett-Barron & Losonczy, 2014), yielding results pertaining to sensory processing functions in primary sensory cortex. We believe that using these tools in the hippocampus can extend the research programs that aim to determine how inhibitory cell types shape hippocampal activity, and how this activity implements memory functions.

In my thesis, I have conducted experiments that have begun to link these fields (**Fig 1.4**). I first examined the impact of CA1 Som+ interneurons on PC excitatory input processing, by controlling circuit elements in acute brain slices. The research in *Chapter 2* is designed to determine how distinct interneuron types contribute to regulating CA1 firing patterns through control of PC input-output transformations. I next examined how CA1 Som+ interneurons contribute to CFC, by recording and perturbing neural circuit activity in behaving mice while they learn and recall fear memories. The research in *Chapter 3* is designed to ask how distinct interneuron types regulate the encoding of memories in PC ensembles. These two studies focus on Som+ dendrite-targeting inhibitory interneurons in the CA1 subfield of the dorsal hippocampus, and together show how these inhibitory interneurons contribute to fundamental neural function at the

cellular level (gain control and burst spiking) and the behavioral level (contextual memory formation).

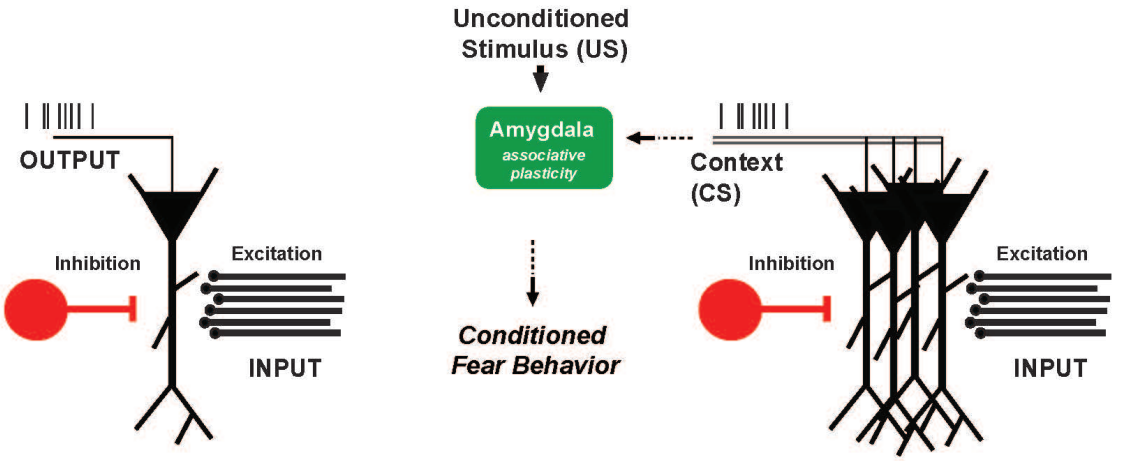

Figure 1.4 – Overview of issues addressed in this thesis. *Chapter 2* will investigate the role of inhibitory interneurons in regulating the transformation of excitatory synaptic input into action potential output in single CA1 PCs, using cell type-specific activation, inactivation, and intracellular recording *in vitro*. *Chapter 3* will investigate the role of inhibitory interneurons in regulating the encoding of context by the hippocampus during contextual fear conditioning, using cell type-specific inactivation, 2-photon Ca^{2+} imaging, pharmacology, and behavioral testing *in vivo*.

Chapter 2 - Regulation of CA1 Pyramidal Cell Input-output Transformations by Dendrite-targeting Inhibitory Interneurons

Introduction

The output of principal cells in the hippocampus can range from silence to high-frequency bursts of action potentials (Kandel & Spencer, 1961; Thompson & Best, 1989). Sparse coding for the cognitive representation of space is implemented by a subset of principal neurons that display location-specific firing during navigation, while other neurons remain silent (O'Keefe & Dostrovsky, 1971; O'Keefe & Nadel, 1978). Similarly, hippocampal principal neurons are sparse and selective in non-spatial tasks, with a small percentage of neurons firing in response to distinct behaviorally relevant events (Eichenbaum et al., 1999). This sparse and selective coding regime is believed to underlie the capacity of the hippocampus to support an extensive memory storage system. The mechanisms by which the hippocampal circuit transforms synaptic input into spike output conducive to this sparse coding scheme remain controversial (Colgin et al., 2008; Ahmed & Mehta, 2009). This transformation can be described by a neuron's input-output (i-o) function – which quantifies the outputs (membrane voltage, spike probability, or spike rate) that are caused by a given level of input (current injection, conductance, synaptic input). Experimental manipulations of the i-o transformation are typically described as being additive/subtractive (typically a shift in the rheobase along the input axis while maintaining the slope of the i-o curve – referred to as a change in 'offset') or multiplicative/divisive (a change in the slope of the i-o curve – referred to as a change in 'gain') (Silver, 2010).

The i-o transformation of PCs can be effectively studied in hippocampal area CA1, due to its relatively uniform population of PCs and minimal recurrent connectivity amongst PCs. Although this question is relevant to other hippocampal subfields, the

neocortex, and other regions of the brain, CA1 can serve as a model cortical circuit to study input-output properties without the complexity of recurrent excitatory circuits, especially when isolated *in vitro*. Spatiotemporal pattern-dependent integration of excitatory inputs can generate distinct spike outputs by promoting linear or supralinear integration schemes in PC dendrites (Larkum et al., 1999; Gasparini & Magee, 2006; Losonczy & Magee, 2006; Nevian et al., 2007), and could potentially provide mechanisms for firing behaviors observed in CA1 PCs *in vivo* (Harvey et al., 2009; Epsztein et al., 2011). Active dendritic electrogenesis and the all-or-none properties of axonal spiking, however, yield a limited dynamic range of input processing because firing rates saturate even to relatively low levels of input. As a consequence, this bistable network behavior constrains the capacity for neural coding, suggesting a requirement for mechanisms that constrain excitatory circuit processing (Ahmed & Mehta, 2009; Isaacson & Scanziani, 2011) to expand the dynamic range of input-output processing.

One candidate for such processing is the diverse population of local inhibitory GABAergic cells in CA1, which provide inhibition to pyramidal cells along their entire somato-dendritic axis through distinct perisomatic- and dendrite-targeting GABAergic circuits (Buhl et al., 1994; Freund & Buzsáki, 1996; Klausberger & Somogyi, 2008). The influence of perisomatic inhibition on pyramidal cells has been well documented, with GABA release from basket and axo-axonic cells acting to control spike timing and oscillations (Cobb et al., 1995; Pouille & Scanziani, 2001; Losonczy et al., 2010) - both aspects of neuronal activity considered relevant for temporal coding.

However, CA1 PCs receive the vast majority of their inhibitory inputs to their dendrites (Megias et al., 2001; Klausberger, 2009), and the activity of dendrite-targeting interneurons coincides with the inferred activity of presynaptic excitatory inputs *in vivo* (Klausberger et al., 2004; Klausberger & Somogyi, 2008; Klausberger, 2009). This raises the possibility that dendritic inhibition serves to regulate local excitatory input processing (Larkum et al., 1999; Murayama et al., 2009; Larkum et al., 2009), which could be particularly important given the active properties of CA1 PC dendrites (Sjostrom et al., 2008; Spruston et al., 2008). Indeed, inhibition has been demonstrated to play a role in controlling both Ca^{2+} spikes in the apical trunk (Miles et al., 1996; Larkum et al., 1999) and *N*-methyl-D-aspartate receptor (NMDAR)-dependent nonlinearities (Collingridge et al., 1988) in thin dendrites of hippocampal pyramidal neurons. The presence or absence of dendritic inhibition in CA1 could contribute to defining the spike output of CA1 PCs to synaptic excitation in a given spatial environment or during particular events. Yet, the causal role of identified dendritic inhibitory circuits in PC i-o transformations remains unknown, due to difficulties in achieving precise experimental control over known excitatory and inhibitory circuit elements. Here we apply a panel of cell type-specific optogenetic and pharmacogenetic techniques to control distinct components of excitation and inhibition in the hippocampal CA1 circuit *in vitro*, and assess the function of dendritic inhibition in CA1 PC i-o transformations.

Results

Manipulating excitatory and inhibitory circuitry in CA1

In the engaged hippocampal network, CA1 PCs are driven by excitatory synaptic inputs that are distributed over multiple branches of their dendritic arborizations, and inhibition exerts its effects with GABAergic interneurons recruited through synaptic excitation. To mimic these input conditions *in vitro* while recording the voltage of PCs, we devised a strategy to activate the CA1 circuit with spatiotemporally distributed photostimulation of the excitatory CA3 Schaffer collaterals (CA3-SCs). To assess the impact of inhibitory interneurons under these conditions, our approach is to concurrently silence genetically-designated subpopulations of local interneurons.

We bilaterally injected the recombinant adeno-associated virus (rAAV) rAAV(*ChR2-sfGFP*) into dorsal CA3 of adult mice to induce Channelrhodopsin-2 (ChR2) expression in CA3-SC axons, located in *strata radiatum* and *oriens* of CA1 (see Experimental Procedures; **Fig 2.1a**). Grid-photostimulation of the CA3-SCs, the numerically largest source of excitatory input to CA1 (Megias et al., 2001; Ahmed & Mehta, 2009), drove pyramidal cells and interneurons in the CA1 circuit with phasic excitatory synaptic input in acute coronal hippocampal slices. We determined the suprathreshold i-o transformation by systematically varying the intensity of CA3-SC photostimulation and measuring the firing rate output of CA1 PCs (*f*) with whole-cell recordings from the soma. As detailed in the introduction, the low levels of recurrent excitatory connectivity present in the CA1 area (Knowles & Schwartzkronin, 1981) permitted us to quantify photostimulation intensities in terms of mean excitatory currents ($I_{E(syn)}$) measured in PCs under $GABA_A$ receptor ($GABA_AR$) blockade (20 μM gabazine)

at the end of each experiment (**Fig 2.1b**). Grid photostimulation produced a spatially disperse activation of CA3-SC axons, comparable to estimates of CA3-SC inputs during theta-exploratory states *in vivo* (Ahmed & Mehta, 2009; Buzsáki, 2002; see

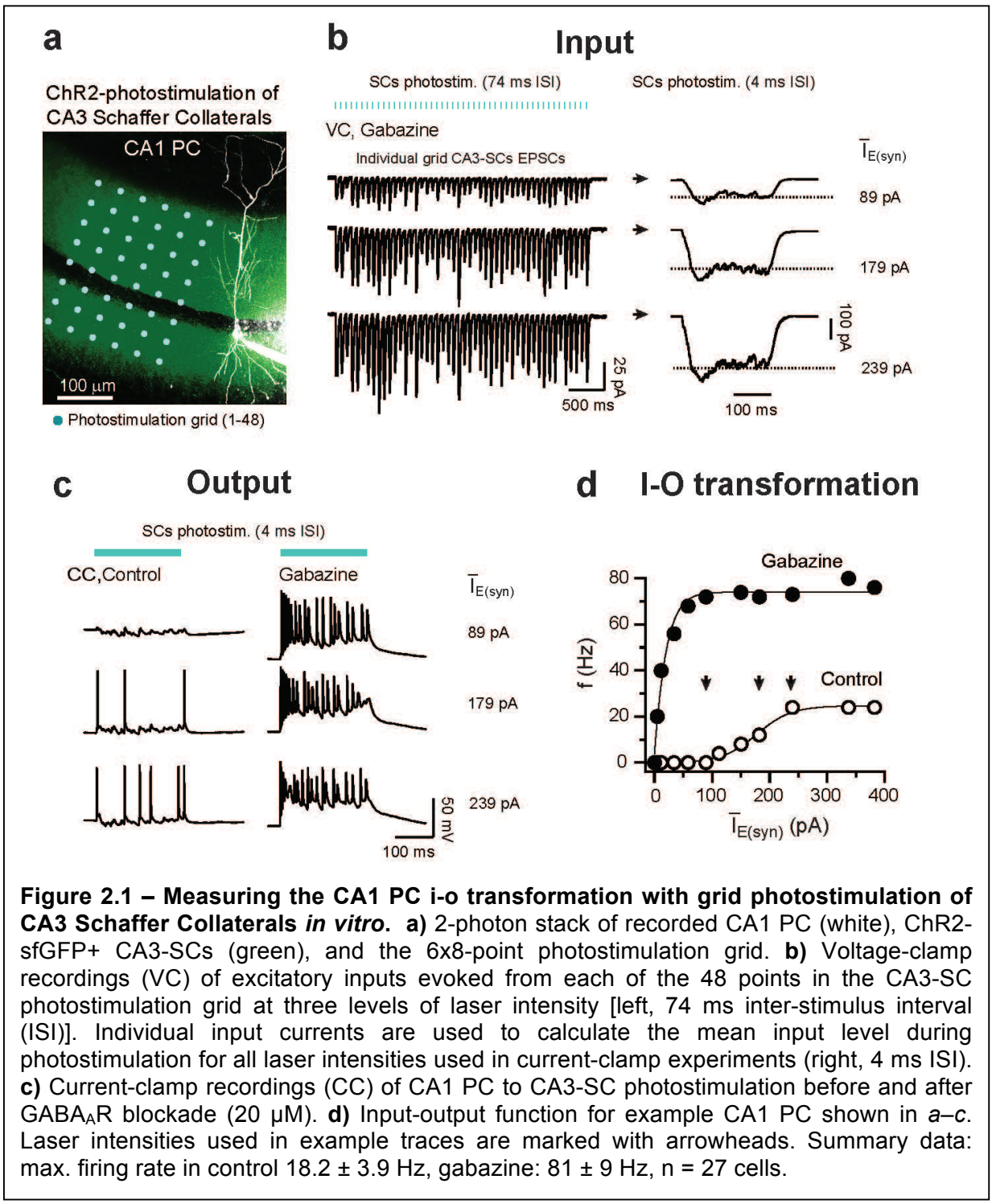

Figure 2.1 – Measuring the CA1 PC i-o transformation with grid photostimulation of CA3 Schaffer Collaterals *in vitro*. a) 2-photon stack of recorded CA1 PC (white), ChR2-sfGFP+ CA3-SCs (green), and the 6x8-point photostimulation grid. **b)** Voltage-clamp recordings (VC) of excitatory inputs evoked from each of the 48 points in the CA3-SC photostimulation grid at three levels of laser intensity [left, 74 ms inter-stimulus interval (ISI)]. Individual input currents are used to calculate the mean input level during photostimulation for all laser intensities used in current-clamp experiments (right, 4 ms ISI). **c)** Current-clamp recordings (CC) of CA1 PC to CA3-SC photostimulation before and after $GABA_AR$ blockade (20 µM). **d)** Input-output function for example CA1 PC shown in *a–c*. Laser intensities used in example traces are marked with arrowheads. Summary data: max. firing rate in control 18.2 ± 3.9 Hz, gabazine: 81 ± 9 Hz, n = 27 cells.

Experimental Procedures). CA3-SC photostimulation effectively recruited polysynaptic GABAergic inhibition that strongly counteracted excitation, resulting in low CA1 PC firing rates even for relatively high levels of excitatory input. Upon pharmacological blockade of $GABA_A$Rs, PCs greatly increased their firing rates (**Fig 2.1c,d**).

To selectively and completely inhibit defined populations of highly-active GABAergic neurons, we required a genetically-encoded neuronal silencing system that could be acutely engaged and strongly suppresses neuronal activity. For this, we employed a chimeric ligand-gated ion channel ($PSAM^{L141F}$-GlyR) (Magnus et al., 2011) targeted exclusively to genetically-defined subpopulations of GABAergic interneurons in CA1 using the cre-loxP system (Atasoy et al., 2008). Application of its small-molecule agonist ($PSEM^{308}$) results in rapid silencing of $PSAM^{L141F}$-GlyR+ cells (Magnus et al., 2011) though activation of a shunting Cl^- conductance. We verified this approach using conditional viral expression of $PSAM^{L141F}$-GlyR non-selectively in local GABAergic interneurons to achieve complete pharmacological blockade of inhibition in CA1 (**Fig 2.2a**). For this we injected rAAVs into the dorsal hippocampus of *Gad65-Cre* mice (Losonczy et al., 2010) [rAAV(*ChR2-sfGFP*) into bilateral CA3; rAAV($PSAM^{L141F}$-*GlyR*)^{Cre} and rAAV(*tdTomato*)^{Cre} into unilateral CA1], driving robust expression of ChR2-sfGFP in the CA3-SCs, and $PSAM^{L141F}$-GlyR/tdTomato in Gad65+ local inhibitory neurons (**Figs 2.3**; see Experimental Procedures). Bath application of $PSEM^{308}$ completely silenced recorded $PSAM^{L141F}$-GlyR+ interneurons in all cases (3 μM, n = 18), with no spikes elicited by somatic current injection or maximal phasic CA3-SC photostimulation (**Fig 2.2b,c**), and without affecting the intrinsic properties of $PSAM^{L141F}$-GlyR-negative interneurons and PCs (**Fig 2.3**). Pharmacogenetic silencing

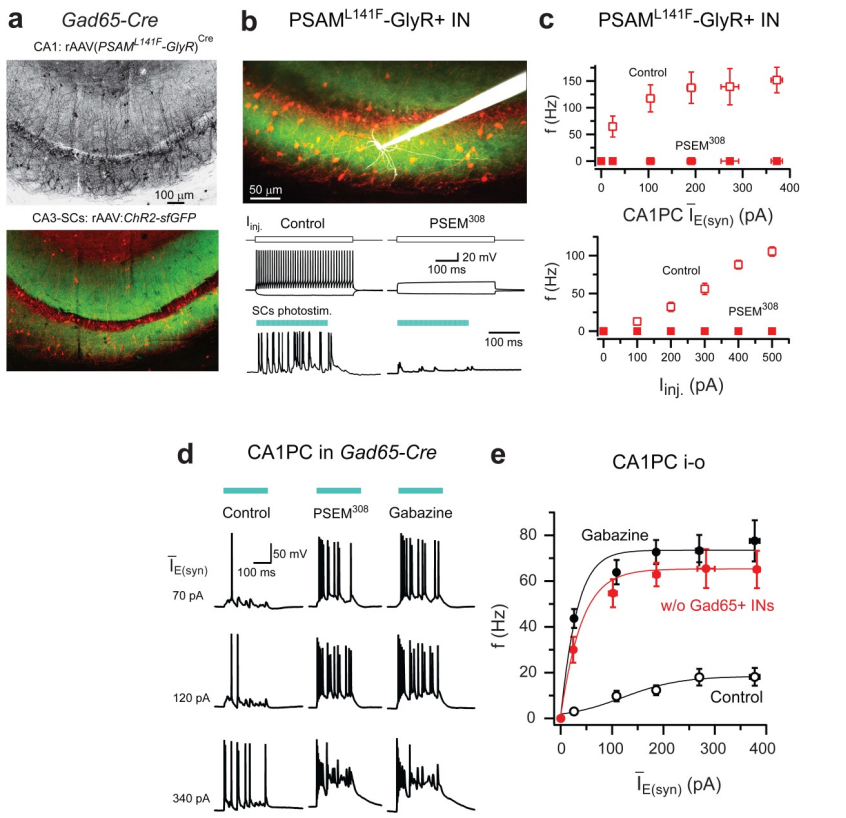

Figure 2.2 – Pharmacogenetic inactivation of CA1 GABAergic interneurons with PSAM^{L141F}-GlyR. **a)** Confocal image stacks of PSAM^{L141F}-GlyR/tdTomato-expressing interneurons (tdTomato fluorescence pseudo-coloured to black on a white background) in *Gad65-Cre* mice, and overlay (native red tdTomato color) with ChR2-sfGFP expression in the CA3-SCs (green). **b)** 2-photon image stack of recorded interneuron (IN, white), ChR2-sfGFP+ CA3-SCs (green), and PSAM^{L141F}-GlyR/tdTomato + INs (red), and responses to somatic current injection and CA3-SC photostimulation before and after bath application of 3 µM PSEM^{308}. **c)** Summary plots of firing rates recorded in PSAM^{L141F}-GlyR+ INs in response to CA3-SC photostimulation (input measured as CA1 PC $I_{E(syn)}$) and somatic current injection ($I_{inj.}$). **d)** Current-clamp recordings from a CA1 PC during CA3-SC photostimulation in control conditions, after silencing Gad65+ INs with PSEM^{308} (max firing in PSEM^{308}: 67 ± 8 Hz, n = 6), and after subsequent application of gabazine. **e)** Summary i-o function for CA1 PCs comparing control conditions, pharmacogenetic removal of inhibition by silencing Gad65+ interneurons, and blockade of $GABA_A$Rs (20 µM gabazine). Δgain/gain: PSEM^{308}: 677 ± 150%, n = 6, gabazine: 732 ± 85%, n = 22; offset: PSEM^{308}: 79 ± 19 pA, gabazine: 82 ± 12 pA. Error bars indicate ± s.e.m.

of Gad65+ interneurons closely mimicked the effects of blocking $GABA_A$Rs pharmacologically, and substantially increased CA1 PC firing rate to CA3-SC photostimulation (**Fig 2.2d**). Together, these results revealed a major divisive and moderate subtractive influence of local GABAergic neurons on the PC i-o relationship (**Fig 2.2e**). We confirmed the selective silencing of genetically-defined interneurons during CA3-SC input by quantifying the efficiency of viral infection, and determining that PSEM^{308} application

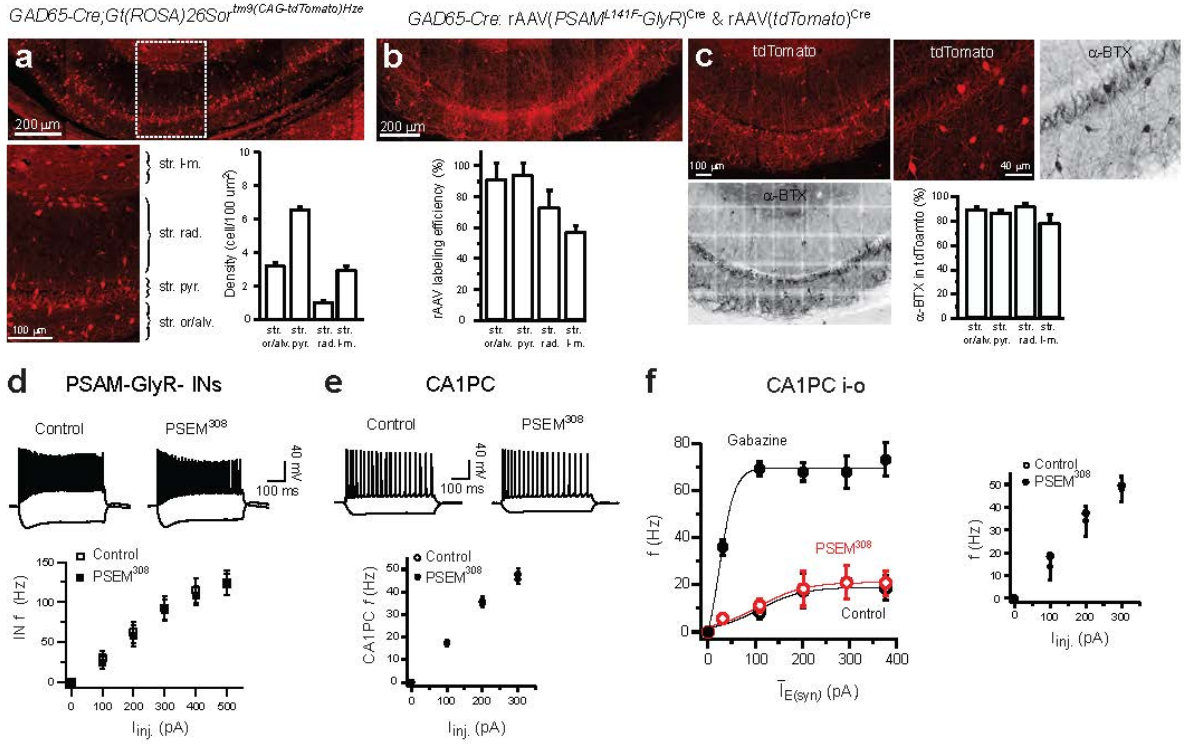

Figure 2.3 – Controls for selective silencing of Gad65+ interneurons in CA1 with cre-dependent expression of PSAM^{L141F}-GlyR, and application of its ligand PSEM^{308}. a) Top: low magnification confocal stack image of tdTomato-expressing interneurons in the CA1 area of the dorsal hippocampus of an offspring of a GAD65-Cre and a Cre-dependent tdTomato reporter mouse (Gt(ROSA)$^{26Sortm9(CAG-tdTomato)Hze}$). Bottom left: dashed boxed area is expanded to show labeling in various layers of the hippocampal CA1 region. Bottom right: summary bar graph of the density of tdTomato labeled interneurons in the layers of CA1 area (n = 16 in n = 8 mice; str. or./alv.: strata oriens/alveus, str. pyr.: stratum pyramidale, str. rad.: stratum radiatum, str. l-m: stratum lacunosum-moleculare). **b)** Top: low magnification confocal stack image of tdTomato-expressing interneurons in the CA1 area of the dorsal hippocampus injected with a mixture (3:1 ratio) of Cre-dependent rAAV expressing PSAM^{L141F}-GlyR [(rAAV(PSAM^{L141F}-GlyR)^{Cre}] and tdTomato [(rAAV(tdTomato)^{Cre}] in a Gad65-Cre mouse. Bottom: summary bar graph of rAAV labeling efficiency in layers of the dorsal hippocampal CA1 region in Gad65-Cre mice (labeling efficiency: 78 ± 5%, n = 8 slices in n = 8 mice). **c)** Top: low-(left) and high-(middle) magnification confocal images of viral tdTomato labeling. Below is the high-magnification image pseudocolored to black on a white backgound. Right: high magnification of alpha-bungarotoxin immunofluorescence (α-BTX) from the CA1 region of the injected hippocampus. Bottom right: summary graph showing the co-localization of α-BTX and tdTomato labeling in Gad65+ interneurons in layers of the hippocampal CA1 region (n = 16).

selectively blocked spiking in cre+/ PSAM^{L141F}-GlyR+ interneurons to current injection and CA3-SC stimulation, while sparing non-expressing interneurons and pyramidal cells (**Fig 2.3**).

Figure 2.3 continued… **d)** Top: representative voltage traces for somatic depolarizing and hyperpolarizing current injections from PSAM-GlyR-negative interneurons in control and in the presence of 3 μM PSEM^{308}. Bottom: summary of somatic current injection-evoked firing rate for PSAM-GlyR-negative interneurons in control and in the presence of PSEM^{308} (n = 16). **e)** Top: representative voltage traces for somatic depolarizing and hyperpolarizing current injections in control and in the presence of PSEM^{308} from CA1 PCs in slices injected with rAAV(PSAM^{L141F}-GlyR)^{Cre} in control and in the presence of PSEM^{308}. Bottom: summary of somatic current injection-evoked firing rate for CA1 PCs in control and in the presence of PSEM^{308} (n = 30). **f)** Left: summary i-o relationship of CA1 PCs in response to CA3-SC photostimulation from slices lacking PSAM^{L141F}-GlyR-exression (n = 5) in control, in the presence of PSEM^{308}, and 20μM gabazine. Lines are sigmoidal fit to the data. Right: somatic f-I relationship for CA1 PCs from slices lacking PSAM^{L141F}-GlyR in control and in PSEM^{308} (n = 5).

Together, these data justify the use of this approach to investigate the influence of GABAergic interneuron subtypes on the CA1 PC i-o transformation, specifically dendrite-targeting Som+ and perisomatic-targeting Pvalb+ interneurons using the mouse lines illustrated in **Fig 1.3**.

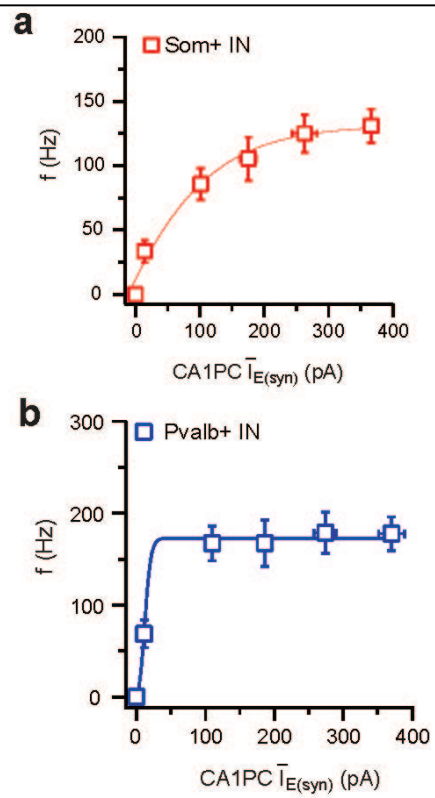

Figure 2.4 – CA3-SC grid photostimulation drives Som+ and Pvalb+ interneurons. I-o function of Som+ interneurons (**a**; n = 8) and of Pvalb+ interneurons (**b**; n = 11) in response to CA3-SCs ChR2-photostimulation. Interneuron firing rates are plotted as functions of mean excitatory CA3-SCs input obtained from consecutively recorded CA1 PCs. Lines are sigmoidal fits.

Effects of silencing Som+ or Pvalb+ interneurons on CA1 PC i-o transformations

We found that CA3-SC photostimulation effectively drove high firing rates in both Pvalb+ and Som+ interneurons, with i-o curves that scaled with the relative input to CA1 PCs. After each interneuron recording, we measured PC

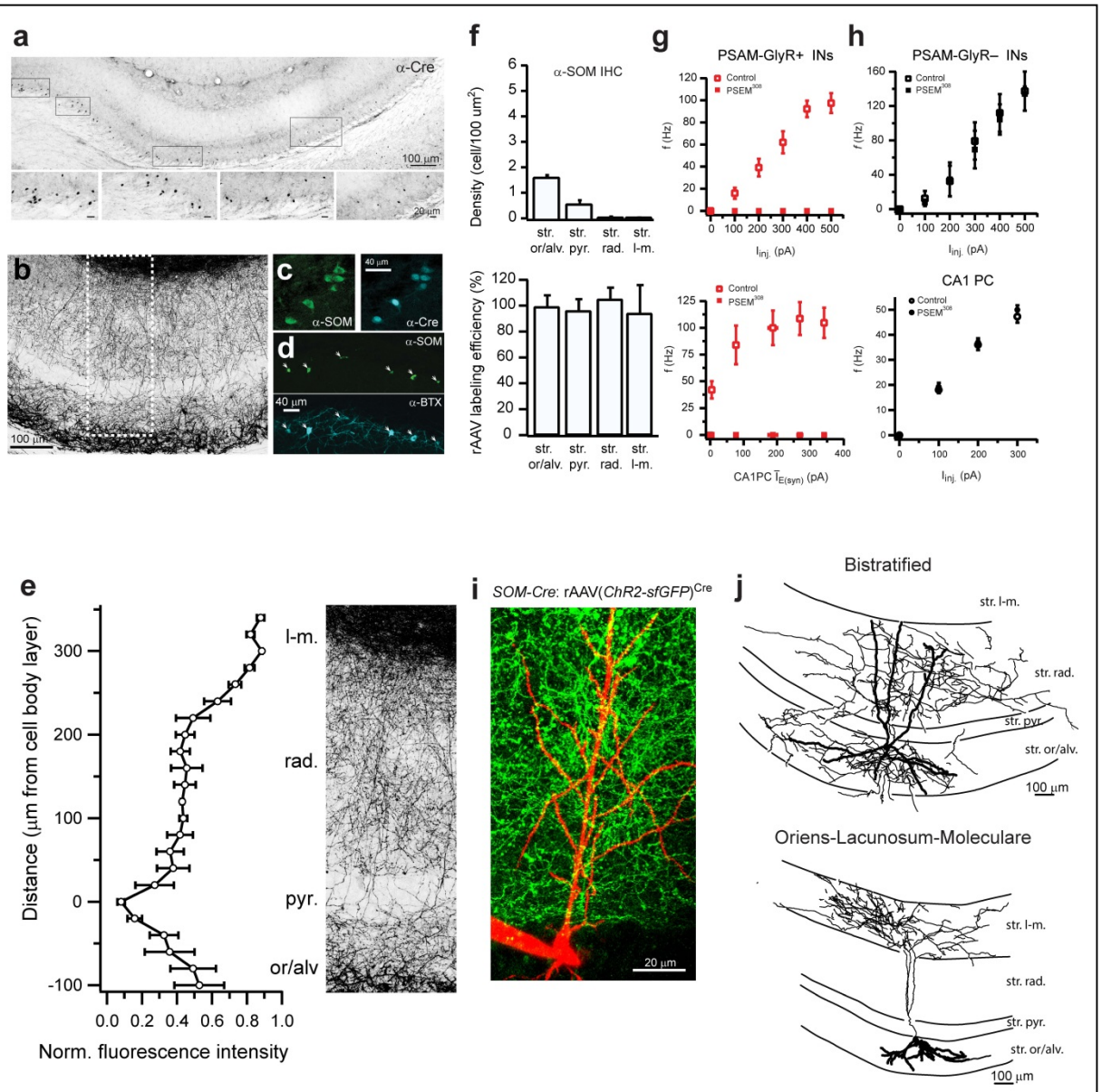

Figure 2.5 – Selective silencing of Som+ interneurons in CA1 with cre-dependent expression of PSAM^{L141F}-GlyR, and application of its ligand PSEM^{308}. **a)** Low magnification bright-field image of the hippocampal CA1 region with Ni-DAB immunostaining for cre recombinase. Boxed areas are expanded in insets to show Ni-DAB labeled nuclei *in strata oriens/alveus and pyramidale* **b)** Low magnification pseudocolored grayscale confocal image stack (20 μm) showing labeling pattern in layers of CA1 in *Som-cre* mice injected with rAAV(sfGFP)^{Cre}. **c)** Co-localization of somatostatin (α-Som) and Cre recombinase (α-cre) in CA1 *stratum oriens/alveus* interneurons in *Som-cre* mice. **d)** Co-localization of somatostatin (α-Som) and alpha-bungarotoxin (α-BTX) in CA1 *stratum oriens/alveus* interneurons in *Som-cre* mice injected with rAAV(PSAM^{L141F}-GlyR)^{Cre}.

Figure 2.5 continued… **e)** Left**:** summary plot of normalized fluorescence intensity as a function of distance from the cell body layer in (bins: 20 µm) in *Som-cre* mice (n = 3) injected with rAAV(sfGFP)^{Cre} into CA1. Background was corrected on 8-bit binary images and average pixel intensity was calculated in 20 x 20 µm areas spanning from *str. oriens* to *str. lacunosum-moleculare*. Normalized average pixel intensity, triggered by the position of the pyramidal layer, was displayed as a function of the distance from the pyramidal layer center for both lines. Right: expanded boxed area from *b*. **f)** Top: summary bar graph of the density of Som+ labeled interneurons in the layers of CA1 area (n = 8, *str. or./alv.: strata oriens/alveus, str. pyr.: stratum pyramidale, str. rad.: stratum radiatum, str. l-m: stratum lacunosum-moleculare*). Bottom: summary of rAAV labeling efficiency in layers of the dorsal hippocampal CA1 region in *Som-cre* mice injected with a mixture (3:1 ratio) of cre-dependent rAAV expressing PSAM^{L141F}-GlyR [(rAAV(PSAM^{L141F}-GlyR)^{Cre}] and tdTomato [(rAAV(tdTomato)^{Cre}]. PSAM Labeling efficiency: 84 ± 11 %, n =15. **g)** Top: bath application of 3 µM PSEM^{308} completely silences PSAM^{L141F}-GlyR+ interneurons to somatic current injection in *Som-cre* mice. Bottom: PSEM^{308} completely silences PSAM^{L141F}-GlyR+ interneurons to CA3-SCs photostimulation in *Som-cre* mice (n = 11 of 11 Som+ interneurons). **h)** Top: PSEM^{308} application has no effect on f-I curves of PSAM^{L141F}-GlyR-negative interneurons (n = 6) in *Som-cre* mice. Bottom: PSEM^{308} application has no effect on f-I curves of CA1 pyramidal neurons (n = 11) in *Som-cre* mice. **i)** Representative example of *Som-cre* labeling. 2-photon image stack of virally labeled interneurons in *Som-cre* mice [green; injected with rAAV(ChR2-sfGFP)^{Cre}] with respect to CA1 PC morphology (red; intracellularly filled with Alexa 594. **j)** Representative examples of reconstructions of the axonal and dendritic arborizations of Som+ interneurons. Top: interneuron with axonal arborization confined to the proximal dendritic layers of CA1. Bottom: interneuron with axonal arborization confined to the distal dendritic layer of CA1. Out of the five identified Som+ interneurons, three had axonal arborizations in proximal dendritic layers of CA1, and two were identified as OLM interneurons with axons confined to the *str. lacunosum-moleculare*

input currents in response to the same photostimulation grid to establish a common measure of synaptic input across cell types (**Fig 2.4**).

To silence a major subpopulation of dendrite-targeting interneurons in CA1, we generated knock-in mice expressing cre recombinase under the control of the somatostatin promoter (*Som-cre*; see Methods). In agreement with previous reports of Som+ interneurons in CA1 (Freund & Buzsáki, 1996; Losonczy et al., 2002; Klausberger et al., 2003; Klausberger & Somogyi, 2008), cre-positive interneurons in *Som-cre* mice had axonal arborizations in *strata oriens, radiatum,* and *lacunosum-moleculare* of the CA1 area, overlapping with the dendritic regions of PCs and excluding the perisomatic regions (**Fig 2.5a-e**). Viral expression of PSAM^{L141F}-GlyR in Som+ interneurons was

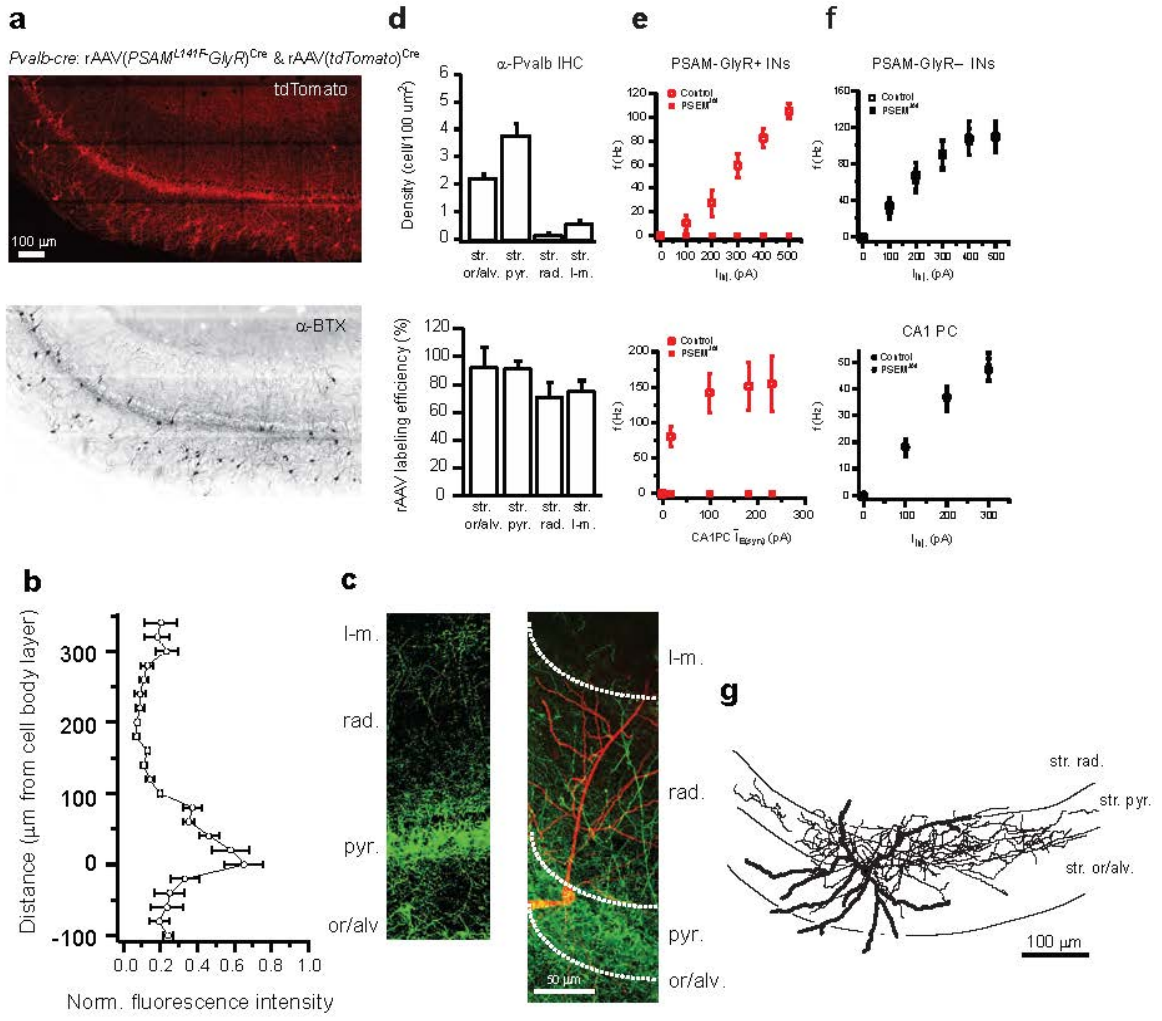

Figure 2.6 – Selective silencing of Pvalb+ interneurons in CA1 with cre-dependent expression of PSAM^{L141F}-GlyR, and application of its ligand PSEM^{308}. a) Co-localization of virally expressed tdTomato and α-BTX in sections of CA1 from *Pvalb-cre* mice injected with rAAV(PSAM^{L141F}-GlyR)^{Cre} and rAAV(tdTomato)^{Cre}. **b**) Summary plot of normalized fluorescence intensity as a function of distance from the cell body layer in (bins : 20 µm) in *Pvalb-cre* mice (n = 3) injected with rAAV(sfGFP)^{Cre} into CA1. **c)** Left: example confocal image stack from CA1 area from Pvalb-mice injected with rAAV(sfGFP)^{cre} into CA1. Right: 2-photon image stack of virally labeled interneurons in *Pvalb-cre* mice [green; injected with rAAV(ChR2-sfGFP)^{cre}] with respect to CA1 PC morphology (red; intracellularly filled with Alexa 594). **d)** Top: summary bar graph of the density of tdTomato labeled interneurons in the layers of CA1 area (n = 6; *str. or./alv.: strata oriens/alveus, str. pyr.: stratum pyramidale, str. rad.: stratum radiatum, str. l-m: stratum lacunosum-moleculare*). Bottom: summary of rAAV labeling efficiency in layers of the dorsal hippocampal CA1 region in *Pvalb-cre* mice injected with a mixture (3:1 ratio) of cre-dependent rAAV expressing PSAM^{L141F}-GlyR [(rAAV(PSAM^{L141F}-GlyR)^{Cre}] and tdTomato [(rAAV(tdTomato)^{Cre}]. PSAM labeling efficiency: 84 ± 9%, n = 15.

highly efficient, and we observed complete and selective silencing upon bath application of PSEM^{308} (**Fig 2.5g,h**), which included both Som+ bistratified cells and OLM cells (**Fig 2.5i,j**).

In separate experiments, we drove conditional expression of PSAM^{L141F}-GlyR in parvalbumin-expressing perisomatic-targeting interneurons of *Pvalb-cre* mice. These conditions permitted silencing of predominantly perisomatic inhibition using the same viral approach (Losonczy et al., 2010) while keeping dendritic inhibitory circuits intact (**Fig 2.6a-c**; see Experimental Procedures). Similar to the viral expression patterns we observed in *Som-cre* mice, we observed high expression of PSAM^{L141F}-GlyR in Pvalb+ interneurons (**Fig 2.6d**) and complete silencing upon application of PSEM^{308} (**Fig 2.6e-g**).

Silencing Som+ interneurons during phasic CA3-SC photostimulation caused a robust increase in the maximal firing rate of CA1 PCs (**Fig 2.7a,b**), revealing a marked divisive influence of dendritic inhibition on the gain of the CA1 PC i-o transformation (**Fig 2.8a,c,d**). These results demonstrate that removal of dendritic inhibitory input is sufficient to increase the firing rate of CA1 PCs in response to excitatory synaptic input. To test whether dendritic inhibition is necessary to effectively regulate CA1 PC firing rate, we repeated these experiments in *Pvalb-cre* mice to silence perisomatic inhibition

Figure 2.6 continued… **e)** Top: bath application of PSEM^{308} (3 μM) completely silences PSAM^{L141F}-GlyR+ interneurons to somatic current injection in *Pvalb-cre* mice. Bottom: PSEM^{308} (3 μM) completely silences PSAM^{L141F}-GlyR+ interneurons to CA3-SCs photostimulation in *Pvalb-cre* mice (n = 5 out of 5 interneurons). **f)** Top: PSEM^{308} application has no effect on f-I curves of PSAM^{L141F}-GlyR-negative interneurons (n = 10) in *Pvalb-cre* mice. Bottom: PSEM^{308} application has no effect on f-I curves of CA1 pyramidal neurons (n = 12) in *Pvalb-cre* mice. **g)** Example of reconstruction of the axonal and dendritic arborizations of a Pvalb+ interneuron showing axonal arborization confined to cell body layer of CA1. Two additional identified interneurons showed similar axonal arborization**.**

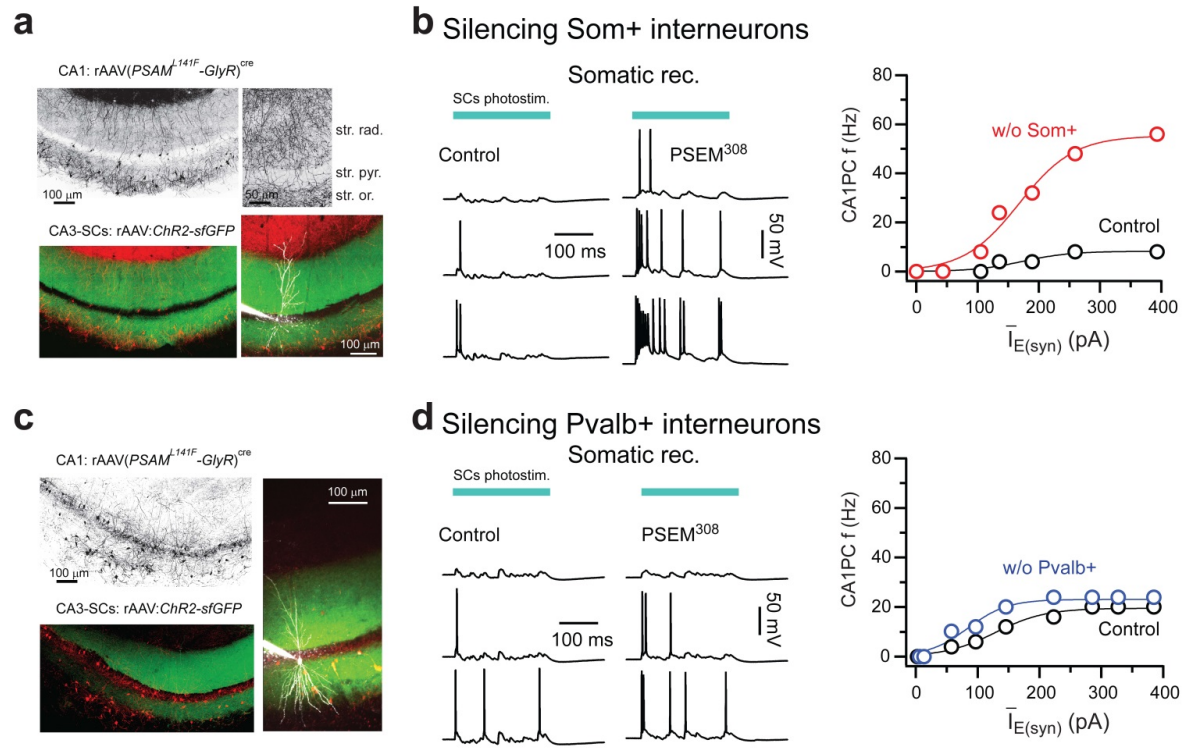

Figure 2.7 – Differential effects of silencing Som+ and Pvalb+ interneurons in CA1 PC i-o: example cells. a) Confocal image stacks of PSAM^{L141F}-GlyR/tdTomato + interneurons in a *Som-cre* mouse (pseudo-colored to black, low and high magnification), and overlay (native red tdTomato color) with ChR2-sfGFP expression in the CA3-SCs (green). 2-photon image stack of recorded CA1 PC in *Som-cre* mouse (bottom right). **b)** Current-clamp recordings from CA1 PC during CA3-SCs photostimulation, before and after silencing Som+ interneurons with PSEM^{308}, and i-o function for example CA1 PC. **c)** Confocal image stacks of PSAM^{L141F}-GlyR/tdTomato + interneurons in a *Pvalb-cre* mouse (pseudo-colored to black, low magnification), and overlay (native red tdTomato color) with ChR2-sfGFP expression in the CA3-SCs (green). 2-photon image stack of recorded CA1 PC in *Pvalb-cre* mouse (right). **d)** Current-clamp recordings from CA1 PC during CA3-SCs photostimulation, before and after silencing Pvalb+ interneurons with PSEM^{308}, and i-o function for example CA1 PC.

during synaptic excitation from CA3-SCs. However, this perturbation resulted in only a minor change in the CA1 PC firing rate (**Fig 2.7c,d** and **2.8b-d**). These results indicate that dendritic inhibition, but not perisomatic inhibition, effectively regulates the gain of CA1 PC i-o transformations.

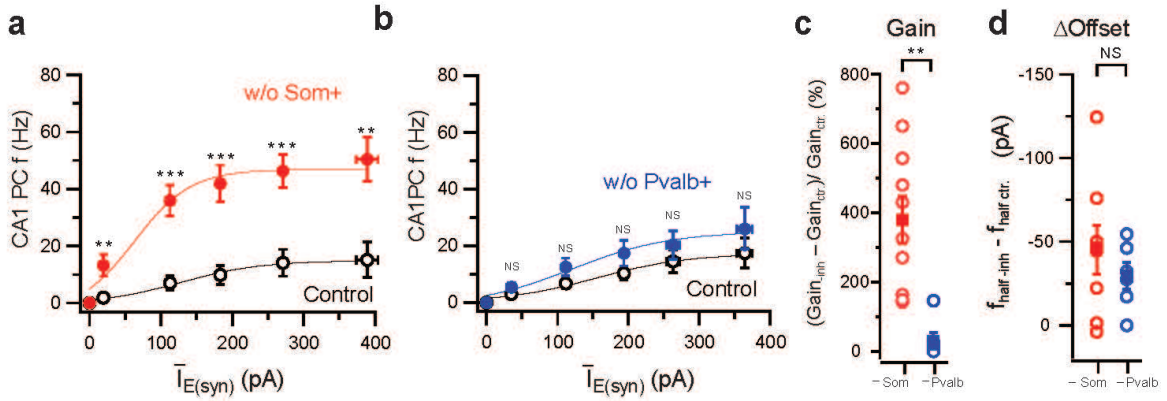

Figure 2.8 – Som+ interneurons, but not Pvalb+ interneurons, regulate the gain of the CA1 PC i-o transformation. a) I-o relationship for population of CA1 PCs before and after silencing Som+ interneurons – maximum firing rate from 15.2 ± 5 Hz to 50.4 ± 6 Hz, n = 12 cells, $p < 0.001$. **b)** I-o relationship for population of CA1 PCs before and after silencing Pvalb+ interneurons - maximum firing rate: from 17.2 ± 5 Hz to 26.2 ± 8 Hz, n = 12 cells, $p = 0.244$. **c)** Calculated gain change in CA1 PCs after silencing Som+ or Pvalb+ interneurons**.** *Som-cre*: Δgain/gain: 381 ± 57% n = 12; *Pvalb-cre*: Δgain/gain: 30 ± 23 %, n= 12 cells. **d)** Calculated offset change in CA1 PCs after silencing Som+ or Pvalb+ interneurons. *Som-cre*: Δoffset 45 ± 15 pA, n = 12 cells; *Pvalb-cre*: Δoffset: 29.6 ± 8 pA, n = 12 cells. Significance was tested with Student's t-test or ANOVA with Tukey's significance of difference test (HSD) for *post hoc;* $p < 0.05$ was considered as significant. All data are given in mean ± s.e.m. Symbols with error bars indicate mean ± s.e.m. **, p<0.01; ***, p<0.001; NS, p>0.05.

Som+ interneurons modulate CA1 PC i-o transformations: Local inhibition of dendritic spikes and bursting

The increase in CA1 PC firing rate upon silencing of Som+ dendrite-targeting interneurons was characterized by a switch to burst spiking output mode in response to CA3-SC input, reflected in a large increase in the duration of the initial slow depolarization underlying spikes measured at the soma (**Fig 2.9**). PCs also switched to burst-spiking output mode upon complete removal of inhibition from CA1 with $GABA_AR$

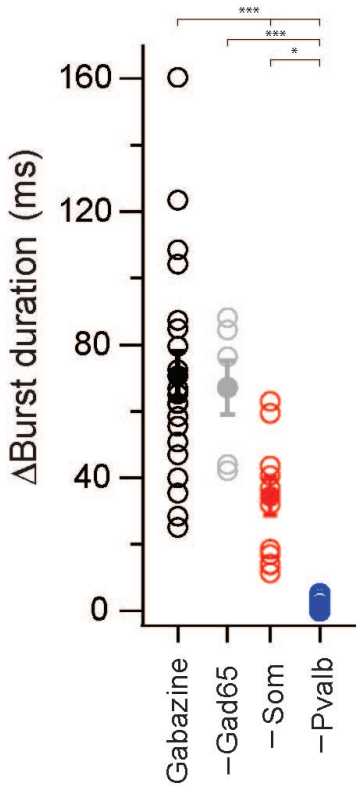

Figure 2.9 – Som+ interneurons, but not Pvalb+ interneurons, regulate CA1 PC burst spiking. Summary plot of calculated change in somatic burst duration from control conditions during CA3-SC photostimulation upon pharmacological blockade of inhibition (20 μM gabazine: 1080 ± 121 % of control, n = 22 cells, black), and pharmacogenetic silencing of Gad65+ interneurons (*Gad65-cre*: 886 ± 171 % of control, n = 6 cells, grey), Som+ interneurons (*Som-cre*: 508 ± 72 % of control, n = 12 cells, red), or Pvalb+ interneurons (*Pvalb-cre*: 120 ± 8% of control, n = 11 cells, blue) interneurons. Significance was tested with Student's t-test; symbols with error bars indicate mean ± s.e.m. *, p<0.05; ***, p<0.001.

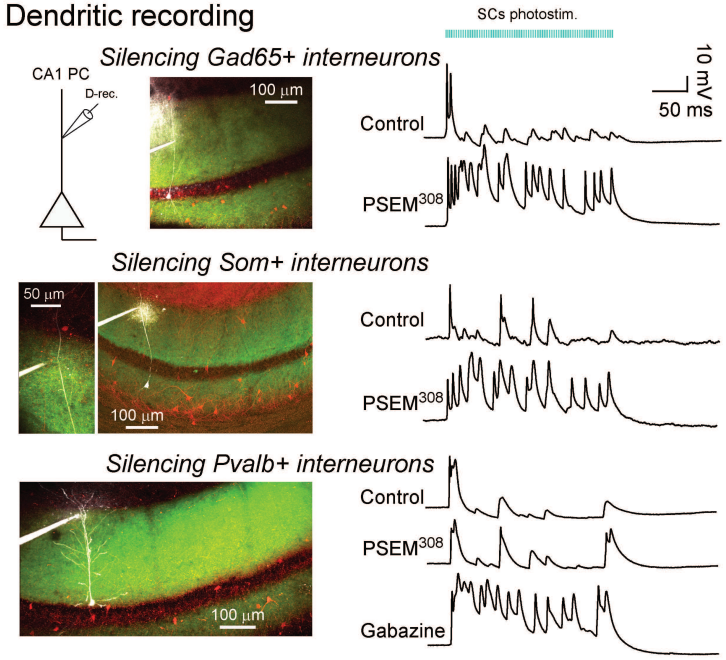

Figure 2.10 – Som+ interneurons, but not Pvalb+ interneurons, regulate CA1 PC dendritic electrogenesis. Schematic and 2-photon image stacks of patch-clamp recordings from the distal apical dendrites of CA1 PCs (left; CA1 PCs white, ChR2-sfGFP+ CA3-SCs green, PSAM^{L141F}-GlyR/tdTomato+ interneurons red) in *Gad65-Cre*, *Som-cre*, and *Pvalb-cre* mice. Current-clamp recordings from the distal apical dendrites in control conditions and upon pharmacogenetic silencing of Gad65+, Som+, or Pvalb+ interneurons during CA3-SC photostimulation (right). Note the prominent local spikes recorded from the dendrites of CA1 PCs upon silencing of Gad65+ and Som+ interneurons, but not upon silencing of Pvalb+ interneurons. Further pharmacological blockade of inhibition (20 μM gabazine) was required to induce dendritic spikes in these cells (bottom trace). *Gad65-cre*: n = 2 dendrites; *Som-cre*: n = 3 dendrites; *Pvalb-cre*: n = 3 dendrites.

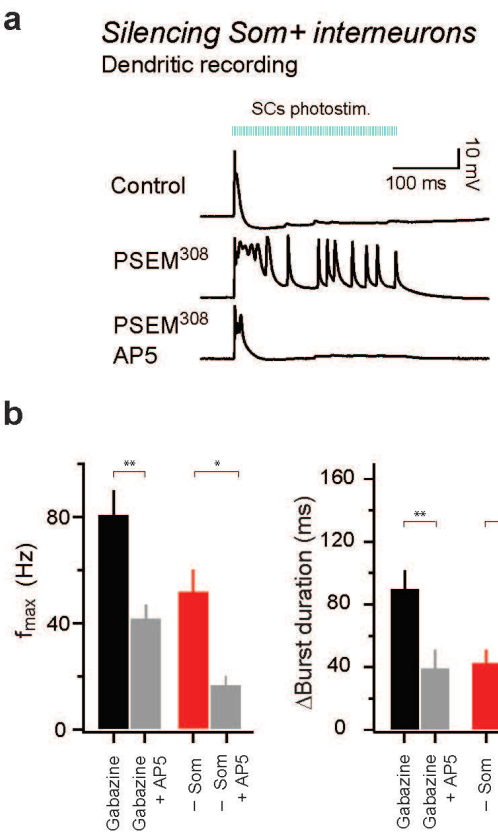

Figure 2.11 – Blockade of NMDA receptors rescues effects of silencing Som+ interneurons in CA1 PC dendritic spikes, firing rate, and burst spiking. **a)** Example intracellular recording from CA1 PC apical dendrite during CA3-SCs photostimulation in *Som-cre* mice, showing the effect of NMDAR blockade (100 μM D,L-AP5) on dendritic spiking induced by Som+ interneuron silencing. **b)** Summary plots of maximum firing rate and burst duration measured in CA1 PCs to CA3-SC photostimulation during pharmacological blockade of inhibition (20 μM gabazine, black) or pharmacogenetic silencing of Som+ interneurons (red), and after subsequent blockade of NMDARs with D,L-AP5 (grey). Gabazine: max. firing rate: from 81.3 ± 9 Hz to 42.1 ± 5 Hz, $p < 0.01$; somatic burst duration: from 1130 ± 120 % to 580 ± 110 %, $p < 0.01$, $n = 6$; Silencing Som+ interneurons: max. firing rate: from 52.2 ± 8 Hz to 17.2 ± 3 Hz, $p < 0.05$; $n = 3$, somatic burst duration: from 648 ± 72 % to 88 ± 9% of control, $p < 0.05$, $n = 3$. Student's t-tests; error bars indicate ± s.e.m.

block but, notably, not upon silencing Pvalb+ perisomatic-targeting interneurons (**Fig 2.9**). Since dendritic supralinearities contribute to somatic burst spiking (Larkum et al., 1999; Magee & Carruth, 1999; Takahashi & Magee, 2009), dendritic inhibition may regulate this switch to burst spiking by gating active dendritic electrogenesis. To test this possibility, we performed whole-cell recordings from distal parts of the main apical dendrites of CA1 PCs (**Fig 2.10**). Consistent with the proposed role for local inhibition in constraining dendritic spike generation (Miles et al., 1996; Larkum et al., 1999; Murayama et al., 2009), CA3-SC photostimulation evoked large amplitude dendritic spikes when dendrite targeting interneurons were silenced, but not when only perisomatic targeting interneurons were silenced (**Fig 2.10**). These

results indicate that a reduction in dendritic inhibition is required to allow dendritic electrogenesis, which switches the output mode of CA1 PCs to burst spiking.

Thin basal and apical oblique dendrites of CA1 PCs, which receive the majority of glutamatergic input from the CA3-SCs, primarily generate local Na^+/NMDAR-dependent spikes (Losonczy & Magee, 2006; Losonczy et al., 2008), whereas the distal apical trunk and dendritic tuft support global Ca^{2+}/NMDA plateau spikes (Miles et al., 1996; Golding et al., 1999; Dudman et al., 2007; Takahashi & Magee, 2009). Because Som+ neurons primarily inhibit thin dendrites (Buhl et al., 1994; Freund & Buzsáki, 1996; Klausberger et al., 2004; Klausberger & Somogyi, 2008), we reasoned that pharmacological blockade of NMDARs would reduce local dendritic electrogenesis and burst spiking observed upon silencing Som+ interneurons. Indeed, bath application of an NMDAR antagonist D,L-2-amino-5-phosphonovaleric acid (D,L-AP5, 100 μM) abolished dendritic electrogenesis (**Fig 2.11a**), somatic burst spiking, and the firing rate increase induced by silencing Som+ interneurons (**Fig 2.11b**). In contrast, when inhibition was completely removed from the entire somato-dendritic axis of CA1 PCs (20 μM gabazine), blockade of NMDARs only partially suppressed burst spiking (**Fig 2.11b**). These data indicate that Som+ dendrite-targeting interneurons primarily influence the transformation of CA3-SC input into spike output by inhibiting NMDAR-dependent branch-specific supralinearities in CA1 PC radial oblique and basal dendrites. A more pronounced suppression of inhibition allows for more global spiking, perhaps including Ca^{2+} electrogenesis in the apical trunk and tuft (Takahashi & Magee, 2009).

Because Som+ interneurons can be further separated into bistratified cells (which inhibit PC proximal dendrites receiving CA3 input) and OLM cells (which inhibit PC

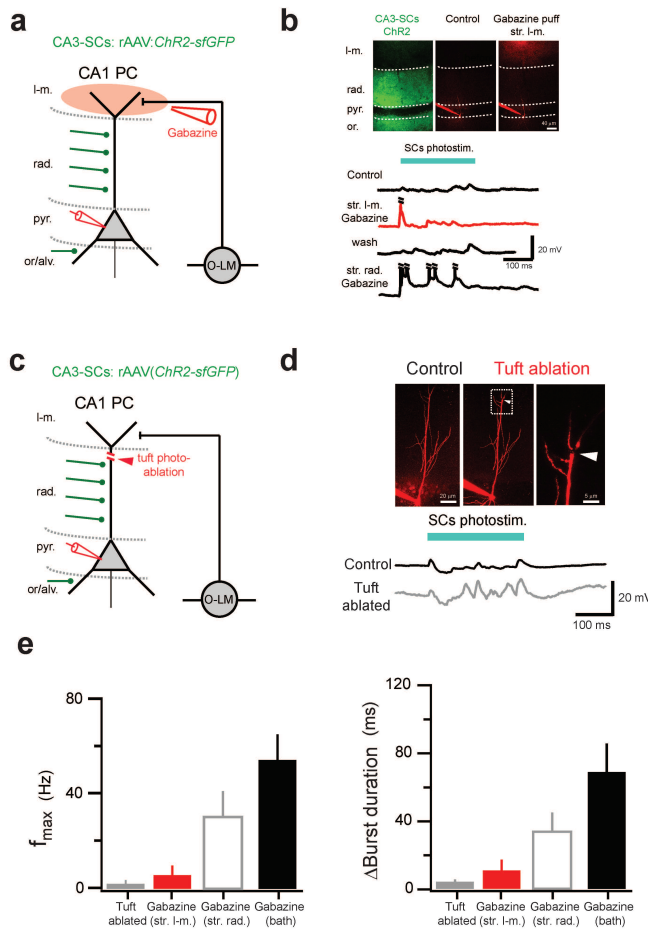

Figure 2.12 – Inhibition of CA1 PC distal tuft dendrites in *stratum lacunosum-moleculare* does not influence integration of CA3-SC input to proximal dendrites. **a)** Schematic of recording configuration, in which the responses of a CA1 PC are recorded to CA3-SCs photostimulation, with and without local gabazine puff (20 μM) applied to the distal dendritic tuft in *stratum lacunosum-moleculare* (focally blocking GABAergic input in the tuft). **b)** Top: single-plane 2-photon images of intracellularly recorded CA1 PC (red) before and after distal gabazine puff (red bolus; Alexa594 included in gabazine puff solution) and geometry with respect to the ChR2-sfGFP+ CA3-SCs (green). Bottom: responses of CA1 PC to CA3-SCs photostimulation in control conditions, (top, black), upon gabazine puff to *stratum lacunosum-moleculare* (middle, red), subsequent washout (middle, black), and upon gabazine puff to *stratum radiatum* (bottom, black). For focal application of 20 μM gabazine (with 50 μM Alexa 594), a puffer pipette (~2-5 μm tip diameter) was positioned above the tuft region. Duration of gabazine application (10-15 sec) was controlled by a Picospritzer. The spatial extent of the Alexa 594 signal was used the estimate the spread of gabazine application in the tissue. **c)** Schematic of recording configuration, in which the responses of a CA1 PC are recorded to CA3-SCs photostimulation, with and without the presence of an apical tuft. **d)** Top: 2-photon image stack of patch-clamped CA1 PC, before and after 2-photon photo-ablation of the distal tuft dendrites at the border of *strata radiatum* and *lacunosum-moleculare*, and expanded boxed inset (arrowhead denotes location of 2-photon ablation). Bottom: responses of CA1 PC to CA3-SCs photostimulation in control conditions (black) and upon ablation of the tuft (grey). Repeated two-photon line scans (200-300 lines, 820 nm, 20 mW) with slow pixel dwell times (40-60 μs/pixel) were used to photo-ablate apical distal apical trunk at the border of *str. radiatum* and *strata lacunosum-moleculare*. Successful photo-ablation produced an apparent gap on the distal dendrite and removed the prominent sag from voltage responses evoked by hyperpolarizing somatic current injections (data not shown). **e)** Left: population summary data showing maximum the maximum firing rate from control conditions after tuft ablation (n = 5), or puffing gabazine to *strata lacunosum-moleculare* (n = 4) or *radiatum* (n = 4), compared to bath application of gabazine (n = 8), which completely blocks inhibition in the slice. Right: summary graph of change in burst duration upon tuft ablation and upon local or bath application of gabazine.

distal dendrites receiving EC input), we devised experiments to assess the relative contribution of these inhibitory neurons to processing of the CA3-SC input we use in the experiments described above. While Som+ OLM cells send a dense projection to CA1 PC dendritic tufts in *stratum lacunosum-moleculare*, we found that distal inhibition of the dendritic tuft minimally affected responses to CA3-SC input. First, we found PCs did not substantially change their responses to CA3-SC input upon local $GABA_AR$ block in *stratum lacunosum-moleculare* (**Fig 2.12a,b**), induced by local puff application of 20μM gabazine to this layer. Conversely, similar puff application of gabazine to *stratum radiatum* induced burst spiking (**Fig 2.12b**). In agreement with this finding, we used 2-

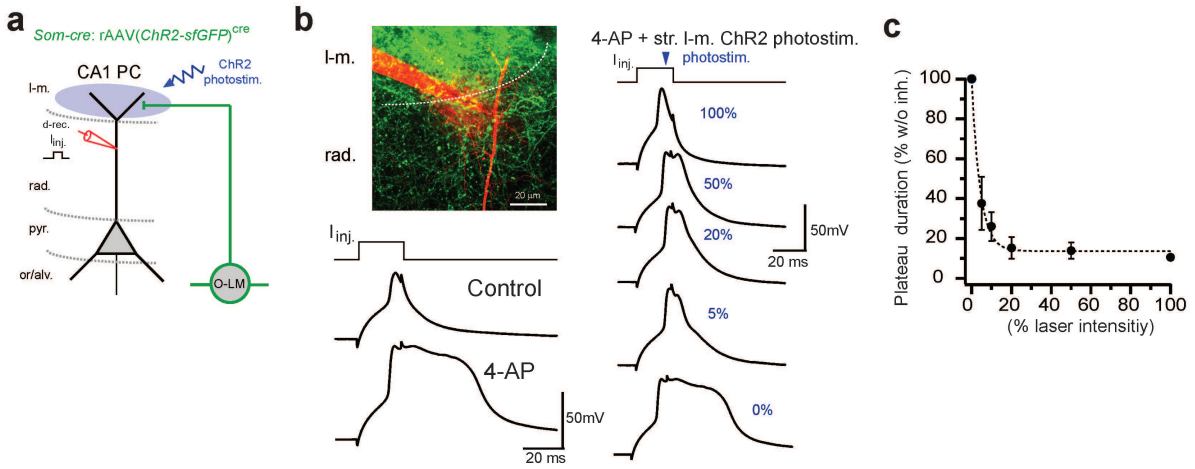

Figure 2.13 – Inhibition CA1 PC distal tuft dendrites in *stratum lacunosum-moleculare* powerfully regulates global dendritic plateaus. a) Schematic of recording configuration in which CA1 PCs are patched in the distal apical dendrite, and inhibition is delivered via focal photostimulation of ChR2+ axons from Som+ OLM cells, which synapse on distal apical tuft dendrites. **b)** Top left: high-magnification 2-photon image stack of intracellular recording from the distal apical dendrite of a CA1 PC (red) and ChR2-sfGFP+ axons from Som+ OLM cells (green). Recordings are performed in acute slices from *Som-cre* mice injected with $rAAV(ChR2\text{-}sfGFP)^{Cre}$ into dorsal CA1. Bottom left: V_m responses recorded from distal dendrite to brief current injection (+400pA, 20ms) in control conditions, and upon blockade of K^+ channels with bath application of 2mM 4-AP. Blockade of K^+ channels turn the dendritic response to current injection into a long-lasting dendritic plateau. Right: V_m responses to dendritic current injection in the presence of 4-AP, paired with ChR2-photostimulation of *strata lacunosum-moleculare* at various laser intensities (blue). **c)** Population summary data (n = 3 dendrites) showing the effect of distal OLM inhibition on the duration of dendritic plateau potentials evoked by dendritic current injection in the presence of 4-AP.

photon laser ablation to completely remove the dendritic tuft, and thus the OLM synapses to this compartment, and found minimal effects on PC processing of CA3-SC input (**Fig 2.12c,d**). Together, this data indicates that CA3-SC excitation of CA1 PCs is more effectively regulated by co-aligned inhibition (**Fig 2.12e**), which arises in part from Som+ bistratified cells.

Despite negligible impact on CA3-SC input processing, the dense inhibition of PC dendritic tufts is likely to serve an important role in input processing that engages this dendritic compartment (Miles et al., 1996; Larkum et al., 1999; Murayama et al., 2009). Because CA3-SC input does not engage this compartment, we excited CA1 PC dendritic tufts by direct current injection in the apical dendrite through a patch pipette during whole-cell current clamp recording (**Fig 2.13a**). To allow for large-scale dendritic plateau potentials (Takahashi & Magee, 2009), we blocked potassium (K^+) channels with bath application of 2mM 4-AP, allowing for propagation of current-injection-mediated depolarization throughout the tuft dendrites (**Fig 2.13b**). We conducted these experiments in slices from *Som-cre* mice injected with rAAV(*ChR2-sfGFP*)^{cre} into CA1. Under these conditions, focal optical activation of ChR2-expressing Som+ axons in *stratum lacunosum-moleculare* (corresponding to OLM cell axons) effectively blocked plateau potentials (**Fig 2.13b,c**). Therefore, although Som+ OLM cell axons in *lacunosum-moleculare* do not regulate CA3-SC input processing by CA1 PCs, these inhibitory inputs will play an important role in regulating PC dendritic tuft excitation via entorhinal cortex input and/or CA3-EC interactions in PC apical dendrites (Jarsky et al., 2005; Dudman et al., 2007; Takahashi & Magee, 2009).

Pvalb+ interneurons do not modulate CA1 PC i-o transformations: Cell type-specific disinhibition in CA1

We next sought to explain the mechanisms by which Pvalb+ interneurons failed to substantially regulate CA1 PC i-o gain and burst spiking. The inability of perisomatic inhibition to regulate PC output mode could not be explained by ineffective activation of Pvalb+ interneurons by the CA3-SCs, as these cells fired at high frequencies even to low levels of photostimulation (**Fig 2.4b**), and are effectively silenced using the PSAM-PSEM system (**Fig 2.6e**). Furthermore, CA1 PC firing rates did not further increase when Pvalb+ interneuron silencing was complemented with bath application of the CB_1 receptor agonist WIN-55,212-2 (1 μM), which reduces GABAergic release from a separate population of perisomatic-targeting interneurons that express cholecystokinin (Katona et al., 1999; **Fig 2.14**). Part of this minor effect could be explained by the location of these synapses on PCs, as somatic inhibition is not spatially aligned with the sources with the source of dendritic electrogenesis (Miles et al., 1996; Larkum et al., 1999).

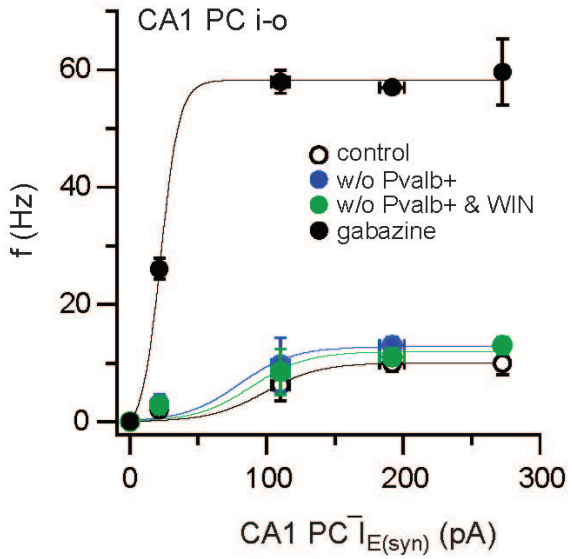

Figure 2.14 – Concurrent silencing of Pvalb+ interneurons and reduction GABA release from Cck+ interneurons via presynaptic endocannabinoids does not increase CA1 PC i-o gain. Summary plot of CA1 PC i-o relationships in control conditions, during silencing of Pvalb+ INs, and during subsequent application of the CB_1 receptor agonist WIN-55,212-2 (1 μM) in the presence of PSEM[308] (n = 7 cells).

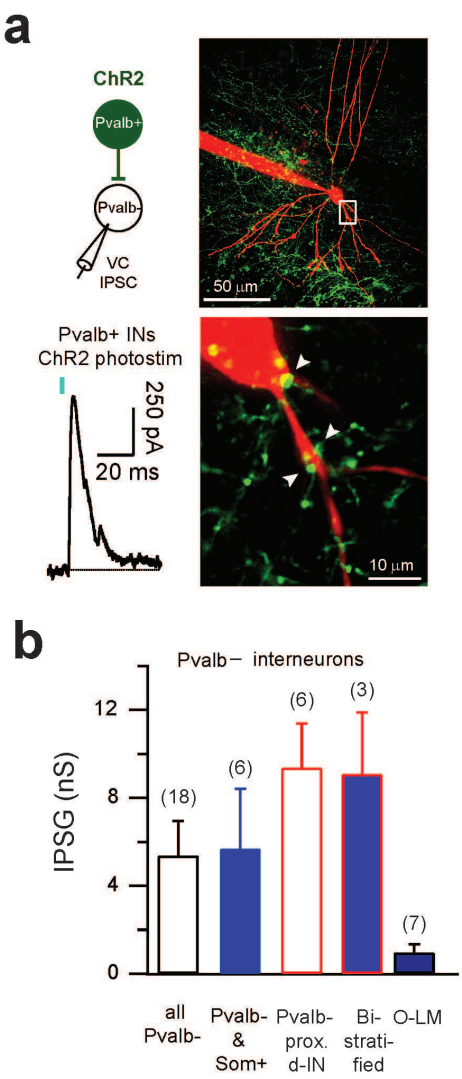

Figure 2.15 – Pvalb+ interneurons inhibit Som+ bistratified cells. **a)** Left: Schematic of recording configuration and example IPSC in Pvalb– interneuron to photostimulating Pvalb+ interneurons expressing ChR2 (bottom, VC at –40mV). Right: 2-photon stack of a Pvalb- interneuron (red) in *str. oriens* of CA1 in a slice expressing ChR2-sfGFP in Pvalb+ interneurons (right, green). Boxed region shows putative contacts (white arrowheads). **b)** Mean ChR2-photostimulation-evoked IPSG from Pvalb-negative cells in *Pvalb-cre* mice (n = 18 cells), subdivided as: all Pvalb– interneurons, Som+ cells (6 out of 10 Pvalb– interneurons tested for Som immunoreactivity), all proximal dendrite-targeting interneurons (prox. d-IN, axons in *strata oriens/radiatum*), bistratified cells (axonal identification + Som+ immunoreactivity - 9.07 ± 2.8 nS, n = 3 cells), and from OLM cells (0.94 ± 0.4 nS, n = 7 cells).

However, interconnectivity among inhibitory neurons in CA1 may play a role as well – a type of disinhibition that has been proven to contribute to circuit processing in neocortex (Letzkus et al., 2011).

We hypothesized that the minor influence of Pvalb+ interneurons on CA1 PC i-o transformations may reflect synaptic interactions between perisomatic and dendritic inhibitory circuits. We first tested this hypothesis by examining the connectivity between inhibitory interneurons using ChR2-mediated photostimulation. In slices from *Pvalb-cre* mice injected with rAAV(*ChR2-sfGFP*)^{Cre} into dorsal CA1, we photostimulated Pvalb+ perisomatic-targeting interneurons

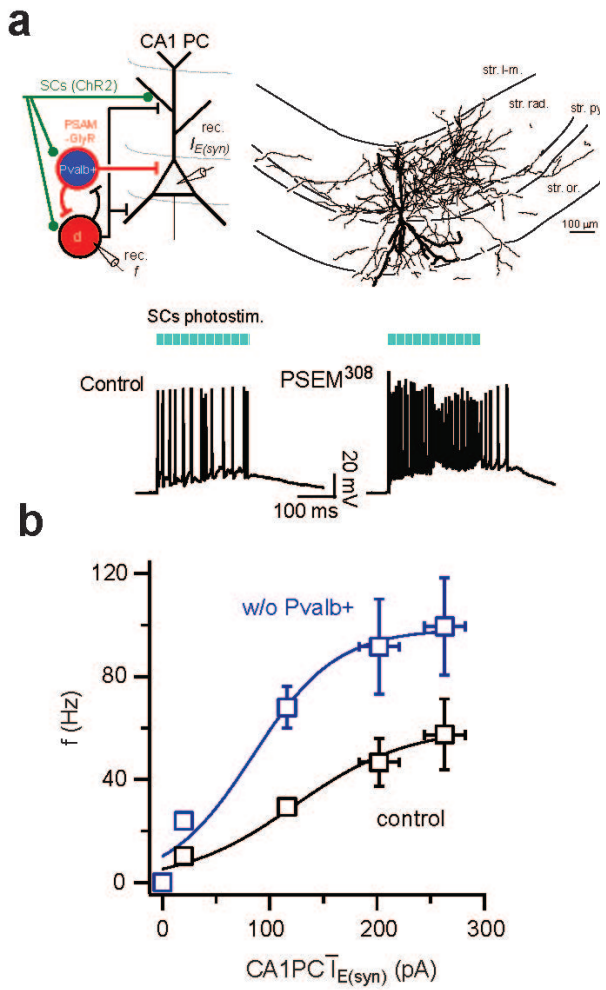

Figure 2.16 – Silencing Pvalb+ interneurons increases the activity of Som+ bistratified cells during CA3-SC input. a) Schematic and morphological reconstruction of a proximal dendrite-targeting Pvalb– interneuron (top, thin lines are axons). Current-clamp recordings from the reconstructed interneuron during CA3-SCs photostimulation in control and after silencing Pvalb+ interneurons (bottom). **b)** Summary of i-o relationship for proximal-dendrite-targeting interneurons before and after Pvalb+ silencing, n = 3 cells.

and recorded ChR2-evoked inhibitory postsynaptic responses in Pvalb-negative interneurons in *strata pyramidale* and *oriens/alveus* of CA1 (**Fig 2.15a**). Bistratified interneurons, identified by *post hoc* somatostatin immunoreactivity and axonal arborization confined to *strata oriens* and *radiatum* (Buhl et al., 1994; Maccaferri et al., 2000; Klausberger, 2009), received large-amplitude GABAergic input from Pvalb+ interneurons (Cobb et al., 1997). In contrast, OLM cells (Maccaferri et al., 2000), with somata located in *stratum oriens* and axons targeting the distal dendritic tuft of CA1 PCs in *stratum lacunosum-moleculare*, received small-amplitude inputs (**Fig 2.15b**). To test the relevance of this connectivity to CA1 circuit processing, we measured the i-o transformation of dendrite-targeting interneurons during CA3-SC photostimulation, before and after silencing Pvalb+

perisomatic interneurons. Indeed, the firing rates of bistratified cells markedly increased (**Fig 2.16**), and the firing rates of OLM cells were unchanged (**Fig 2.17d**).

Therefore OLM cells, which do not influence CA3-SCs input, are not regulated by Pvalb+ interneurons. Together, these results suggest that integration of CA3-SC input in thin basal and oblique dendrites of CA1 PCs is specifically regulated by co-aligned

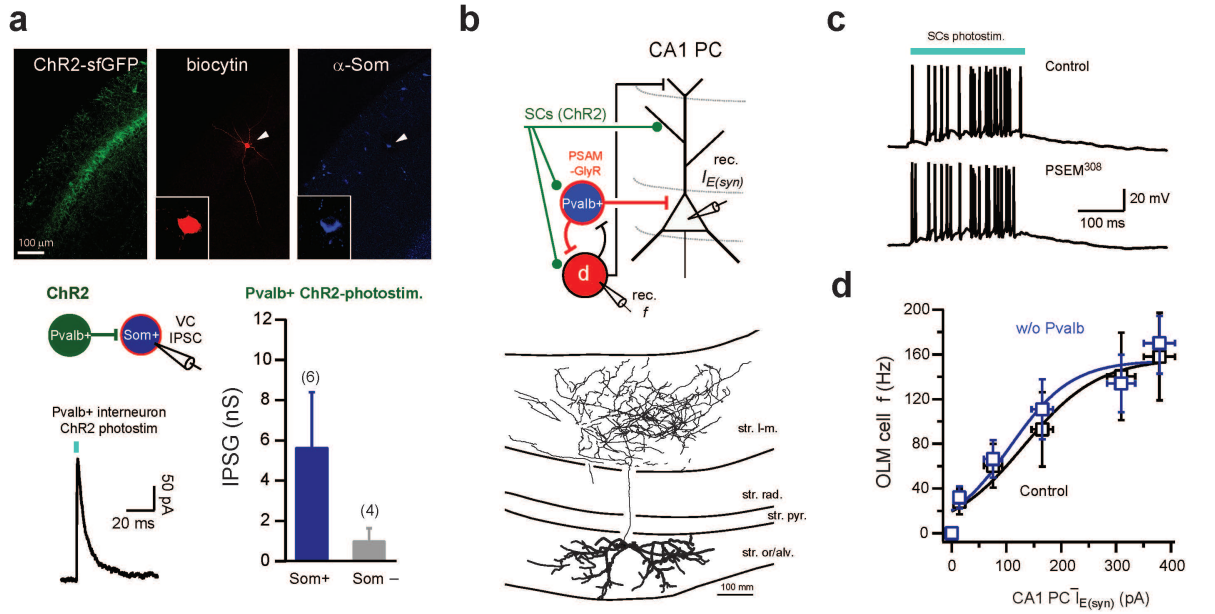

Figure 2.17 – Silencing Pvalb+ interneurons does not increase the activity of Som+ OLM cells during CA3-SC input. **a)** Top: Low magnification confocal image stacks of Som-immunopositive interneuron revealed by intracellularly-filled Alexa594 and Som immunofluorescence, blue pseudocolored) recorded from a CA1 slice with ChR2-sfGFP expression in Pvalb+ interneurons. Enlarged insets showing perinuclear somatostain immunoreactivtiy at image plane of the cell body. Middle: Schematic of recording configuration and voltage-clamp trace from Som+ interneuron receiving large amplitude IPSC upon ChR2 photostimulation of Pvalb+ axons (middle) Bottom: summary bar graphs of inhibitory postsynaptic conductances (IPSGs) recorded from all Som immunopositive (Som+, n = 6 out of n = 10 tested for Som-immunoreactivity, blue) and all Som immunonegative (Som-, n = 4 out of n = 10 tested for Som-immunoreactivity, grey) interneurons during photostimulation of Pvalb+ interneurons in *Pvalb-cre* mice injected with rAAV(ChR2-sfGFP)^{Cre}. **b)** Top: schematic of recording configuration (*d*: dendrite-targeting). Bottom: reconstruction of the axonal and dendritic arborizations of a recorded Pvalb- OLM interneuron showing axonal arborization confined to the distal dendritic layers of CA1. **c)** Representative voltage traces from an OLM interneuron to CA3-SCs photostimulation in control and after silencing Pvalb+ interneurons. **d)** Summary of i-o relationship for identified OLM cells before and after silencing Pvalb+ interneurons (n = 6 cells).

inhibition from Som+ bistratified cells, which are strongly inhibited by Pvalb+ perisomatic-targeting interneurons. We quantified the postsynaptic consequences of this disinhibition, using direct measurements of inhibitory conductance in PC soma and dendrites, by measuring the difference between input resistance at rest (no inhibition) and during CA3-SC input (inhibition active) (**Figs 2.18a**). As expected, we found a compartmentalized switch in GABAergic conductance - as silencing Pvalb+ perisomatic-targeting interneurons decreased somatic inhibitory conductance and increased dendritic inhibitory conductance during CA3-SC input (**Fig 2.18b**).

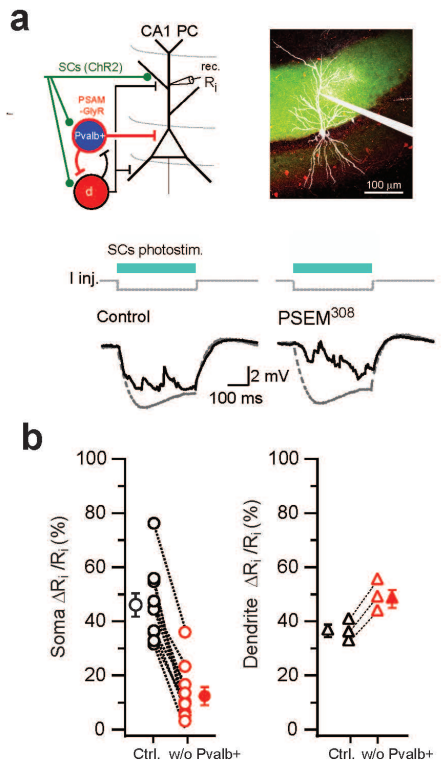

Figure 2.18 – Silencing Pvalb+ interneurons shifts inhibitory conductance from soma to dendrite during CA3-SC input. a) Schematic and 2-photon stack of dendritic recording from CA1 PC from *Pvalb-cre* mouse (top; CA1 PCs white, ChR2-sfGFP+ CA3-SCs green, $PSAM^{L141F}$-GlyR/tdTomato+ interneurons red). Example dendritic voltage traces of CA1 PC input resistance during CA3-SC input in control and after silencing Pvalb+ interneurons. **b)** Summary of changes to somatic and dendritic input resistance in control and after silencing Pvalb+ interneurons, reflecting changes in inhibitory synaptic conductance.

Finally, we found disinhibitory interactions in the opposite direction as well. Silencing of Som+ dendrite-targeting interneurons increased the firing rate of fast-spiking basket cells and decreased somatic input resistance in CA1 PCs (**Fig 2.19**). This result is most likely due to a combination of removing direct inhibition from Som+ interneurons (**Fig 2.19a**) and increasing feedback excitation from CA1 PCs that are spiking more under these conditions, as in **Figs 2.7** and **2.8**. However, this disinhibition of basket cells was

not able to compensate for PC burst firing upon removal of dendritic inhibition. Our results indicate that Pvalb+ interneurons inhibit interneurons targeting the proximal dendrites of CA1 PCs during CA3-SC input, the release of which can compensate for a withdrawal of perisomatic inhibition and amplify the asymmetric influences of perisomatic and dendritic inhibition on PC firing rates. This synaptic interaction between inhibitory circuit elements shapes excitatory synaptic integration by switching inhibitory conductance from one compartment of CA1 PCs to another – which may be a general mechanism for favoring some types of excitatory synaptic integration over others.

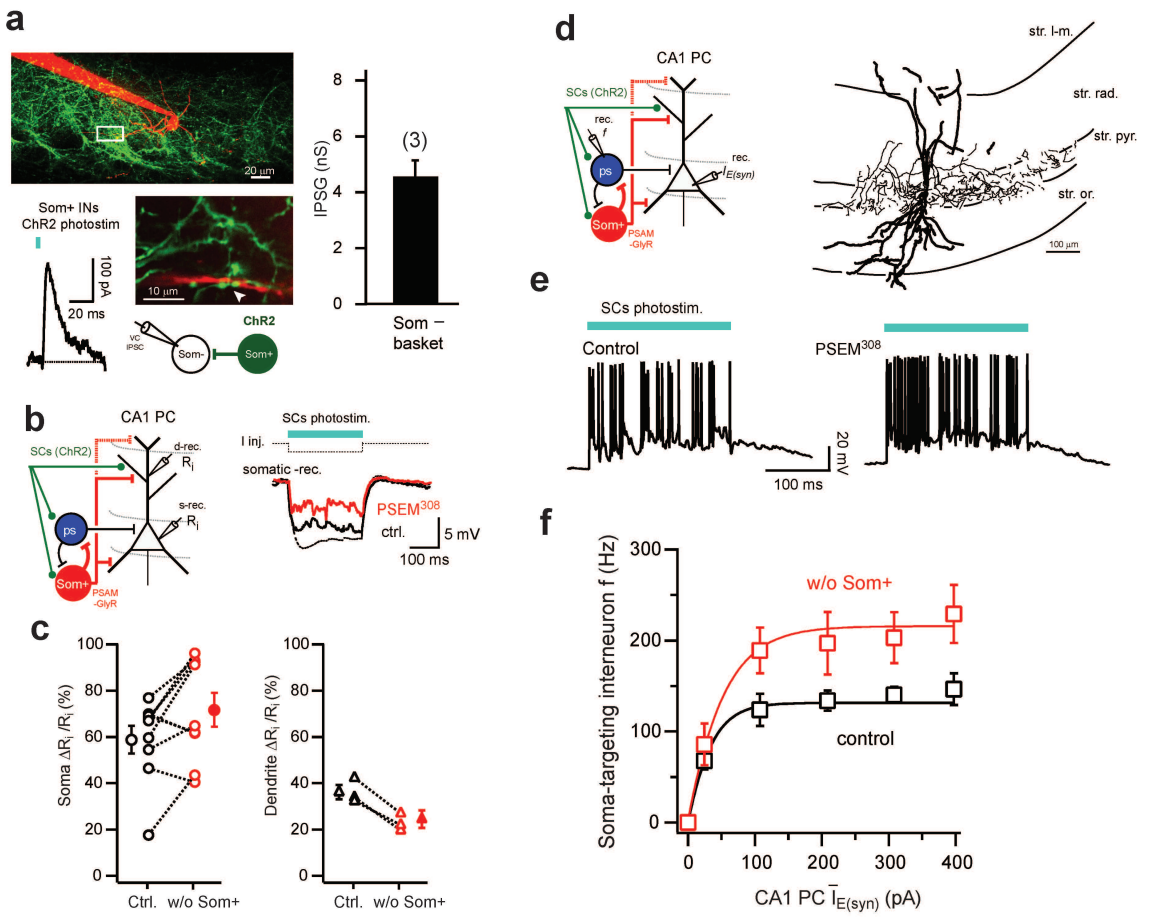

Figure 2.19 – Details of connectivity and disinhibitory effects of Som+ interneurons inhibition of Pvalb+ basket cells. **a)** Top: 2-photon image stack of intracellularly recorded Som-negative interneurons (Alexa 594, red) in CA1 slice expressing ChR2-sfGFP in Som+ interneurons (green), with boxed inset showing putative axo-dendritic contacts (arrowhead). Voltage-clamp recording shows ChR2 photostimulation-evoked IPSC recorded in Som- interneuron. Right: summary of mean conductance recorded from identified perisomatic-targeting INs (Som-, 4.58 ± 0.6 nS, n = 3 cells, black) during Som+ interneuron photostimulation in *Som-cre* mice injected with rAAV(ChR2-sfGFP)^{Cre} . **b)** Left: schematic of recording configuration (*ps*: perisomatic targeting). Right: example voltage traces from somatic whole-cell recordings from a CA1 PC in control and after silencing Som+ interneurons, showing an increase in perisomatic conductance. **c)** Summary of changes to somatic (left) and dendritic (right) input resistance induced by synaptic conductance in control and after silencing Som+ interneurons. **d)** Left: schematic of recording configuration. Right: reconstruction of the axonal and dendritic arborizations of the recorded Som- basket cell showing axonal arborization confined to the cell body layer of CA1. **e)** Representative voltage traces of recordings from a Som- basket cell during CA3-SC photostimulation in control and after silencing Pvalb+ interneurons. **f)** Summary of i-o relationship for of identified Som- perisomatic targeting interneurons before and after silencing Som+ interneurons (n = 5 cells).

Discussion

Dendritic inhibition regulates PC i-o gain by gating the dendritic source of burst spike generation

In summary, selectively silencing genetically-defined local inhibitory interneurons permitted us to identify dendritic inhibition as a key regulator of burst spiking in CA1 PCs. Dendritic inhibition was more effective than perisomatic inhibition at regulating excitatory synaptic integration, a difference that was amplified in active networks through interactions within the local inhibitory circuitry. From a computational perspective, our results suggest the role of dendritic inhibition is to primarily regulate the gain of PC i-o transformations during sustained excitatory input, which greatly expands the dynamic range over which cells can produce rate changes in the presence of active dendritic electrogenesis. We also show that the influence of dendritic inhibition on PCs can be tuned by the activity of perisomatic-targeting interneurons through asymmetric disinhibition. This organization may permit flexible and state-dependent extrinsic modulation over PC output through interneuron-specific targeting with long-range subcortical inputs (Freund & Antal, 1988; Mulligan & Tork, 1988; Toth et al., 1997; Varga et al., 2009).

Roles for other interneurons in PC gain control and bursting

We found that silencing of Som+ dendrite-targeting interneurons accounts for about half of the firing rate and burst duration change observed in PCs during complete removal of inhibition. This demonstrates the key role of Som+ bistratified interneurons in CA1 PC processing of CA3-SC input, but suggests that other interneuron classes

targeting dendrites in *strata oriens* and *radiatum* also contribute to regulating PC dendritic integration and electrogenesis. Indeed, the differential firing of bistratified (Klausberger et al., 2004), Schaffer-collateral associated (Cope et al., 2002), apical dendrite innervating, and Ivy cells (Fuentealba et al., 2008) during network oscillations *in vivo* suggest that these interneurons may regulate CA3-SC input integration in a state-dependent manner. Furthermore, other classes of dendrite-targeting interneurons that inhibit the distal tuft (eg. OLM, perforant path-associated, or neurogliaform cells; Klausberger & Somogyi, 2008; Klausberger, 2009) may contribute to regulating the interaction between CA3-SC input and input to the distal dendritic tuft from the EC during generation of global NMDAR/Ca^{2+} plateau spikes (Jarsky et al., 2005; Takahashi & Magee, 2009).

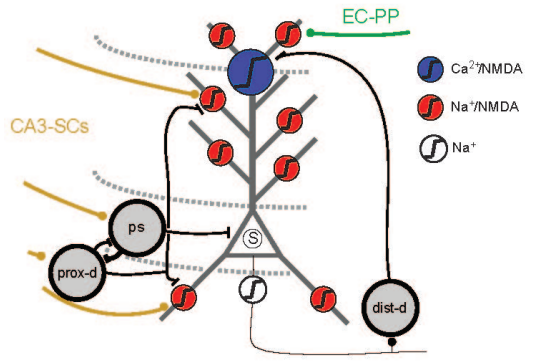

Figure 2.20 – Conceptual model of multicompartmental dendritic integration, and inhibition, in CA1 PCs. CA1 PCs can generate local Na+/NMDAR-mediated dendritic spikes in thin dendrites, in addition to global Ca^{2+} spikes in the apical trunk and tuft. Each of these integrative steps (thin dendritic spikes, global Ca^{2+} plateau spikes, and axonal output spikes) can be regulated by one or more inhibitory interneurons, which also inhibit one another.

Our findings support a multimodal synaptic integration scheme in hippocampal CA1 PCs, in which the initiation of local NMDAR-dependent spikes in radial oblique and basal dendrites, the predominant regenerative event in these thin branches (Losonczy & Magee, 2006; Losonczy 2008), is primarily regulated by co-aligned inhibition (**Fig 2.20**). A suppression of dendritic inhibition of thin dendrites allows for generation of local NMDAR spikes and somatic burst spiking, while a more complete

removal of dendritic inhibition allows the output of thin dendrites to also recruit the Ca^{2+} spike initiation zone, presumably located in distal apical trunk or in the tuft region, and to generate global Ca^{2+}/NMDAR plateaus (Miles et al., 1996; Jarsky et al., 2005; Dudman et al., 2007; Takahashi & Magee, 2009) that elicit longer lasting or higher frequency burst spiking. Thus our results suggest that the compartmentalized excitatory synaptic integration scheme proposed recently for neocortical layer V PCs (Larkum et al., 2009) may also apply to excitatory integration in hippocampal CA1 PCs. Our results further implicate a role for subcellular domain-specific inhibitory circuits within this compartmentalized integration scheme.

Potential behavioral consequences

While these experiments were performed *in vitro*, our findings are relevant to understanding CA1 PC activity *in vivo*. In the behaving animal, the relative amount of dendritic inhibition may determine the spike output of CA1 PCs in a particular environment during spatial navigation. For instance, most PCs could display the phenotype of a silent cell even under conditions of high excitation when accompanied by balanced levels of dendritic inhibition. A suppression of this inhibition could permit active dendritic integration in a subset of cells, resulting in place cell activity and sparse population coding in a given environment (Harvey et al., 2009; Epsztein et al., 2011). This is hypothesized to be a potential mechanism by which current injection into CA1 PCs can shift silent cells to active place cells (Lee et al., 2012a). Context-dependent modulation of dendritic inhibitory circuits could also allow relative changes in the firing rates of place cells to encode non-spatial variables via rate remapping (Colgin et al.,

2008). A diversity of dendrite-targeting interneurons could potentially serve to control different aspects of rate remapping in CA1, in which place fields and firing rates change to accommodate a variety of new sensory and contextual information introduced into the environment. Similarly, dendritic inhibition may contribute to shaping the selectivity of hippocampal encoding of memory in non-spatial tasks.

Complementary roles for dendritic and somatic inhibition of PC activity

Our results, demonstrating a role for dendrite-targeting interneurons in controlling CA1 PC firing rate and burst spiking, complement previous studies documenting the role of perisomatic-targeting interneurons in the control of spike timing and network oscillations (Cobb et al., 1995; Pouille & Scanziani, 2001; Losonczy et al., 2010). The distinctions between these inhibitory cell types adds functional implications to the wealth of anatomical and physiological data demonstrating the diversity of local GABAergic interneurons in the hippocampus (Freund & Buzsáki, 1996; Klausberger & Somogyi, 2008). Our data lends further evidence for a division of labor in cortical circuits, in which the tremendous heterogeneity of inhibitory interneurons has evolved to support diverse local circuit computations (Isaacson & Scanziani, 2011).

Corroboration of our findings *in vivo* and in neocortex

The basic conclusions from our data have been corroborated by several experiments since we published these results (Lovett-Barron et al., 2012; *published online January 15, 2012*). To investigate whether Pvalb+ and Som+ interneurons have dissociable functional roles with respect to the place cell activity in CA1 PCs, Royer and

colleagues (2012) recorded from CA1 PCs in head-fixed mice running on a cue-rich treadmill for rewards. This self-generated activity caused reliable place cell-like spiking patterns, where PCs spike at a particular location on the treadmill belt. The authors then used expression of the optogenetic silencer Halorhodopsin in CA1 Pvalb+ or Som+ interneurons to identify the expressing interneurons, as well as document the effects on simultaneously recorded PCs. Although suppression of both cell types resulted in increases in the firing rates of place cells, Pvalb+ interneurons exerted their effects at the beginning of a PC's place field, whereas Som+ interneurons exerted their effects at the end of its place field. Furthermore, the authors confirmed the dissociable roles for Pvalb+ and Som+ cells that we discovered in brain slices (Losonczy et al., 2010; Lovett-Barron et al., 2012), and demonstrated that suppressing Pvalb+ interneurons shifted the timing of PC spikes relative to the phase of the theta oscillations, whereas suppressing Som+ interneurons increased the number of spikes in a burst.

In primary somatosensory cortex, Gentet and colleagues (2012) recorded the activity of GABAergic interneurons during whisker stimulation in awake animals, using 2-photon guided patch-clamp recordings mice. This study focused on Som+ dendrite-targeting interneurons, and found that this cell type hyperpolarized during sensory stimulation with whisker deflection, whereas other inhibitory cell types and PCs did not. The authors hypothesized this selective reduction in dendritic inhibition provides a temporal window for dendritic electrogenesis and burst spiking output in layer II/III PCs. Gentet and colleagues (2012) tested this with optogenetic suppression of Som+ interneurons during quiet wakefulness, which caused bust spiking in PCs resembling the activity of these cells during active whisking. Furthermore, Palmer at al. (2012a)

found that dendrite-targeting interneuron in sensory neocortex exerted a ‘silent inhibition’ on layer V PC tuft dendrites in layer I (Palmer et al., 2012a; 2012b), which inhibited dendritic electrogenesis via postsynaptic $GABA_BRs$. This form of inhibition was not evident from spiking or somatic voltage recording due to its compartmentalization and electrotonic distance, but only exercised its effects on dendritic Ca^{2+} spikes during dendritic electrogenesis, when this conductance is activated.

Together, our results, and the subsequent findings of the other groups listed above, demonstrate that dendrite-targeting interneurons control dendritic spikes and output bursts in PCs. This is a powerful form of neuronal control that exists in many brain regions, and is widely applicable to the study of neural systems.

Experimental Procedures

All experiments were conducted in accordance with the National Institutes of Health guidelines and with the approval of the Columbia University Institutional Animal Care and Use Committee (to A. Losonczy).

Preparation of knock-in mice and viruses

Gad65-cre, *Pvalb-cre* and *Som-cre* knock-in mice were generated using homologous targeting constructs to insert an internal ribosome entry site (*IRES*) followed by the cre recombinase coding sequence into the 3′ UTR of the respective mouse genes. Constructs were electroporated into hybrid C57BL/6-129/SV stem cells, with colonies screened using PCR analysis for correct construct integration. Progeny carrying the transgene were bred to homozygosity. *Som-cre* and *Pvalb-cre* animals were maintained as a mixed strain. *Gad65-cre* mice were backcrossed repeatedly to C57BL/6 and maintained as a C57BL/6 strain. The *loxP-STOP-loxP-tdTomato* cre-reporter strain B6;129S6-*Gt(ROSA)26Sor*$^{tm9(CAG\text{-}tdTomato)Hze}$/J, (Jackson Laboratory) was bred with *Gad65-cre* animals to express tdTomato in the GABAergic cells of the double-hemizygous *Gad65-cre;tdTomato* progeny. For electrophysiology experiments, both homozygous and hemizygous (bred with C57BL/6) cre mice were used. No differences in the intrinsic properties of CA1 PCs or in the effect of PSAM^{L141F}-GlyR between homozygous and hemizygous mice were found, therefore the data were pooled. For anatomical characterization, homozygous or hemizygous *Gad65-cre* and hemizygous *Som-cre* and *Pvalb-cre mice* were used.

PSAM^{L141F}-GlyR was constructed from a mutated (L141F) alpha 7 nAChR ligand binding domain fused to the ion pore domain of the glycine receptor and was codon-optimized for the mouse. PSEM^{308} is a second-generation ligand for PSAM^{L141F}-GlyR that shows improved potency properties. The details of PSEM^{308} and its properties are described elsewhere.

To prepare cre-independent rAAV:*ChR2-sfGFP*, the codon-optimized coding sequence of *ChR2* (1-304, H134R) was joined to that of superfolder GFP (sfGFP) using the 10 amino acid linker EAGAVSGGVY, and cloned into a recombinant adeno-associated virus (rAAV) cassette containing the human *synapsin* promoter (*hSYN*), a woodchuck post-transcriptional regulatory element (*WPRE*), SV40 poly-adenylation sequence, and two inverted terminal repeats. To prepare cre-dependent rAAV(*ChR2-sfGFP*)^{Cre}, rAAV(*sfGFP*)^{Cre} and rAAV(*tdTomato*)^{Cre} and rAAV(*PSAM^{L141F}-GlyR*)^{Cre}, the respective coding sequences were cloned into the same vector in the inverted (with respect to promoter) orientation. Viruses were assembled using a modified helper-free system (Stratagene) as a serotypes 2/1 (*rep/cap* genes) for rAAV:*ChR2-sfGFP* and as serotype 2/7 for the cre-dependent constructs.

Viral injection

Viruses were stereotaxically injected into the dorsal hippocampi of adult mice using thin glass pipettes (10 μm tip diameter) and Nanoject II injectors (Drummond Scientific). Virus was injected into bilateral dorsal CA3 of (rAAV:*ChR2-sfGFP*; 6 penetrations, 2 injections per penetration) and dorsal CA1 [rAAV(*PSAM^{L141F}-GlyR*)^{Cre} and rAAV(*tdTomato*)^{Cre}, 3:1 ratio; 4 penetrations, 5–7 injections per penetration]. In

separate experiments rAAV(*ChR2-sfGFP*)^{Cre} was injected into dorsal CA1 (3 penetrations, 5 injections per penetration). Individual injections of ~30 nL high-titer virus were made in each pipette penetration along the z-axis of the tract as pipettes were withdrawn dorsally. Mice were returned to their home cage for 4–6 weeks before acute slice preparation.

Slice preparation and electrophysiology

Coronal slices (350 μm) were prepared in from the dorsal hippocampus of adult mice, as described previously (Losonczy & Magee, 2006). Slices were secured on mesh in a custom-made double-perfusion recording chamber, and perfused over both sides at 5–7 ml/min with ACSF maintained at 32–33 °C and containing (in mM): NaCl 125, $NaHCO_3$ 25, KCl 2.5, NaH_2PO_4 1.25, $MgCl_2$ 1, $CaCl_2$ 2, glucose 22.5, Na-pyruvate 3, ascorbate 1, and saturated with 95% O_2 and 5% CO_2. During most recordings, 500 nM CGP55845 (Tocris) was added to the ACSF. Slices were visualized with Dodt contrast optics using a Zeiss Examiner.Z1 with a 40x objective (NA 0.75) for somatic recordings and 63x objective (NA 1.0) for dendritic recordings (Zeiss). Neurons expressing sfGFP, tdTomato, or containing Alexa594/488 were imaged with a 2-photon scanning upright microscope (Prairie Technologies).

Whole-cell patch clamp recordings from somata or dendrites of CA1 pyramidal neurons or from somata of CA1 interneurons were obtained using a Dagan BVC-700A amplifier in the active "bridge" mode, filtered at 1–10 kHz and digitized at 50 kHz. Recording pipettes were pulled from borosilicate glass to tip resistances of ~4–7 MΩ for somatic recordings and ~8–10 MΩ for dendritic recordings and contained (in mM): K-

gluconate 130, KCl 8, NaCl 4, HEPES 10, Mg_2ATP 4, $Tris_2GTP$ 0.3, phosphocreatine 14, Alexa 594 or Alexa 488 0.1, pH 7.25. Biocytin (0.2%, Sigma) was included in the intracellular solution for recordings from interneurons. In current-clamp recordings, membrane potential was kept close to the $GABA_AR$ reversal measured in voltage-clamp (~ –65 mV).

Photostimulation of CA3 Schaffer Collaterals

For ChR2-photostimulation of the CA3-SCs, a blue DPSS laser (473 nm, CrystaLaser) was coupled to the uncaging path of the 2p scan-head with a 20x objective to access the extent of ChR2-sfGFP+ CA3-SC axons in *strata radiatum* and *oriens* of CA1. Photostimuli consisted of 1 ms pulses in the range of 10-200 μW directed at the specimen. Timing, position and intensity of the laser pulses were controlled using the laser's analog modulation circuitry (PrairieView-TriggerSync, Prairie Technologies). A 6x8-point grid of stimulation points was spread over the CA1 *strata radiatum/oriens*, away from the recorded cell and towards CA3 to avoid direct ChR2-depolarization of terminals. Each point in the photostimulation grid (1–48) was stimulated once, sequentially in a random spatial order, with an ISI of 4 ms for phasic photostimulation or 74 ms for recording individual EPSCs. After recordings under various conditions in current-clamp mode (4 ms ISI), 20 μM SR95531 was added to the extracellular solution to block $GABA_A$ receptors, CA1 PCs were voltage-camped, and grid-photostimulation was repeated with 74 ms ISI. This allows EPSCs from each photostimulation point to be independently measured and summed together to estimate a 'mean input current' for laser intensities used in current-clamp experiments. This was

repeated for all laser powers used throughout the experiment, and constituted the *x*-axis of suprathreshold input-output curves. After recording the firing rate of interneurons, the pipette was removed and a pyramidal cell was patched in the vicinity of the interneuron (< 50 μm) in order for mean currents to be measured with the same temporal order and spatial position of the grid as was used for the previously recorded interneuron. This gave a standard measure of synaptic input to compare the spike output from pyramidal cells and interneurons of different types across slices.

Under various conditions, CA1 PC firing rates saturated at high levels of input, possibly reflecting biophysical constraints. However the possibility cannot be excluded that, at high photostimulation levels, partial overlap of laser foci for individual points in the grid could desensitize ChR2 in CA3-SCs axons that are stimulated more than once. Any resulting reductions in input current during 4 ms ISI grid photostimulation would not have been fully detected when isolated EPSCs were measured due to the relative temporal isolation (74 ms ISI).

This spatially dispersed and temporally asynchronous activation of the CA3-SCs *in vitro* was designed to simulate the activity of CA3 ensembles during exploratory theta-states *in vivo*, in which individual CA3 PCs fire at low frequency and excite neurons in CA1 through high convergence (Ahmed & Mehta, 2009; Buzsáki, 2002). The mean rate of presynaptic CA3-SCs inputs during ChR2 photostimulation was estimated to range from ~0.2 up to 20 kHz, by averaging measured currents elicited from stimulating each individual photostimulation point in the 6x8 grid in isolation, dividing by this single-point average by the CA3-SCs unitary input measured at the soma (~10 pA;

Ahmed & Mehta, 2009), and multiplying by the number of stimulation points over the stimulation time.

Drug application

PSEM^{308} was dissolved in DMSO, stored in 100 mM aliquots, diluted in ACSF to a final concentration of 3 μM, and applied for 20–30 min for maximal effect. There was complete silencing of neurons expressing PSAM^{L141F}-GlyR without changing the excitability of interneurons not expressing PSAM^{L141F}-GlyR, or altering the intrinsic or input-output properties of pyramidal cells upon bath application of PSEM^{308} at this concentration (**Figs 2.3, 2.5,** and **2.6**). Other drugs used in our experiments include gabazine (20 μM, Tocris), D,L-2-amino-5-phosphonovaleric acid (D,L-AP5, 100 μM, Tocris), CGP55845A (500 nM, Tocris), 4-aminopyridine (4-AP, 2 mM, Sigma), and WIN-55,212-2 (1 μM, Tocris), which were dissolved in water or DMSO and diluted to final concentration in ACSF ([DMSO]< 0.005%).

Characterization of knock-in *Cre* mice

Adult heterozygous mice were deeply anesthetized with Isoflurane and transcardially perfused first with 0.1 M phosphate buffered saline (PBS, pH 7.4) and then with 4% paraformaldehyde. For light microscopic immunocytochemistry, sections (50 μm) were rinsed in PBS and pretreated with 1% H_2O_2 in PBS eliminate endogenous peroxidase activity. Nonspecific antibody binding sites were blocked and tissues were permeated with 2% normal goat serum (NGS) in PBS/0.3% Triton X-100. Sections was transferred into a 1:200,000 dilution of a monoclonal mouse antibody to cre

recombinase (Millipore; diluted with Triton X-100-free blocking reagent) for 48 hours at 4 °C. Immunoreactivity was detected after tissue incubations in anti-mouse biotinylated secondary antibodies (Jackson ImmunoResearch Laboratories; 1:1000), then in ABC-Elite reagent (Vector Laboratories, 1:1000 dilutions of solutions A and B in TBS), for 1 hour each. The peroxidase developer contained diaminobenzidine (DAB), nickelammonium-sulfate, and 0.002% H_2O_2 in TBS. Sections were mounted and cover slipped with DPX Mountant (Electron Microscopy Sciences).

For fluorescence immunocytochemistry, slices were incubated in 5% NGS, 0.1% Triton X-100 and one of the following primary antibodies: polyclonal rabbit anti-parvalbumin (α-PV, 1:300, Code, PV-28; Swant), monoclonal rat anti-somatostatin (α-SOM, 1:100, Millipore) or monoclonal anti-*Cre* recombinase (α-Cre, 1:1000, Millipore). After several washes, sections were incubated with secondary antibodies: Alexa Fluor(r) 633 conjugated donkey-α-rabbit (1:200), DyLight 649 conjugated goat-α-rat (1:500) or DyLight 488 conjugated goat-α-mouse (1:300, all from Jackson ImmunoResearch Laboratories). Confocal stack images (25–35 slices, 1 μm optical thickness) from the CA1 region of the hippocampus were acquired (40x objective) using a Leica DM6000 B confocal microscope. The numbers of fluorescent cell bodies were counted on maximum-projected stack confocal images.

Double-labeling for somatostatin and cre recombinase shown in **Fig 2.5c** was done as follows. First, sections were pretreated with 2% NGS in PBS/0.3% Triton X-100 followed by incubation in monoclonal rat antibody to somatostatin (1:100, Millipore) for 48 hours at 4 °C. Somatostatin immunoreactivity was detected with DyLight 649 conjugated goat α-rat IgG (1:500, Jackson ImmunoResearch Laboratories).

Immunolabeled sections were then incubated in mouse monoclonal α-cre recombinase antibody (1:1000, Millipore) then in DyLight 488 goat α-mouse secondary antibody.

Analysis of viral labeling efficiency

Following electrophysiological recordings, slices were processed for quantification of viral labeling efficiency. Slices were fixed in paraformaldehyde, washed, and re-sectioned (50 μm). Viral labeling efficiency was quantified as the ratio of the density of PSAM^{L141F}-GlyR-expressing interneurons in layers of CA1 and the total density interneurons in CA1 layers. For *Gad65-cre* mice, the total density of interneurons was determined in progeny of crosses of *Gad65-cre* with a cre-dependent tdTomato reporter strain (n = 15). For *Som-cre* and *Pvalb-cre* mice, the total densities were obtained from somatostatin (n = 8) and parvalbumin (n = 6) fluorescence immunocytochemical stainings, respectively. For immunocyochemical characterization, hemizygous (*C57BL/6;Som-cre* and *C57BL/6;Pvalb-cre*) mice were used.

The strong fluorescence signal in ChR2-sfGFP-expressing CA3-SCs masked the weak GFP fluorescence of PSAM^{L141F}-GlyR expressing interneurons. To visualize PSAM^{L141F}-GlyR+ interneurons during targeted electrophysiological recordings, mice were injected with rAAV(*PSAM^{L141F}-GlyR*)^{Cre} together (3:1 ratio) with rAAV(*tdTomato*)^{Cre}. The overlap of tdTomato+ cells and PSAM^{L141F}-GlyR+ cells was first quantified by performing a *post hoc* immunofluorescence procedure to directly detect the hybrid PSAM^{L141F}-GlyR using Alexa-647 conjugated α-bungarotoxin (α-BTX, 1:3000, Invitrogen), selective for the mutated α7-nAChR receptor binding site of PSAM. The α-BTX staining in PSAM^{L141F}-GlyR+ cells could be clearly separated from the weak

staining of endogenous α7-nAChRs in the hippocampus. Confocal stack images (25–35 slices, 1 μm optical thickness) were collected from the entire CA1 region, by stitching together multiple stacks made with a 40x objective. Stitched-together stacks covering all of CA1 were collapsed into one z-plane, and cell bodies labeled with tdTomato and/or α-BTX-Alexa647 were counted in each layer (ImageJ, US National Institutes of Health), allowing for quantification of the density and overlap of neuronal expression. We found high degree of overlap between tdTomato and α-BTX signal (percentage of α-BTX in tdTomato in all layers: *Gad65-cre* = 87 ± 3%, n = 16, **Fig 2.3c**; *Som-cre* = 98 ± 2%, n = 7; *Pvalb-cre* = 88 ± 6 %, n = 9) and therefore in subsequent experiments the expression of tdTomato was routinely used to estimate the density of $PSAM^{L141F}$-GlyR+ cells.

Digital images of α-bungarotoxin staining were pseudo-colored to either blue (**Fig 2.5d**) or black on a white background instead of its dark red native color on a black background (**Figs 2.3c, 2.5b** and **2.6a**). Similarly, digital images of tdTomato or GFP staining were sometimes pseudo-colored to black on a white background instead of its red native color on a black background (**Figs 2.2a, 2.6b,e** and **2.7a,c**).

Identification of intracellularly labeled interneurons

Slices containing biocytin-filled (0.2%) interneurons, were fixed, washed, cryo-protected, permealized and re-sectioned (50 μm). The endogenous peroxidase activity was then blocked, followed by permealization with TBS containing 0.3% Triton X-1000. Sections were then incubated in avidin-biotin complex in TBS (1:200; Elite ABC kit, Vector Labs), pre-incubated with 0.05% DAB in TB, and developed with added H_2O_2. Some recovered neurons were later reconstructed in Neurolucida (MBF Bioscience).

For somatostatin immunocytochemistry on biocytin-filled interneurons (n = 10; **Figs 2.15b** and **2.17a**), filled cells were visualized with Alexa 594-conjugated streptavidin (1:1000 or 1:3000, ImmunoResearch Laboratories) and somatostatin immunoreactivity was detected with monoclonal rat somatostatin (α-SOM, 1:100, Millipore) followed by DyLight 649 conjugated goat-α-rat (1:500). Following immunocytochemical evaluation, the sections were de-mounted and the recorded cells were labeled with avidin-biotin complex as described above.

Data analysis

Data was analyzed in Igor Pro 6.04 (Wavemetrics). To produce suprathreshold i-o curves, individual EPSCs recorded with a 74 ms ISI between each point of the photostimulation grid were first summed off-line with a 4 ms ISI and the mean amplitude of the summed current was measured. Firing rate was calculated based on the number of action potentials during the 250 ms of phasic photostimulation. Changes in gain for the subthreshold branch i-o and for suprathreshold i-o curves were calculated as [(control slope-experimental slope)/control slope] where slopes were determined from the peak of first derivative of the sigmoid fits to the data in a form: *base+max/1+(exp(xhalf–x))/rate*, where base is the baseline frequency, max is maximum frequency, and rate is the slope parameter. For i-o curves, input shifts (Δoffset) were determined from the xhalf of sigmoid functions. The relative input resistance (R_i) change in somatic and dendritic compartments (**Figs 2.18b** and **2.19b**) was calculated by comparing the mean level of hyperpolarization to a current injection (–100 pA) with responses to current injection paired with CA3-SCs photostimulation (< 100 pA mean input level, responses to synaptic input alone subtracted from paired

traces). Action potentials, if present, were removed by blanking the traces from 2 ms before the action potential's peak to 5 ms after the peak and the traces were subsequently linearly interpolated. Burst duration was calculated by filtering spikes from current-clamp recordings and calculating the full width at half-maximum depolarization across the first 100 ms of CA3-SCs photostimulation. Significance was tested with Student's t-test or ANOVA with Tukey's significance of difference test (HSD) for *post hoc;* $p < 0.05$ was considered as significant. All data are given in mean ± s.e.m. In all figures, symbols with error bars indicate mean ± s.e.m. *, $p<0.05$; **, $p<0.01$; ***, $p<0.001$; NS, $p>0.05$.

Experiments described in Chapter 2 have been published as:

Lovett-Barron M, Turi GT, Kaifosh P, Lee P, Bolze F, Sun X-H, Nicoud J-F, Zemelman BZ, Sternson SM, and Losonczy A (2012). Regulation of Neuronal Input Transformations by Tunable Dendritic Inhibition. *Nature Neuroscience,* **15**, 423-430.

Chapter 3 - Dendritic Inhibition in the Hippocampus Supports Contextual Fear Conditioning

Prelude

The results outlines in *Chapter 2* indicate a distinct functional role for Som+ dendrite-targeting interneurons in controlling burst spiking in CA1 PCs. This distinct role complements the known roles of Pvalb+ perisomatic-targeting interneurons, which have been identified as playing a critical role in controlling the spike timing of CA1 PCs (Cobb et al., 1995; Klausberger et al., 2003; Losonczy et al., 2010; Royer et al., 2012). Therefore each of these broadly defined interneuron types inhibits a particular compartment of the PC membrane surface, and thus has a unique effect on the pattern of PC spiking. It remains to be seen, however, whether these differences translate into unique behavioral functions for these interneurons, via control over the neural coding schemes that implement them. One challenge in addressing these concerns is to determine whether the distinct CA1 PC spiking regimes play critical roles in some behaviors, but not others (as reviewed in *Chapter 1*).

One example is the role of Pvalb+ interneurons in the control of spike timing, and the role of spike timing in spatial working memory tasks. The temporal precision of spike transmission from CA1 PCs to the mPFC (Siapas et al., 2005) has been suggested to be critical for spatial working memory in the rat (Jones & Wilson, 2005) and the mouse (Sigurdsson et al., 2010). To link these two hypotheses, Murray et al. (2011) found that destroying Pvalb+ interneurons in CA1 impaired the spatial working memory abilities of mice, while sparing spatial reference memory. Together, this suggests that Pvalb+ interneurons are required for spatial working memory because they organize CA1 PC spike timing relative to the extracellular theta rhythm (Losonczy et al., 2010; Royer et al., 2012).

In light of our findings that Som+ interneurons regulate CA1 PC burst spiking, we sought to determine whether these cells were analogously critical for behaviors that depend on CA1 PC burst spikes. As reviewed in *Chapter 1*, contextual fear conditioning (CFC) has been recently demonstrated to depend on the burst spiking output of the hippocampus (Xu et al., 2012b). This exciting finding motivated us to investigate the role of Som+ interneurons in CFC, in an effort to link cellular identity to neural spiking pattern to memory function in a well characterized hippocampal circuit.

Introduction

Aversive stimuli cause animals to associate their environmental context with these fearful experiences, allowing for adaptive defensive behaviors during future exposure to the context. This process of contextual fear conditioning (CFC) is dependent upon the brain performing two functions in series: first developing a unified representation of the multisensory environmental context (the conditioned stimulus, CS), then associating this CS with the aversive event (unconditioned stimulus, US) for memory storage (Fanselow, 1986; Fanselow, 1990; Maren, 2001; Rudy et al., 2004; Fanselow & Poulos, 2005). This is conceptually similar to cued fear conditioning, where the CS is a unimodal cue such as a tone or a light (**Fig 3.1**). Experiments in rodents have demonstrated that the context CS is encoded by the dorsal hippocampus, whose outputs are subsequently associated with the US through synaptic plasticity in the amygdala (Kim & Fanselow, 1992; Phillips & LeDoux, 1992; Young et al., 1994; Maren & Fanselow, 1995; Frankland et al., 2004). The hippocampus must incorporate multisensory features of the environment into a representation of context, but

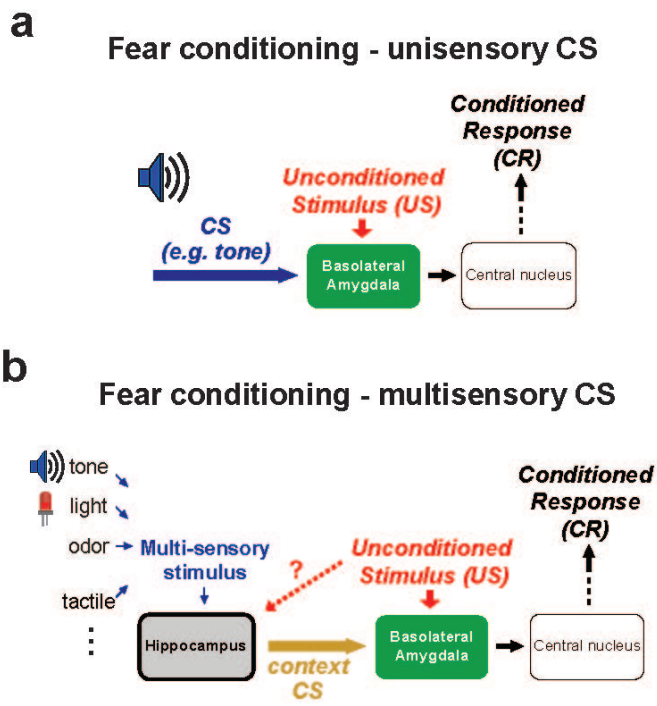

Figure 3.1 – Sensory processing during fear conditioning. **a)** Schematic of sensory processing in the case of fear conditioning to a unimodal CS, such as a tone. **b)** Schematic of sensory processing in the case of fear conditioning to a multimodal contextual CS, which requires the hippocampus to form a unified respresentation of the context from multiple sensory cues.

paradoxically must exclude sensory features during the moment of conditioning – when the primary sensory attribute is the US. The sensory features of the US may have a disruptive effect on learning (Fanselow et al., 1993). Although the cellular and circuit mechanisms of fear learning and sensory convergence have been extensively studied in the amygdala (LeDoux, 2000; Maren, 2001; Sah et al., 2003; Fanselow & Poulos, 2005), much less is known about the mechanisms by which the neural circuitry of the hippocampus contributes to fear conditioning.

The primary output neurons of the hippocampus, PCs in area CA1, are driven to spike by proximal dendritic excitation from CA3 and distal dendritic excitation from the entorhinal cortex (EC; Ahmed & Mehta, 2009). While CA3 is believed to store a unified representation of the multisensory context (Kesner, 2007), the EC is thought to convey information pertaining to the discrete sensory attributes of the context (Maren & Fanselow, 1997). At the cellular level, supralinear interactions between inputs from CA3 and EC in the dendrites of PCs can result in burst spiking output (Takahashi & Magee,

2009) and plasticity (Dudman et al., 2007). PCs can carry behaviorally relevant information in the timing of single spikes (Jones & Wilson, 2005), spike rate (Ahmed & Mehta, 2009), and spike bursts (Harris et al., 2001), but information conveyed with just bursts of spikes is sufficient for hippocampal encoding of the context CS during CFC (Xu et al., 2012b).

Distinct CA1 PC firing patterns are under the control of specialized local GABAergic inhibitory interneurons (Freund & Buzsáki, 1996; Klausberger & Somogyi, 2008). Whereas spike timing is regulated by Pvalb+ interneurons that inhibit the perisomatic region of PCs (Cobb et al., 1995; Losonczy et al., 2010; Royer et al., 2012), burst spiking is regulated by Som+ interneurons that inhibit PC dendrites (Lovett-Barron et al., 2012; Royer et al., 2012). This functional dissociation between cell types suggests that CA1 Som+ interneurons may play an important role in CFC. Despite distinct influences on PC spiking patterns, the activity of specific interneurons during CFC and their causal influence remain unknown.

To facilitate neural recording from multiple genetically and anatomically defined circuit elements in CA1 during CFC with 2-photon Ca^{2+} imaging, we developed a variation of CFC for head-fixed mice (hf-CFC). We combine functional imaging with cell-type specific inactivation techniques in head-fixed and freely-moving mice to show that Som+ interneurons in CA1 are required for CFC, and analyze the mechanisms and consequences of their activity during learning. Our results suggest a new conceptual framework for CFC that addresses the paradox of sensory convergence in the hippocampus, and demonstrates a novel role for dendritic inhibition in exclusion of aversive sensory stimuli from hippocampal contextual representations.

Results

A contextual fear conditioning paradigm for head-fixed mice

Conditioned fear in rodents is typically measured in terms of freezing upon re-exposure to the context where the subject experienced an aversive stimulus, usually a foot-shock (LeDoux, 2000; Maren, 2001; Fanselow & Poulos, 2005). However, using freezing as a conditioned response is problematic in head-fixed mice. To overcome this limitation we measured learned fear using conditioned suppression of water licking (Mahoney & Ayres, 1976; Bouton & Bolles, 1980), an established measure of fear that translates well to head-fixed preparations. We first habituated water-restricted mice to head restraint with an implanted head-post; mice could freely walk on a treadmill and lick a port for small water rewards (~0.5 µL/lick). The hf-CFC paradigm consisted of three consecutive days where we presented mice with two different multisensory contexts for three minutes each. Each context CS consisted of a distinct set of auditory, visual, olfactory, and tactile cues that we presented to mice using a microcontroller-driven stimulus presentation and behavioral recording system (**Fig 3.2a**; Kaifosh et al., 2013). On the first day (Habituation), mice licked for water at similar frequencies in both contexts. On the second day (Conditioning) we presented mice with both contexts again, but paired one context (CtxC) with a US: six air-puffs to the snout (200 ms, 0.1Hz) during the final minute of the context. The other context was neutral and not paired with a US (CtxN). On the third day (Recall), we exposed mice to the conditioned context (CtxC) and the neutral context (CtxN) again, and assessed the rate of licking in each context. We found that US pairing caused a decrease in the rate of licking in CtxC, but not CtxN (**Fig 3.2b,c**). These results indicate that mice can be robustly and

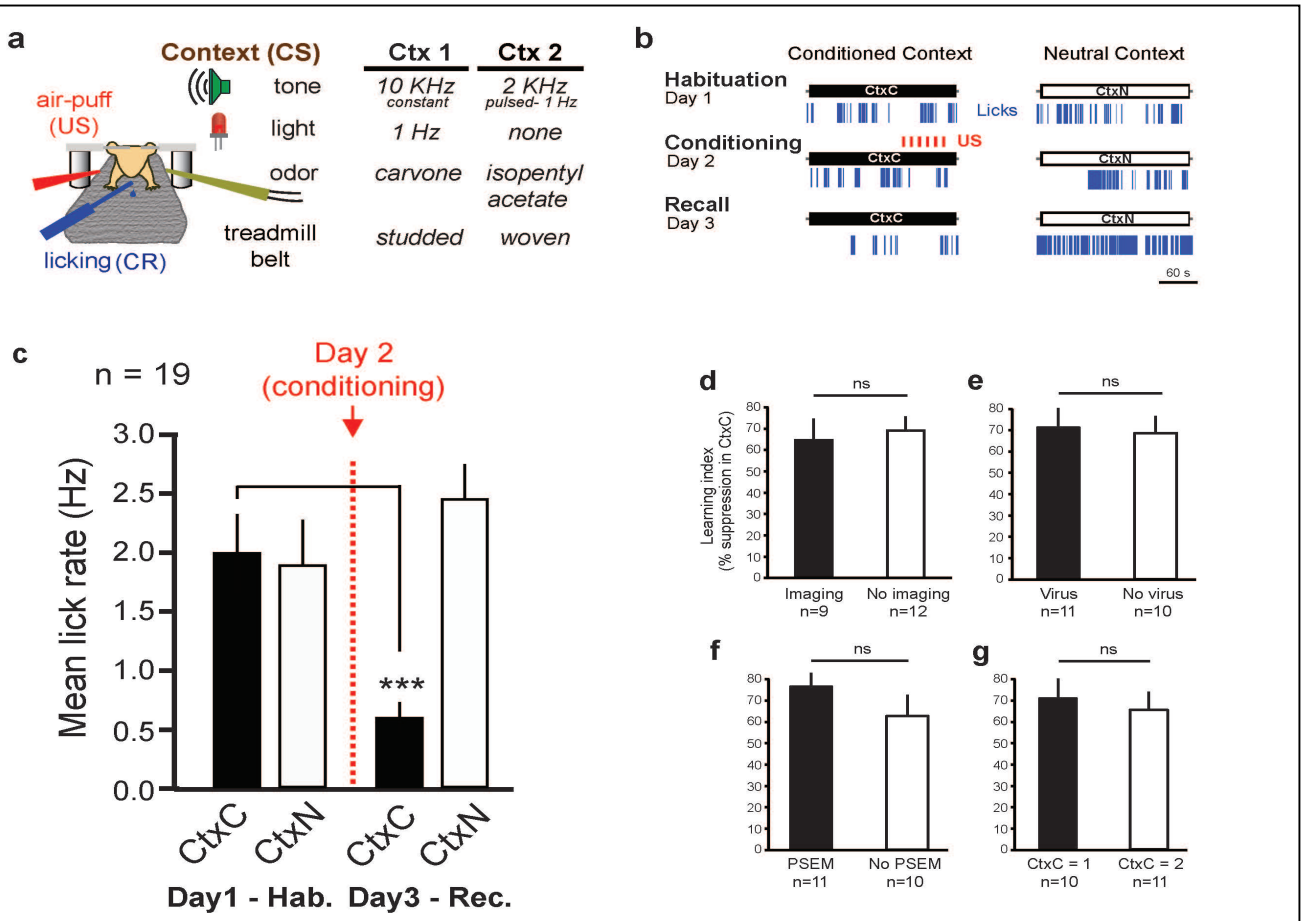

Figure 3.2 – Contextual fear conditioning for head-fixed mice (hf-CFC). a) Schematic of hf-CFC task. A head-fixed mouse on a treadmill is exposed to contexts (conditioned stimuli, CS) defined by distinct sets of multisensory stimuli. We used air-puffs as the unconditioned stimulus (US), and suppression of water-licking as a measure of learned fear (conditioned response, CR). The two distinct contexts used in this study are described at right. **b)** Behavioral data from an example mouse over the 3 day hf-CFC paradigm. Conditioned (CtxC) and neutral contexts (CtxN) are each presented once a day, and licking is assessed during the 3 minute context. **c)** Summary data for 19 mice (2-way ANOVA, context x session, $F_{(1,19)} = 9.34$, $p < 0.01$). Mice showed a selective decrease in mean lick rate between Habituation and Recall in CtxC, but not CtxN (paired sign tests). **d)-g)** Control experiments for the hf-CFC task – of mice that received no experimental manipulation, some received surgical or behavioral treatments whereas others did not. None of these treatments altered hf-CFC performance. **d)** Implant and imaging control: 'Imaging' group (n = 9) – mice express GCaMP, have a hippocampal window implanted, and have CA1 imaged with a 2-photon microscope during hf-CFC. 'No imaging' group (n = 12) – mice are implanted with a headpost alone with no window surgery or imaging. Unpaired t-test: p = 0.705. **e)** Viral expression control: 'Virus' group (n = 11) – mice have received stereotaxic injections of a virus to express tdTomato, GFP, or GCaMP. 'No virus' group (n = 10) – mice received no viral injection. Unpaired t-test: p = 0.828. **f)** PSEM injection control: 'PSEM' group (n=11) – mice were injected with 60 mg/kg PSEM[89] in saline i.p 15 min before conditioning in CtxC session. These mice were used as the control group in Figure 1e. 'No PSEM' group (n=10) – mice received no PSEM[89] injection. Unpaired t-test: p = 0.252. **g)** Context identity control: 'CtxC = 1' group (n = 10) – mice were conditioned to Context 1 (CtxC), and Context 2 was neutral (CtxN). 'CtxC = 2' group (n = 11) – mice were conditioned to Context 2 (CtxC), and Context 1 was neutral (CtxN). Unpaired t-test: p = 0.652.

reliably conditioned to fear a particular multisensory context, but not another, even though both are presented while the mouse is head-fixed in the same true physical location (**Fig 3.2d-g**).

We used pharmacogenetic neuronal inactivation to test the necessity of the hippocampus and amygdala for the encoding of hf-CFC. We targeted bilateral injections of rAAV(*Synapsin-PSAM^{L141F}-GlyR*) to express the ligand-gated Cl^- channel PSAM^{L141F}-GlyR in either dorsal hippocampal area CA1 or the amygdala in wild-type mice (**Fig**

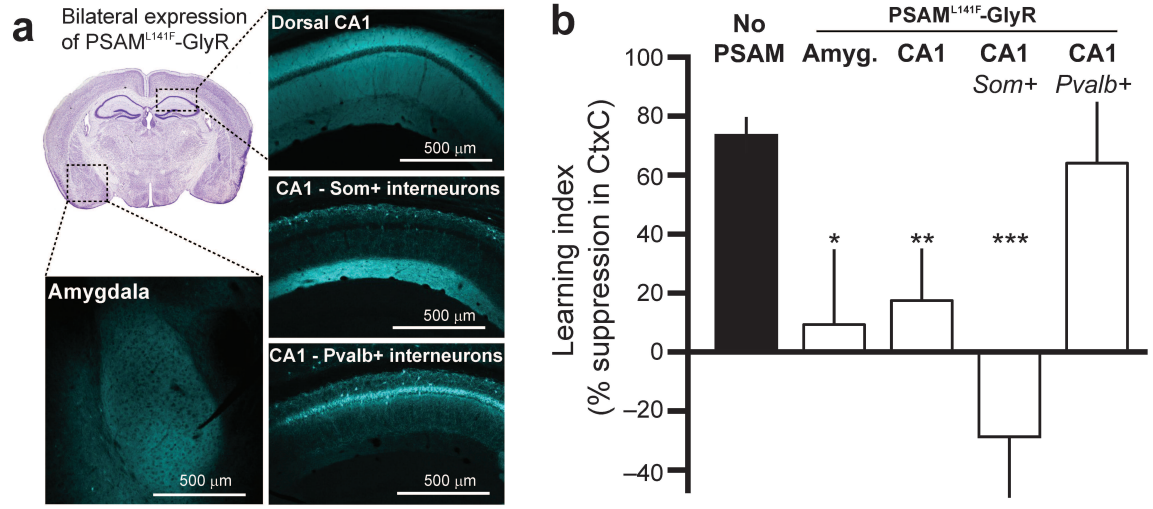

Figure 3.3 – Cell types required for learning hf-CFC. **a)** Viral expression of the ligand-gated Cl^- channel PSAM^{L141F}-GlyR in the amygdala or dorsal CA1, revealed by α-bungarotoxin-Alexa647 immunostaining. PSAM^{L141F}-GlyR+ neurons are inactivated upon systemic application of its ligand, PSEM^{89}. Cells were labeled by injection of cre-independent rAAV2/1(*Synapsin-PSAM^{L141F}-GlyR*) virus in wild-type C57/Bl6 mice ('amygdala' and 'CA1' conditions), or expression was targeted to specific interneuron types by injection of cre-dependent rAAV2/7(*Synapsin-PSAM^{L141F}-GlyR*)^{cre} virus in *Som-cre* or *Pvalb-cre* mice. All injections were bilateral; for simplicity only one hemisphere is shown. Image at top left is from the Allen Brain Atlas. **b)** Summary data for mice injected with PSEM^{89} systemically 15 min before the conditioning session in CtxC (day 2 of hf-CFC paradigm). Learning is assesed by the % lick rate decrease in the CtxC recall session (day 3) relative to the mean lick rate in all sessions. Mice expressing PSAM^{L141F}-GlyR in amygdala cells (*Amyg.*, n = 6 mice), dorsal CA1 cells (*CA1*, n = 5 mice), or CA1 Som+ interneurons (*CA1-Som+*, n = 8 mice) showed impaired learning compared to mice not expressing PSAM^{L141F}-GlyR (*No PSAM*, n = 11 mice), whereas mice expressing PSAM^{L141F}-GlyR in CA1 Pvalb+ interneurons (*CA1-Pvalb+*, n = 4 mice) did not. Comparisons are Mann-Whitney U tests. Bars represent mean ± s.e.m. *p < 0.05, **p < 0.01, ***p < 0.001

3.3a). Neurons expressing PSAM^{L141F}-GlyR are inactivated for ~15-20 minutes upon systemic administration of its ligand PSEM^{89} (60mg/kg i.p.; Magnus et al., 2011). We administered PSEM^{89} to mice before conditioning in CtxC, and tested their memory 24 hours later without the drug by assessing lick suppression in CtxC recall compared to mean licking across all sessions. In agreement with regional inactivation and lesion experiments during conventional freely-moving CFC (Kim & Fanselow, 1992; Phillips & LeDoux, 1992; Anagnostaras et al., 2001; Goshen et al., 2011), we found that inactivating neurons in dorsal CA1 or the amygdala prevented contextual fear learning (**Fig 3.3b**).

Som+ interneurons are required for CFC

To determine the relevance of CA1 inhibitory circuits for the acquisition of hf-CFC, we asked whether acute inactivation of GABAergic interneuron subclasses in CA1 would alter learning. We injected rAAV(*Synapsin-PSAM^{L141F}-GlyR*)^{cre} bilaterally into CA1 of *Som-cre* or *Pvalb-cre* mice to express PSAM^{L141F}-GlyR selectively in either Som+ dendrite-targeting interneurons or Pvalb+ perisomatic-targeting interneurons, respectively (Lovett-Barron et al., 2012; Royer et al., 2012) (**Figs 3.3a**), covering the extent of dorsal CA1 (**Fig 3.4**). Systemic PSEM^{89} administration during conditioning prevented learning in mice expressing PSAM^{L141F}-GlyR in CA1 Som+ interneurons, but not in mice expressing PSAM^{L141F}-GlyR in CA1 Pvalb+ interneurons (**Fig 3.3b**).

To confirm the validity of these results, we repeated our inactivation experiments in conventional CFC experiments with freely-moving mice, with a foot-shock US and freezing as the conditioned response. Again, we found that inactivating CA1 Som+

interneurons during conditioning prevented recall 24 hours later without the drug, while inactivating Pvalb+ interneurons had no effect (**Fig 3.5a,b**). Inactivating Som+

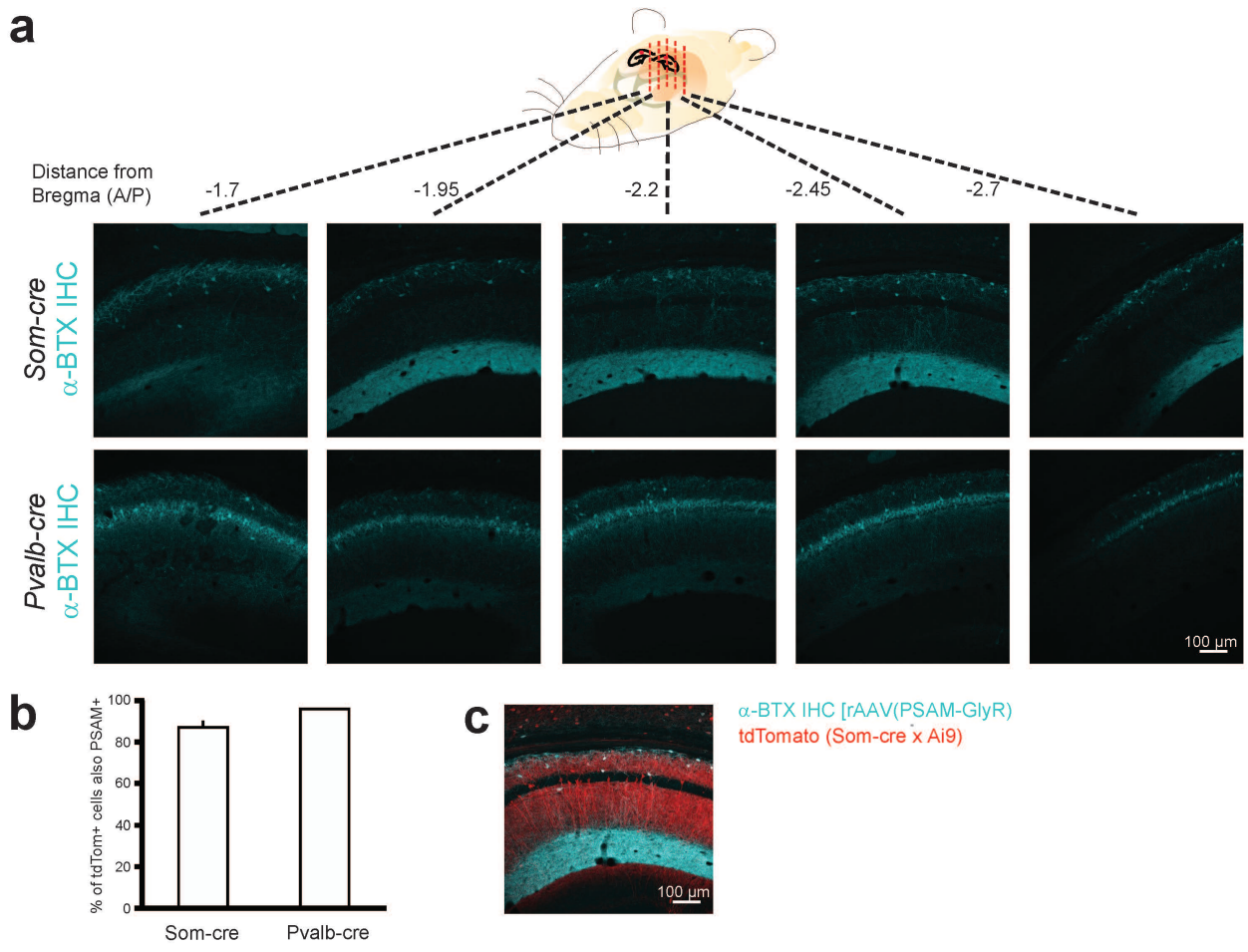

Figure 3.4 – PSAM^{L141F}-GlyR expression in interneurons covers the extent of dorsal CA1. a) Septo-temporal extent of viral expression of the ligand-gated Cl- channel PSAM^{L141F}-GlyR in dorsal CA1, revealed by α-bungarotoxin/Alexa647 (*α-BTX IHC*) immunostaining (example *Som-cre* and *Pvalb-cre* mice). **b)** Mean % of cre/tdTomato+ cells in CA1 that are also PSAM^{L141F}-GlyR+ in *Som-cre/Ai9* (5 sections) and in *Pvalb-cre/Ai9* (6 sections) mice. **c)** Counts in *Som-cre/Ai9* mice from panel b) were restricted to *oriens*, because a sparse subset of CA1 PCs in *pyramidale* express tdTomato developmentally, but do not express *Cre* in adulthood. Red = developmental expression. Blue = viral expression.

interneurons or Pvalb+ interneurons did not alter perception of the US, as hippocampal-independent auditory cued conditioning was left intact (**Fig 3.5c**). This result

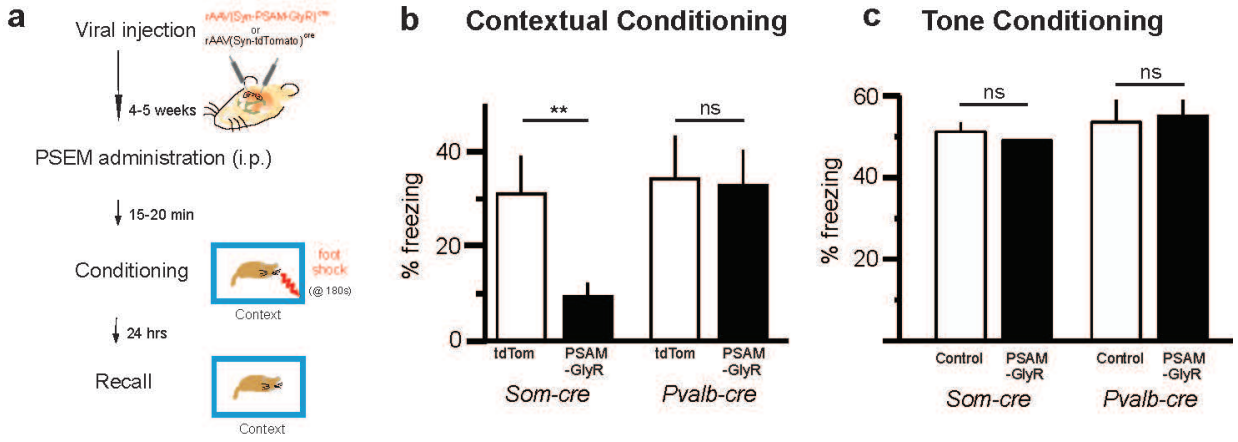

Figure 3.5 – Som+ interneurons in CA1 are required for learning conventional CFC in freely-moving mice, but not cued FC. **a**) Schematic of experimental protocol. Mice were injected with 30 mg/kg PSEM[89] i.p. 15 min before CFC with a single 2 s/1 mA footshock, and are tested in a recall session 24 hours later without PSEM[89]. **b**) Summary data for contextual freezing 24 hours later with *Som-cre* mice and *Pvalb-cre* mice, expressing either tdTomato or PSAM^{L141F}-GlyR in cre+ CA1 interneurons (2-way ANOVA, genotype x virus: $F_{(1,31)} = 5.43$, $p < 0.05$). *Som-cre* mice, control vs. PSAM^{L141F}-GlyR ($p < 0.05$); *Pvalb-cre* mice, control vs. PSAM^{L141F}-GlyR ($p = 0.75$), unpaired 2-tailed t-test. **c**) Summary data for tone-conditioning experiments with *Som-cre* and *Pvalb-cre* mice. Mice were injected with 60 mg/kg PSEM[89] i.p. 15 min before conditioning with four 20 s tones terminating with a 2 s/1 mA footshock. Freezing was assessed 24 hours later in an altered context without PSEM[89], tested with four repetitions of 20 s tones. *Som-cre*: control, n=2; PSAM^{L141F}-GlyR, n=2; $p = 0.56$, unpaired 2-tailed t-test. *Pvalb-cre*: control, n=4; PSAM^{L141F}-GlyR, n=4; $p = 0.839$, unpaired 2-tailed t-test.

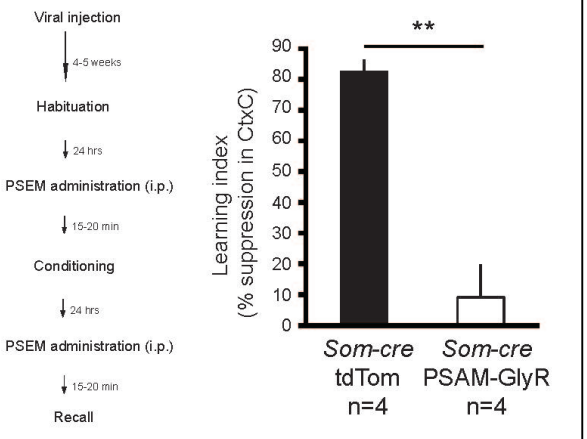

Figure 3.6 – Effects of inactivating CA1 Som+ interneurons on learning is not a consequence of brain-state effects. *Som-cre* mice were injected with 60 mg/kg PSEM[89] in saline i.p. 15 min before CtxC conditioning session, and CtxC recall session. Unpaired 2-tailed t-test: $p < 0.01$. Because these mice were similar to *Som-cre* mice injected with PSEM[89] during conditioning alone, the two groups were merged for Figure 3.3b.

demonstrates that non-hippocampal-based fear conditioning can still occur. Inactivating Som+ interneurons did not merely change the animal's brain state, as inactivation during both conditioning and recall also prevented learning (**Fig 3.6**). If Som+ interneuron silencing did alter the mouse's brain state at the time of conditioning, and

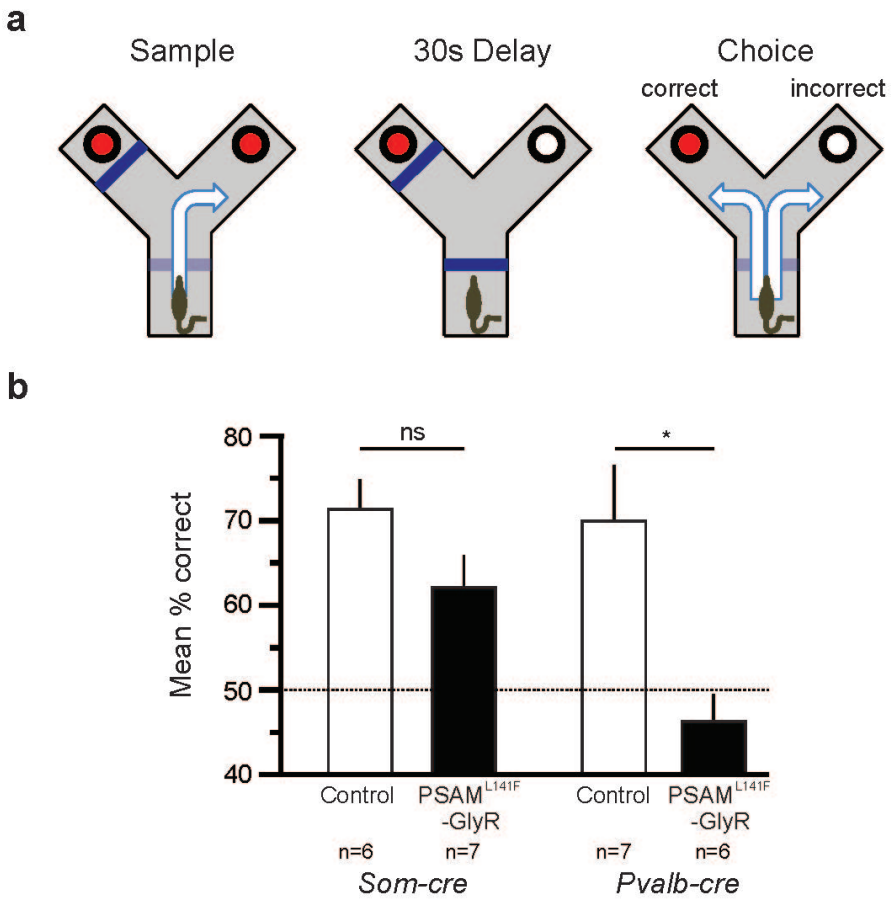

Figure 3.7 - Inactivating CA1 Pvalb+ interneurons with PSAM^{L141F}-GlyR disrupts spatial working memory. **a)** Schematic of experimental protocol. Mice pursued sweetened condensed milk rewards (50% dilution, 30 µL). Mice were injected with 60 mg/kg PSEM^{89} i.p., and tested in a delayed non-match to sample task in a y-maze from 10-35 min post-injection. Mice went through 10 trials beginning in the start box, consisting of a sample phase (shuffling of location across trials), a 30 s delay phase in the start box, and a choice phase. The correct response in the choice phase is to collect a reward in the arm not yet visted, reflecting working memory in a natural foraging behavior. Between trials mice were moved to a clean cage for 60 s. **b)** Summary data for DNMS task, in *Som-cre* and *Pvalb-cre* mice (2-way ANOVA, genotype x virus: $F_{(1,23)} = 2.0$, $p = 0.172$). There was a significant main effect of virus ($p < 0.005$). *Som-cre* mice, Control vs. PSAM^{L141F}-GlyR ($p = 0.173$); *Pvalb-cre* mice, control vs. PSAM^{L141F}-GlyR ($p < 0.05$), Mann-Whitney U tests.

thus changed the perception of the training context, then inducing the same manipulation in recall should allow for more contextual freezing, because the perceived training and recall contexts would be the same.

The absence of a role for Pvalb+ interneurons in CFC was not due to insufficient neuronal inactivation. In agreement with previous findings (Murray et al.,

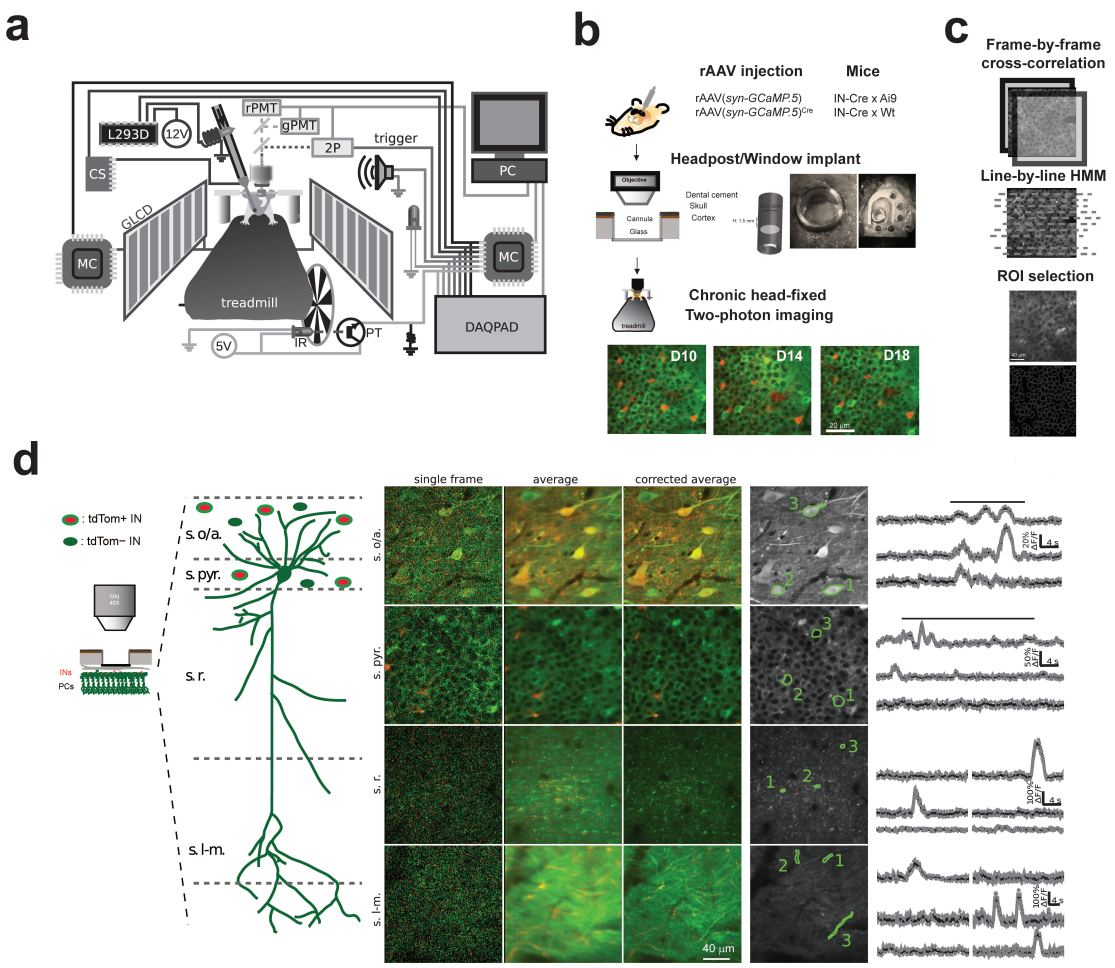

Figure 3.8 – 2-photon Ca^{2+} imaging of GCaMP-expressing neurons in CA1 of awake head-fixed mice. **a)** Schematic of apparatus for imaging the hippocampus of behaving head-fixed mice. Micro-controllers (MC) are used to deliver a variety of sensory stimuli to mice head-fixed on the treadmill, which is synched to imaging acquisition software (on PC) and behavioral read-out through the DAQPAD. **b)** Workflow for preparation of mice for chronic head-fixed 2-photon Ca^{2+} imaging. **c)** Workflow for analysis of Ca^{2+} signals in moving mice. **d)** Example images from all layers of CA1 during running, demonstrating the utility of motion-correction software. Traces at right denote running with horozontal bar.

2011), this manipulation reduced performance in a spatial working memory task (**Fig 3.7**). Together, these data indicate that CA1 Som+ dendrite-targeting interneurons are required for CFC. This result is consistent with the interpretation that CFC depends on hippocampal PC burst spiking (Xu et al., 2012b), which is regulated by Som+ interneurons (Lovett-Barron et al., 2012; Royer et al., 2012).

Using 2-photon Ca^{2+} imaging of hippocampal neurons in head-fixed mice (**Fig 3.8**), we confirmed that systemic PSEM could effectively silence Som+/PSAM-GlyR+ neurons *in vivo* (**Fig 3.9**), although silencing was not complete in all tested neurons.

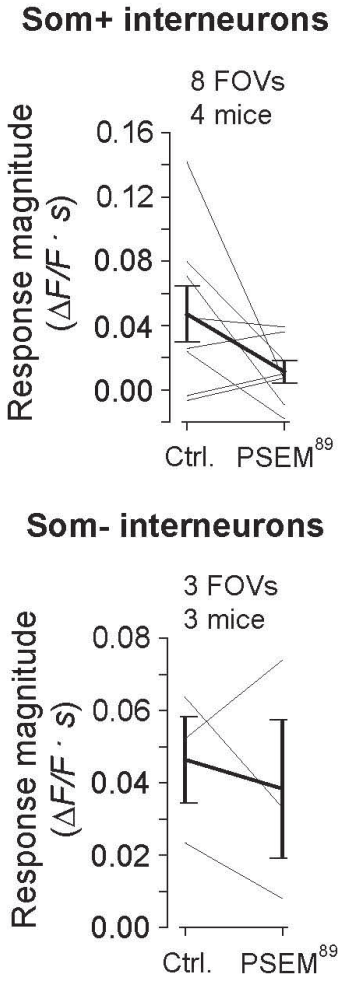

Figure 3.9 - PSEM^{89} inactivation of Som+ interneurons *in vivo.* Mean air-puff responses of Som+/PSAM^{L141F}-GlyR+ interneurons (top) and Som−/PSAM^{L141F}-GlyR− interneurons (bottom) in control and PSEM^{89} administration (60 mg/kg PSEM^{89} i.p. 12-30 min before stimulus presentation).

The US activates Som+ interneurons in CA1

To dissect the role of CA1 Som+ interneurons in contextual learning, we used 2-photon Ca^{2+} imaging (**Fig 3.8)** to record the activity of these neurons over the course of hf-CFC (**Fig 3.10**). We unilaterally injected rAAV(*Synapsin-GCaMP5G*)^{cre} into dorsal CA1 of *Som-cre* mice to express the genetically-encoded Ca^{2+} indicator GCaMP5G (Akerboom et al., 2012) in the somata, dendrites, and axons of

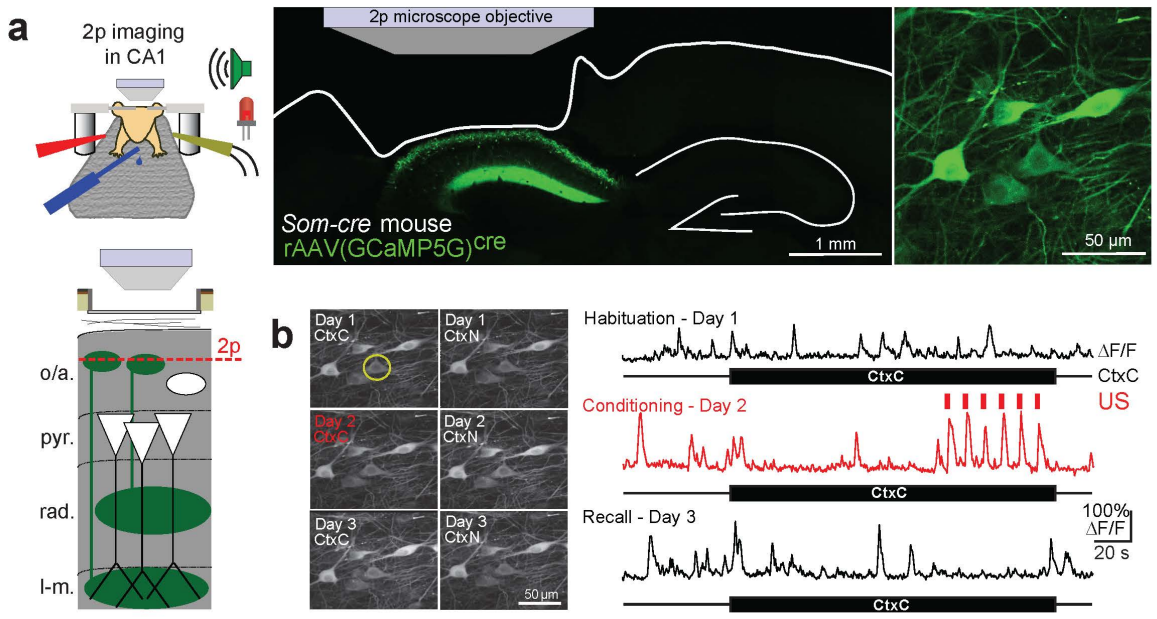

Figure 3.10 – Som+ interneurons are activated by the US during hf-CFC. **a)** Top left: Schematic of hf-CFC during 2-photon imaging from hippocampal neurons. Bottom left: Schematic of recording configuration, with 2-photon (*2p*) imaging from Som+ interneurons in the *oriens*/*alveus* layers of CA1 *in vivo* (*o/a*: strata oriens/alveus, *pyr.*: stratum pyramidale, *rad.*: stratum radiatum, *l-m.*: stratum lacunosum-moleculare). Right: Confocal image of coronal section from mouse expressing GCaMP5G in Som+ interneurons in dorsal CA1. The 2-photon microscope objective and landmarks showing the outline of the brain, including the removed cortex and the contralateral hippocampus, are illustrated. An *in vivo* 2-photon image of GCaMP-expressing Som+ interneurons is shown at far right. **b)** Left: 2-photon images of the same field of view from panel *a*, returning to this same location for the six hf-CFC session over the course of three days. Images are time averages of 2000 motion-corrected imaging frames collected for each imaging session. Right: *ΔF/F* traces from an example Som+ CA1 interneuron (circled in yellow at left) over the 3 daily exposures to CtxC.

Som+ interneurons (**Fig 3.10a**). To visualize CA1 neurons *in vivo*, we used established surgical techniques (Mizrahi et al., 2004; Dombeck et al., 2010; Kaifosh et al., 2013) to implant a chronic imaging window superficial to dorsal CA1 (**Fig 3.8**) – a surgical technique that does not alter CFC performance (Sakaguchi et al., 2012; **Fig 3.2d**). After recovery, water restriction, and habituation to head-restraint, we engaged mice in the hf-CFC task while imaging Ca^{2+}-evoked GCaMP5G fluorescence transients from the cell bodies of Som+ interneurons in the *oriens* and *alveus* layers of CA1. We returned to the

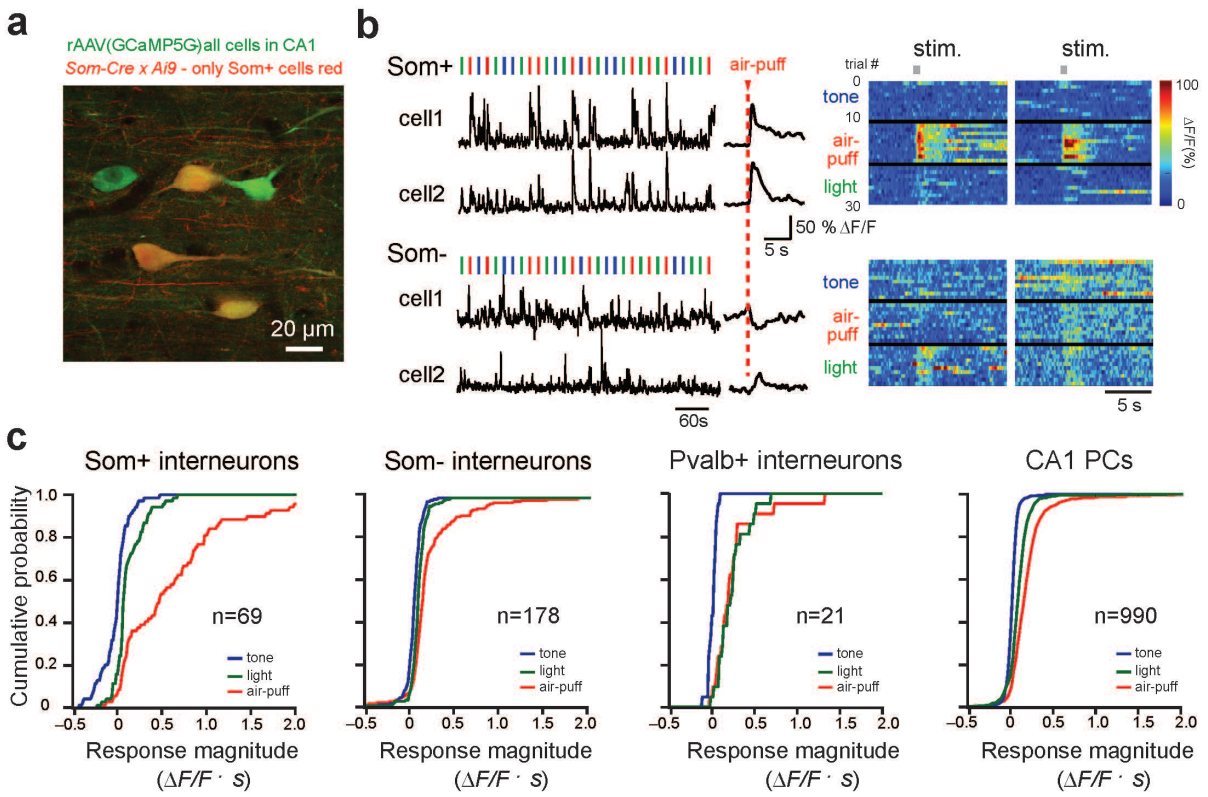

Figure 3.11 – Fraction of sensory-evoked responses in different cell types of CA1.
a) Expression of GCaMP5G in CA1 *oriens* interneurons of a *Som-cre/Ai9* mouse, including parallel recording from Som/tdTom+ and Som/tdTom- interneurons. **b)** Left: traces from example cells in panel *a* during the pseudorandom presentation of discrete sensory stimuli. Traces are concatenated together from 30 individual trials of air-puffs, tones, and lights. Middle: example averaged air-puff responses on an expanded time scale. Right: The same data represented as heat maps, with trials grouped by stimulus type. **c)** Summary data for GCaMP5G responses to discrete sensory stimuli in Som+ and Som- interneurons (*Som-cre/Ai9* mice), Pvalb+ interneurons (*Pvalb-cre/Ai9*), and pyramidal cells (both lines). *ΔF/F* is calculated using the difference between the 5 s before and after stimulus onset.

same field of view for each of the six sessions of hf-CFC (**Fig 3.10b**), and processed fluorescence time-series data using established methods for motion-correction and signal processing (Dombeck et al., 2007; Kaifosh et al., 2013). Strikingly, we found that Som+ interneurons displayed markedly increased activity in response to the US during hf-CFC (example cell in **Fig 3.10b**).

To investigate the dynamics of stimulus-evoked GABAergic signaling in more detail, we imaged CA1 inhibitory cells during the pseudorandom presentation of discrete

sensory stimuli (200 ms) from the hf-CFC task: light-flashes and tones, which were elements of the CS, or air-puffs, which served as the US. To image a greater variety of interneurons simultaneously, we injected cre-independent rAAV(*Synapsin-GCaMP5G*) into CA1 of *Som-cre* mice crossed with a tdTomato reporter line, which allowed us to simultaneously image sensory responses of Som+ and Som- interneurons (**Fig 3.11a,b**). We found that air-puffs activated most Som+ interneurons, whereas a smaller proportion of Som− interneurons, Pvalb+ interneurons, and CA1 PCs had comparable responses (**Fig 3.11b,c**).

Not all Som+ cells were activated by the air-puff (**Fig 3.11c**), which could reflect a difference between bistratified cells and OLM cells, both of which are labeled in *Som-cre* mice (Lovett-Barron et al., 2012; Royer et al., 2012). The axons of bistratified cells arborize in stratum *oriens* and *radiatum*, whereas those of OLM cells arborize in stratum *lacunosum-moleculare* (Freund & Buzsáki, 1996; Klausberger & Somogyi, 2008; Klausberger, 2009). These two inhibitory projections contact the dendritic compartments of CA1 PCs that receive input from CA3 and the EC, respectively, suggesting potentially distinct functions. To isolate the relative contributions of these two inhibitory pathways to US-evoked signaling, we virally labeled Som+ neurons with GCaMP5G in *Som-cre* mice and focused our imaging plane on the axons of bistratified cells in *radiatum*, or the axons of OLM cells in *lacunosum-moleculare* (**Fig 3.12a**). Whole-field recording from the dense Som+ axonal termination in *lacunosum-moleculare* revealed a fast high-amplitude increase in fluorescence in response to the air-puff, but not the tone or light (**Fig 3.12a,b**). In contrast, the lower density axons in *radiatum* revealed little response to these stimuli. We also expressed GCaMP5G in *Pvalb-cre* mice to record from Pvalb+

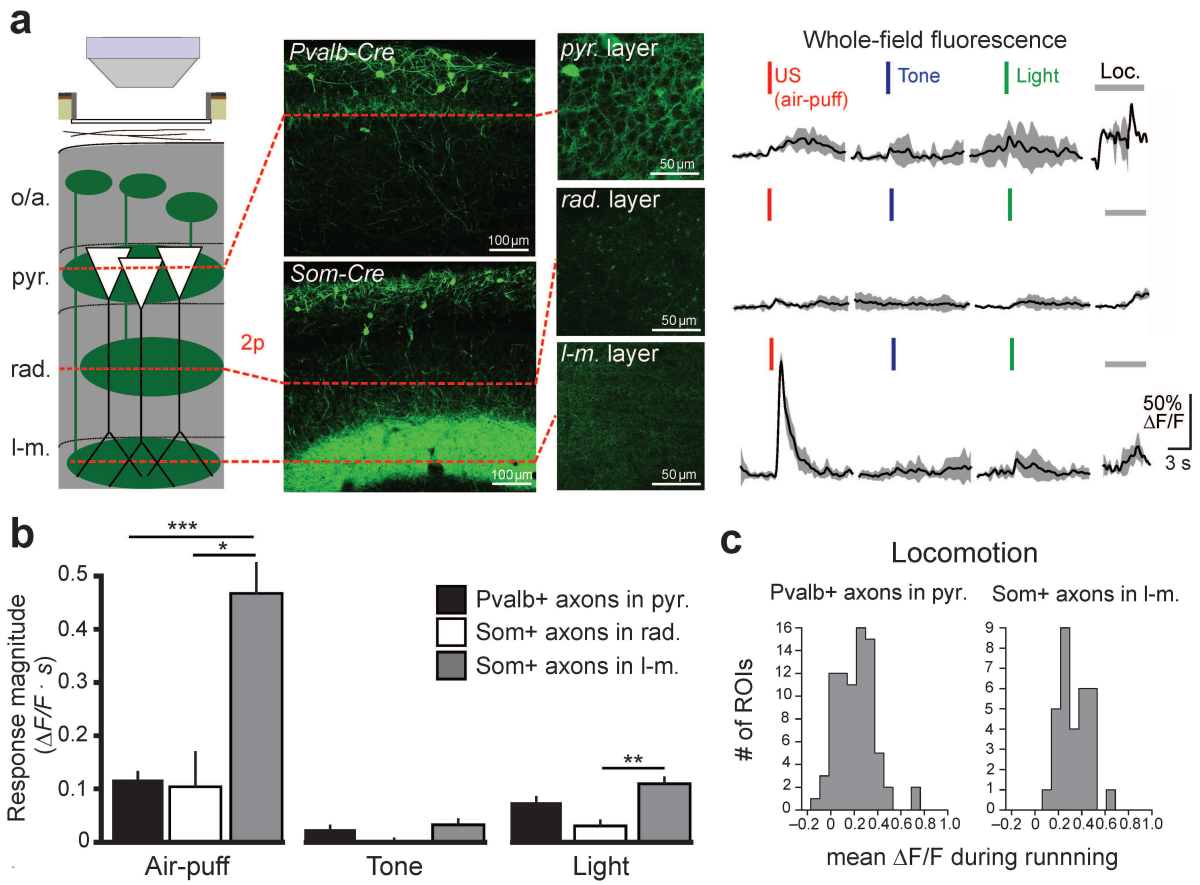

Figure 3.12 – US-responsive Som+ interneurons project to *stratum lacunosum-moleculare*. **a)** Left column: Schematic of recording configuration, with *in vivo* 2-photon imaging from the axons of Som+ interneurons in *radiatum* or *lacunosum-moleculare* layers of CA1, or axons of Pvalb+ interneurons in the *pyramidale* layer. Middle column: Expression of GCaMP5G in layer-specific axonal projections, revealed by confocal images of coronal sections and *in vivo* 2-photon images of each layer. Right column: Example trial-averaged responses (five trials each presented in pseudorandom order) of layer-specific whole-field fluorescence responses to discrete sensory stimuli and locomotion (mean with shaded standard deviation). **b**) Summary data for sensory stimulation experiments shown in panel *c*. Responses are quantified as the mean integral of whole-field *ΔF/F* over the three second after the stimulus. (2-way ANOVA, axon type x stimulus type, $F_{(4,84)} = 16.9$, $p<0.001$; post-hoc Mann-Whitney U tests). Bars represent mean ± s.e.m., *p < 0.05, **p < 0.01, ***p < 0.001. **c)** Summary data for whole-field *ΔF/F* responses to treadmill-running. Pvalb+ axons in *pyramidale* exibit locomotion responses similar to Som+ axons in *lacunosum-moleculare* (Mann-Whitney U test, p=0.101).

basket cell axons in stratum *pyramidale*. These high-density axons displayed smaller responses to the US (**Fig 3.12a,b**) but responded robustly to treadmill running at similar magnitudes to Som+ axons in *lacunosum-moleculare* (**Fig 3.12c**). Previous data have demonstrated that aversive stimuli drive widespread suppression of PC firing activity in

CA1 of anesthetized rodents (Herreras et al., 1988a; Khanna, 1997; Funahashi et al., 1999; Vinogradova, 2001); here we show in behaving mice that these stimuli preferentially activate Som+ OLM cells, which are positioned to drive time-locked inhibition compartmentalized to the distal dendritic tufts of CA1 PCs.

Cholinergic projection neurons in the medial septum drive Som+ interneurons through m1ACh receptors during the US

To drive fast-onset responses to the US, Som+ interneurons in CA1 must receive a time-locked source of US-driven excitation. However, most excitatory inputs to OLM cells are synapses from CA1 PCs (Klausberger & Somogyi, 2008; Klausberger, 2009), and PCs do not encode the US (Frankland et al., 2004; Fanselow & Poulos, 2005) or robustly respond to it (**Fig 3.11c**; Herreras et al., 1988a; Khanna, 1997; Funahashi et al., 1999; Vinogradova, 2001). As an alternative, Som+ interneurons could be excited by extrahippocampal sources such as subcortical neuromodulatory inputs. Indeed, OLM cells in CA1 can be depolarized through both nicotinic and muscarinic acetylcholine receptors (Lawrence et al., 2006; Leão et al., 2012), and lesion of cholinergic inputs from the medial septum are known to prevent the suppressive effects of aversive stimuli on CA1 spiking activity (Miller & Groves, 1977; Rovira et al., 1983; Herreras, 1988b; Khanna, 1997; Zheng & Khanna, 2001). Additionally, neocortical interneurons have recently been demonstrated to respond to aversive stimuli (Pi et al., 2013) through cholinergic input (Letzkus et al., 2011).

To probe the source of US-evoked activation of Som+ OLM cells, we modified our imaging window to allow for local pharmacological manipulation of the imaged

neural tissue (**Fig 3.13a,b**; Kaifosh et al., 2013). We applied antagonists of neuromodulatory receptors through the imaging window, which passively diffused into CA1; there we imaged GCaMP5G-expressing Som+ interneuron responses to stimuli

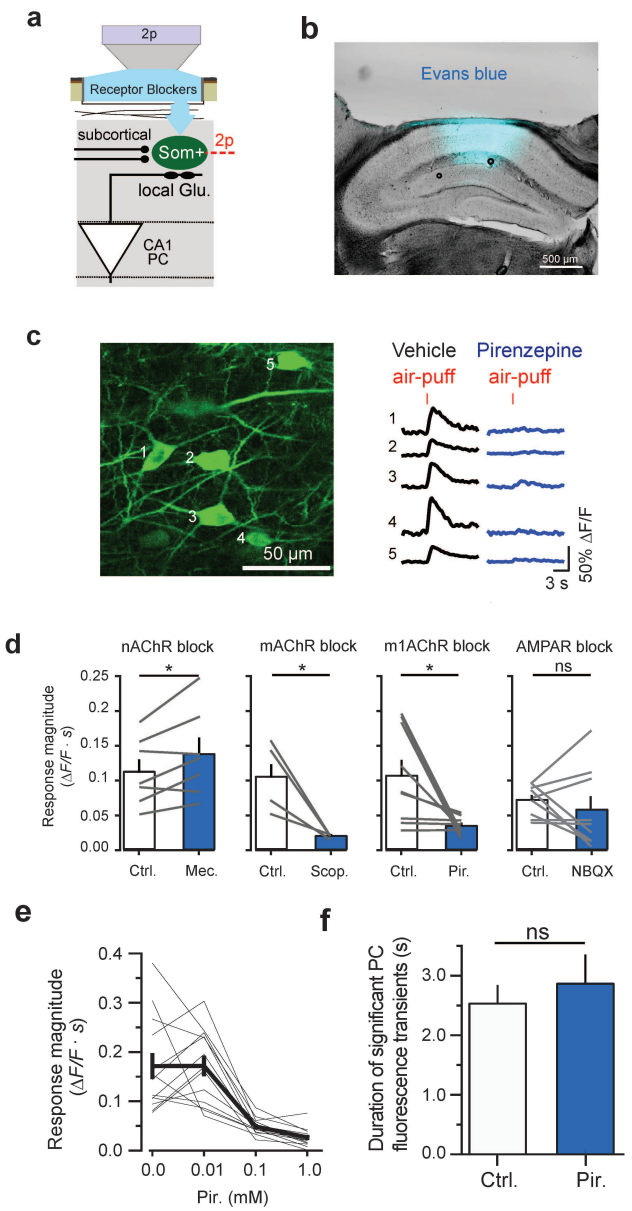

Figure 3.13 – Som+ interneurons lose their responsiveness to the US upon local blockade of m1AChRs. a) Schematic of recording configuration, with 2-photon imaging from Som+ interneurons in the *oriens* and *alveus* layers of CA1 *in vivo*, and local pharmacological manipulations through an aperture in the imaging window. **b)** Confocal image of spread of 1% Evans Blue (in cortex buffer) through the perforated imaging window over the timescale of pharmacological manipulation, followed by perfusion, fixation, and mounting. **c)** Example *in vivo* 2-photon image of GCaMP-expressing Som+ interneurons, and their fluorescence responses to air-puffs in vehicle (cortex buffer) and in the presence of 1 mM pirenzepine. **d)** Summary data for local pharmacological manipulations. Each point is the mean response of all Som+ interneurons within a FOV to air-puffs (5 trials each) in vehicle (Ctrl.) and upon drug application (nAChR block: 1 mM mecamylamine, 7 FOVs in 5 mice; mAChR block: 1 mM scopolamine, 4 FOVs in 3 mice; m1AChR block: 1 mM pirenzepine, 9 FOVs in 5 mice; AMPAR block: 20 µM NBQX, 9 FOVs in 4 mice). Comparisons are paired t-tests between drug conditions. **e)** Concentration-dependence of m1AChR blockade on air-puff-evoked activity in Som+ interneurons. Each line is one Som+ cell (n=13 cells). **f)** Responses of pyramidal cells to air-puffs are not significantly altered by the concentration of pirenzepine (100µM) required to block Som+ interneuron responses to air-puffs. We measured this as the duration of air-puff-evoked transients in PCs active in both drug conditions (ctrl: 2.51 ± 0.3s, Pir.: 2.84 ± 0.5s, n = 5 cells; paired t-test).

before and after drug administration (**Fig 3.13a-c**). Surprisingly, we found that blockade of the nicotinic acetylcholine receptor (nAChR) did not decrease Som+ interneuron responses to air-puffs (1 mM mecamylamine), but instead modestly increased responses (**Fig 3.13d**). However, blockade of the muscarinic acetylcholine receptor (mAChR) significantly reduced air-puff responses in Som+ interneurons (1 mM scopolamine) (**Fig 3.13d**). We recapitulated this result with more selective blockade of type 1 mAChRs (1 mM pirenzepine), which reduced air-puff-evoked Som+ interneuron responses in a dose-dependent fashion (**Fig 3.13c-e**). Metabotropic receptors like mAChRs generally act on slower timescales, but studies in brain slices have demonstrated that muscarinic input can evoke fast-onset depolarization and spiking of CA1 OLM cells (Lawrence et al., 2006; Widmer et al., 2006). mAChRs in dorsal hippocampus are known to be required for encoding CFC (Gale et al., 2001), and our results suggest a possible circuit mechanism that contributes to this requirement. This effect was not a consequence of reduced disynaptic drive from

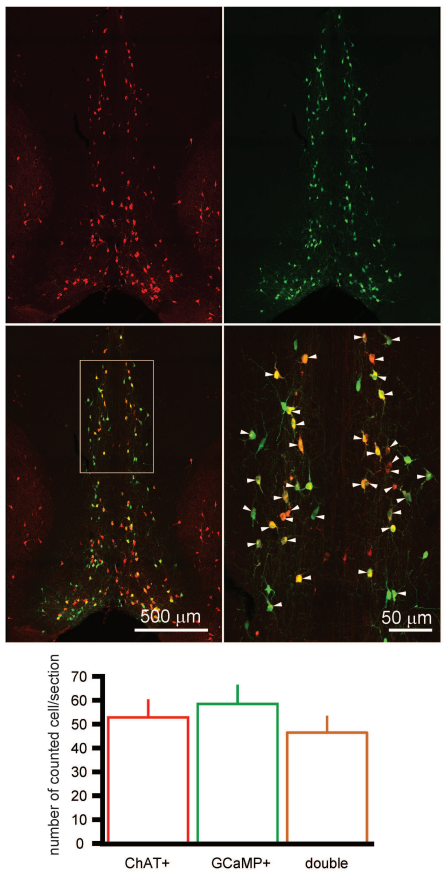

Figure 3.14 – GCaMP6f expression in ChAT+ neurons of the medial septum. Top: Confocal images of the medial septum showing co-localization of virally expressed GCaMP6f and endogenous ChAT with ChAT immunohistochemistry. Bottom: Summary graph of co-localization of ChAT immunohistochemistry and GCaMP labeling (n = 3 section in 3 mice) in ChAT-cre mice injected with rAAV2/1(*ef1α-DIO-GCaMP6f*)^{cre} into the medial septum.

m1AChR-responsive PCs (Dasari & Gulledge, 2011), as m1AChR block did not substantially alter air-puff-evoked activity in the minority of responding PCs (**Fig 3.13f**), and responses of Som+ interneurons were not substantially changed by blockade of glutamatergic AMPA receptors (20 µM NBQX; **Fig 3.13d**).

Cholinergic input to the hippocampus arises from projection neurons in the

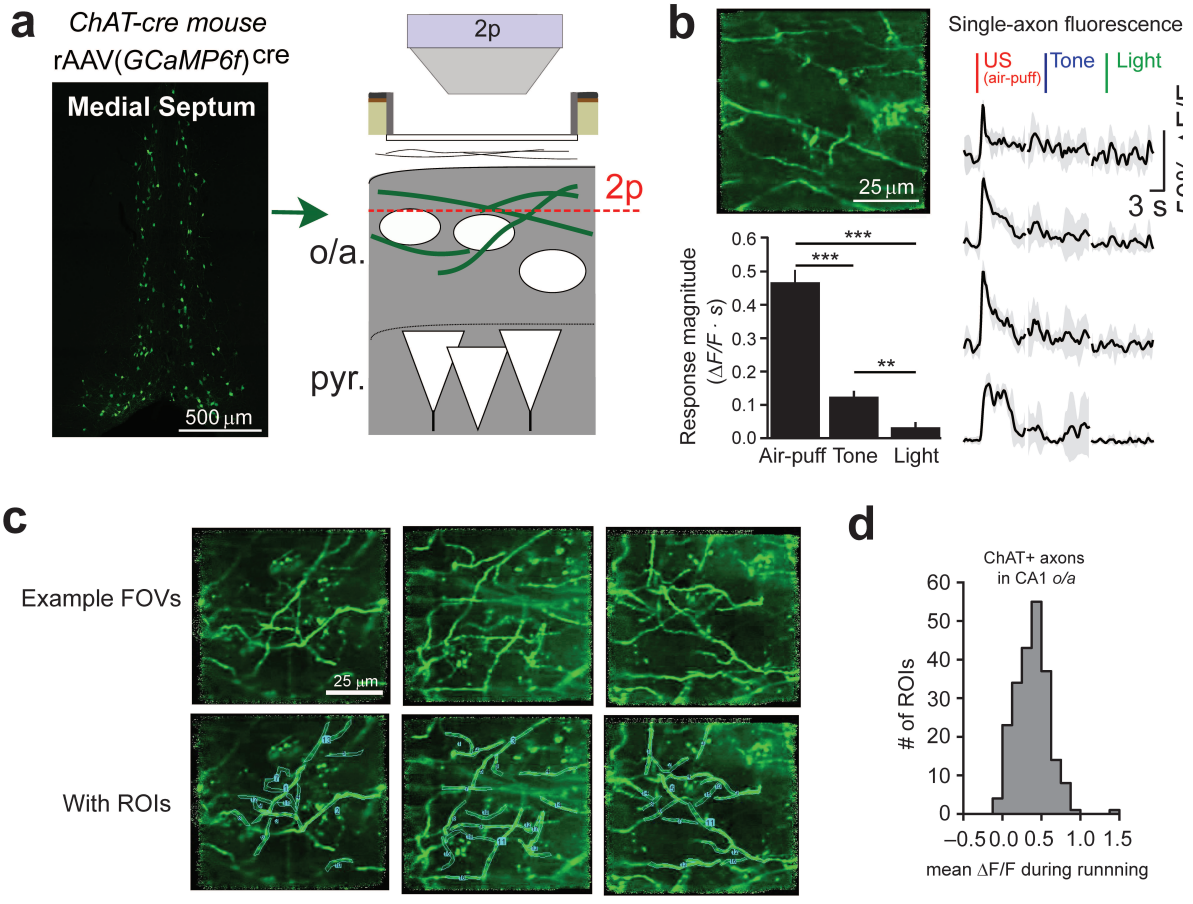

Figure 3.15 – Septohippocampal cholinergic projections to CA1 are activated by the US. **a)** Left: coronal confocal image of GCaMP6f+/ChAT+ neurons in the medial septum of a *Chat-cre* mouse. Right: Schematic of recording configuration, with 2-photon imaging from ChAT+ axons in the *oriens* and *alveus* layers of CA1 *in vivo*. **b)** Top left: example *in vivo* 2-photon image of GCaMP6f-expressing ChAT+ axons in CA1. Right: mean responses of individual axons to discrete sensory stimuli. Bottom left: Summary data from ChAT+ axons averaged within each FOV (sign tests; n = 20 FOVs in n = 2 mice). Bars represent mean ± s.e.m., *p < 0.05, **p < 0.01, ***p < 0.001, ns = non-significant**. c)** More examples of FOVs from *oriens/alveus* in CA1 of ChAT+ mice, and the ROIs drawn to analyze axonal signals. **d)** Responsiveness of ChAT+ axons to locomotion on the treadmill.

medial septum (Hasselmo, 2006), a region required for CFC (Calandreau et al., 2007). To directly record the activity of these projections, we injected rAAV(*ef1α-DIO-GCaMP6f*)^{cre} into the medial septum (MS) of *ChAT-cre* mice to express the sensitive Ca^{2+} indicator GCaMP6f (Chen et al., 2013) in cholinergic neurons that project to the hippocampus, among other structures (**Fig 3.14**). We imaged cholinergic (ChAT+) axons in the *oriens* and *alveus* layers of CA1 during sensory stimulation (**Fig 3.15a-c**), and found that ChAT+ axons responded robustly to air-puffs, with smaller responses to tones and very little response to light flashes (**Fig 3.15b**). Like many circuit elements connected in the septal-hippocampal-entorhinal system, these cholinergic axons were active during treadmill running (**Fig 3.15d**). We also imaged the axonal boutons arising from septohippocampal GABAergic projections (Freund & Antal, 1988) under similar conditions (**Fig 3.16a,b**), and found comparable response properties to ChAT+ axons: prominent responses to air-puffs and treadmill running (**Fig 3.16c-e**; see Kaifosh et al., 2013 for a detailed analysis of this projection). Septal GABAergic neurons may be activated by local connections from septal cholinergic neurons and inputs from various brainstem nuclei (Kaifosh et al., 2013).

We found that ChAT+ axon responses were independent of air-puff duration, similar to Som+ axons in *lacunosum-moleculare* (**Fig 3.17**). These data indicate that the septohippocampal cholinergic projection is triggered by stimulus onset, in contrast with the graded responses of septohippocampal GABAergic projections (Kaifosh et al., 2013). Cholinergic activation of Som+ interneurons thus provides CA1 with onset-locked information about the US from subcortical nuclei.

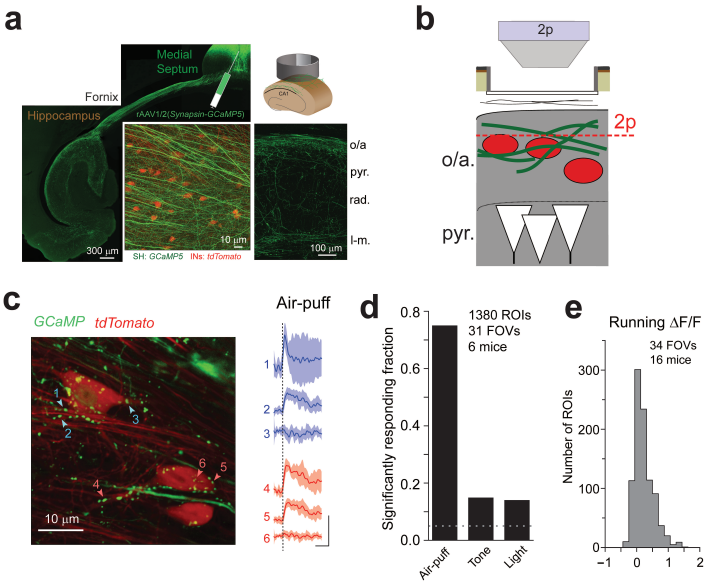

Figure 3.16 – Response properties of septohippocampal GABAergic projections to CA1. **a)** Viral injection site in the medial septum and SH-GABA fibers in the fornix and dorsal hippocampus (left). Confocal image of area under the imaging window (middle) and coronal image of GCaMP-labeled SH-GABA fibers in CA1 (right). o/a, oriens/alveus; pyr., pyramidal layer; rad., radiatum; l-m., lacunosum-moleculare. **b)** Schematic of in vivo two-photon (2p) imaging. **c)** Left: Two-photon image of GCaMP5G+ SH-GABA boutons adjacent to tdTomato+ CA1 interneurons. Right: mean air puff–triggered signals from example boutons (arrows at left). **d)** Fraction of boutons responding to different sensory stimuli. Dotted line indicates chance level. **e)** Elevation of Ca^{2+} signals during running ($P < 0.001$, sign test, n = 935 boutons).

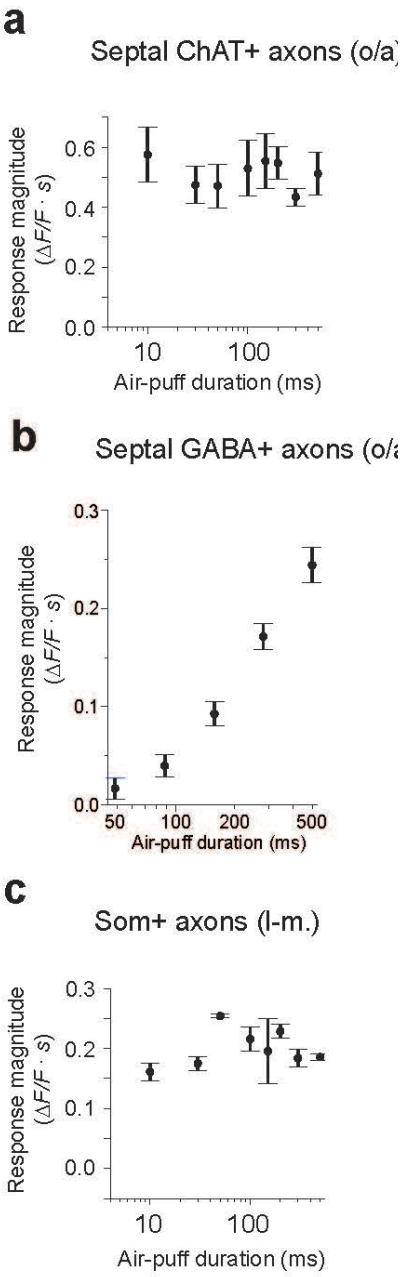

Figure 3.17 – The circuit connecting septo-hippocampal cholinergic inputs to Som+ OLM cells is sensitive to the onset of air-puffs, but not the duration. Mean responses to air-puffs of duration 10 ms, 30 ms, 50 ms, 100 ms, 150ms, 200 ms, 300 ms, and 500 ms in: **a)** Septal ChAT+ axons, **b)** Septal GABA+ axonal boutons, **c)** Som+ OLM cell axons.

Co-aligned inhibition and excitation of PC dendrites in *lacunosum-moleculare* during the US

We have found that Som+ interneurons in CA1 are required for learning CFC, and are driven by cholinergic afferents during the US to inhibit the distal dendrites of CA1 PCs in stratum *lacunosum-moleculare*. The distal tuft dendrites of PCs receive excitatory input from medial and lateral EC (MEC and LEC) and thalamus, raising the possibility that the inhibition we observe is counteracting US-evoked excitation to these

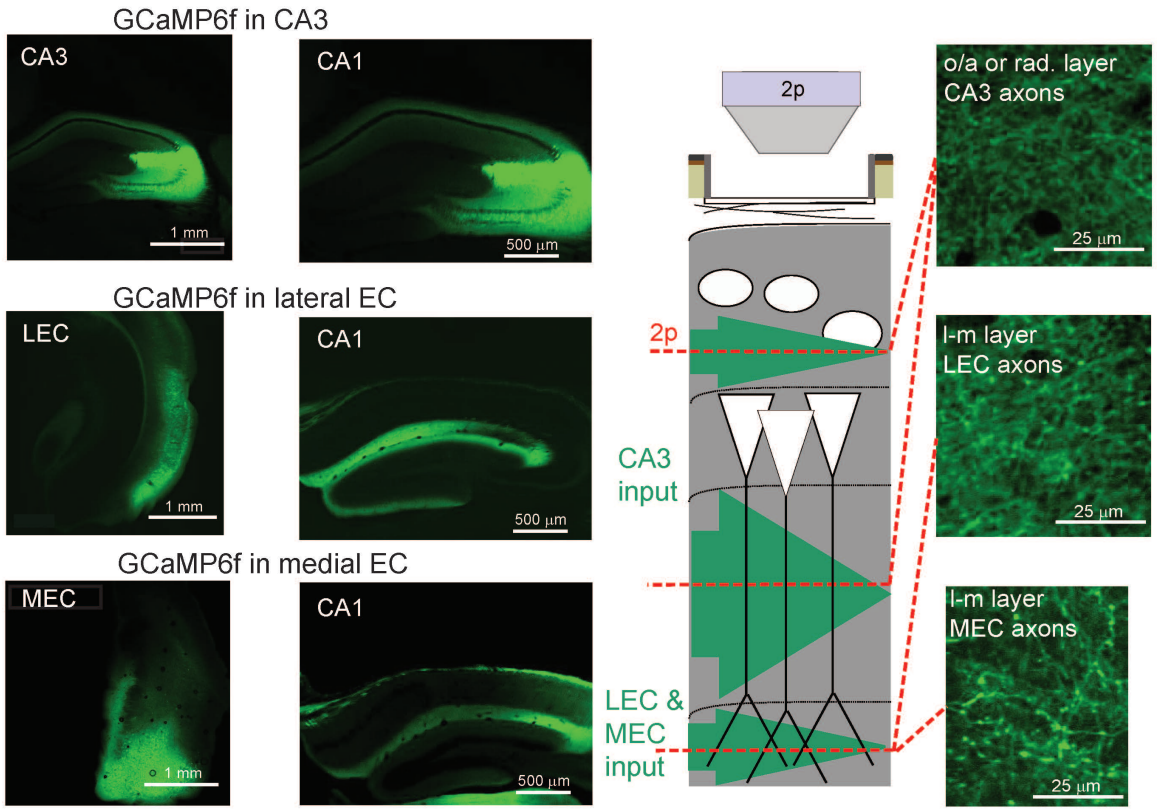

Figure 3.18 – Imaging GCaMP6f-expressing excitatory afferents to different layers of CA1. Left: confocal images of coronal sections from dorsal hippocampus, showing expression of GCaMP6f in CA1-innervating axons from CA3 (top), LEC (middle), and MEC (bottom). Middle: Schematic of recording configuration, with 2-photon imaging from excitatory axons in the *oriens*/*radiatum* layers (CA3 projections) or *lacunosum-moleculare* layer (LEC or MEC projections) of CA1 *in vivo*. Right: example *in vivo* 2-photon images of GCaMP6f-expressing axons in CA1 (CA3, top; LEC, middle; MEC: bottom).

dendrites. The EC is believed to provide sensory information to CA1 (Maren & Fanselow, 1997), particularly through the predominantly non-spatial activity patterns of the LEC (Hargreaves et al., 2005), and some of the non-spatial neurons of the MEC (Zhang et al., 2013). Sensory input to PC distal dendrites contrasts with afferents to their proximal dendrites, which receive input from CA3 believed to carry stored contextual representations rather than sensory information (Kesner, 2007). To directly record from these excitatory inputs we injected rAAV(*Synapsin-GCaMP6f*) into CA3, LEC, or MEC, and imaged axonal activity in ipsilateral CA1 layers *oriens/radiatum* or *lacunosum-moleculare*, respectively (**Fig 3.18**). We found that sensory inputs, particularly aversive air-puffs, evoked stronger signals from LEC and MEC axonal boutons compared to CA3 axonal boutons, reflected by changes in whole-field fluorescence (**Fig 3.19a-c**). These data indicate that US-driven inhibition of PC distal tuft dendrites in stratum *lacunosum-moleculare* is co-aligned with excitatory input, which could effectively limit dendritic depolarization (Palmer et al., 2012b). Compartmentalized inhibition can also prevent propagation of excitation from distal to proximal dendrites (Jarsky et al., 2005; Dudman et al., 2007; Takahashi & Magee, 2009), potentially preserving responses of PCs to sparse excitation from CA3 axons (**Fig 3.19d**). Similar US-driven signals may occur in other excitatory inputs to *lacunosum-moleculare*, such as the thalamic reuniens nucleus. Therefore, US-driven inhibition from OLM cells is poised to inhibit sensory input during the US, while sparing sensory input during other episodes that are not aversive or punishing.

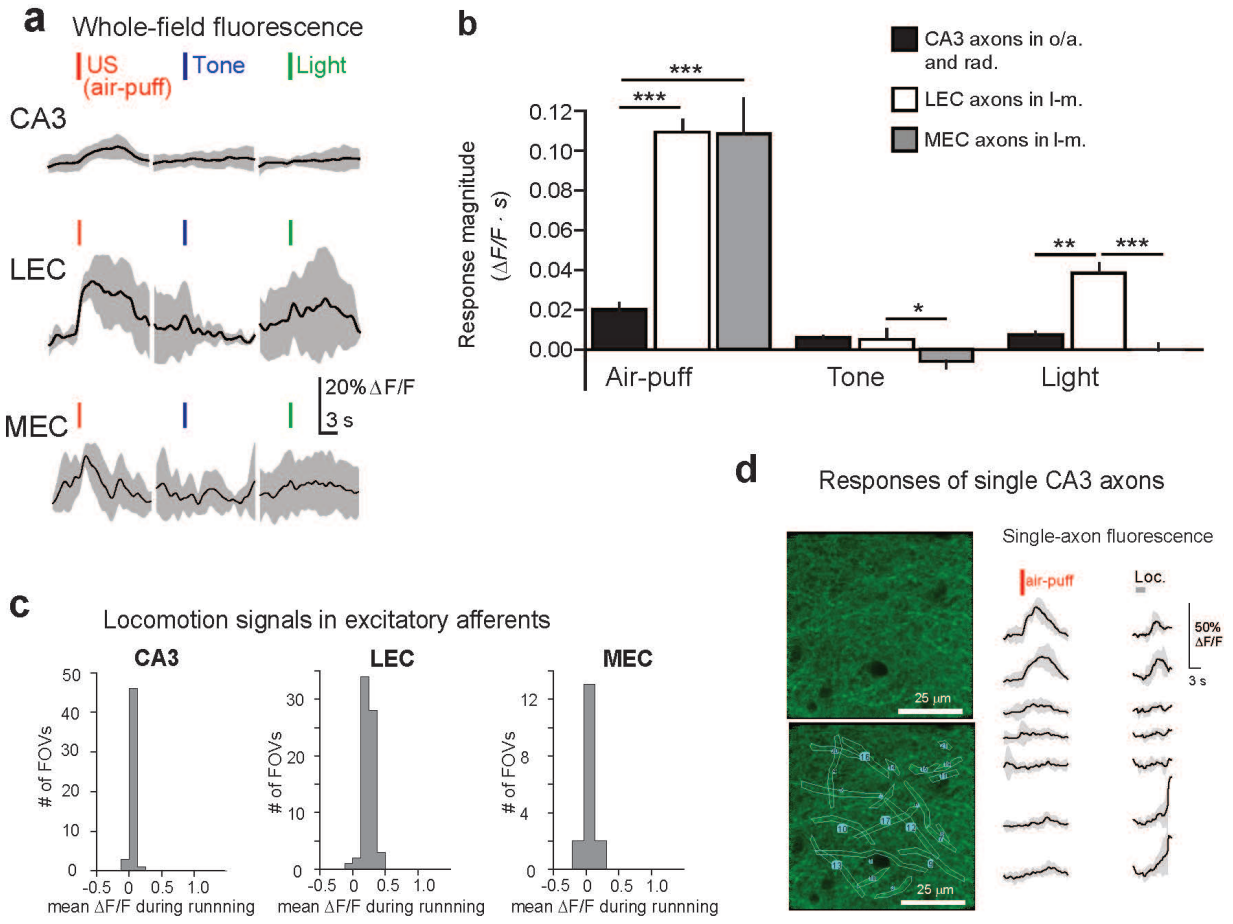

Figure 3.19 – Inputs from EC, but not CA3, robustly respond to the US. **a)** Example mean whole-field fluorescence traces from CA3, LEC and MEC axons (examples in Figure 3.18), in response to discrete sensory (mean with shaded standard deviation). **b)** Summary data for sensory stimulation experiments. Responses are quantified as the mean integral of *ΔF/F* over the 3 s after the stimulus. (2-way ANOVA, axon type x stimulus type, $F_{(4,84)} = 10.7$, $p < 0.001$; post-hoc Mann-Whitney U tests). Bars represent mean ± s.e.m., **p < 0.01, ***p < 0.001. **c)** Locomotion signals in CA3, LEC, and MEC axons (whole-field ROIs). **d)** Example responses of single CA3 axons to running and air-puffs. While most CA3 axons do not respond to air-puffs, as reflected in whole-field fluorescence (panel *a* & *b*), a sparse subset of CA3 axons do respond, potentially providing the drive to excite a sparse subset of CA1 PCs, even though the much stronger EC signals are being inhibited.

Som+ interneurons limit CA1 PC population activity during the US

Ultimately, any dysfunction in the hippocampal encoding of context is likely reflected in changes to the primary hippocampal output neurons – CA1 PCs. Som+ interneurons appear poised to inhibit excitation during the US and are required for CFC, but the response of PCs in their absence is unknown. To probe the consequences of

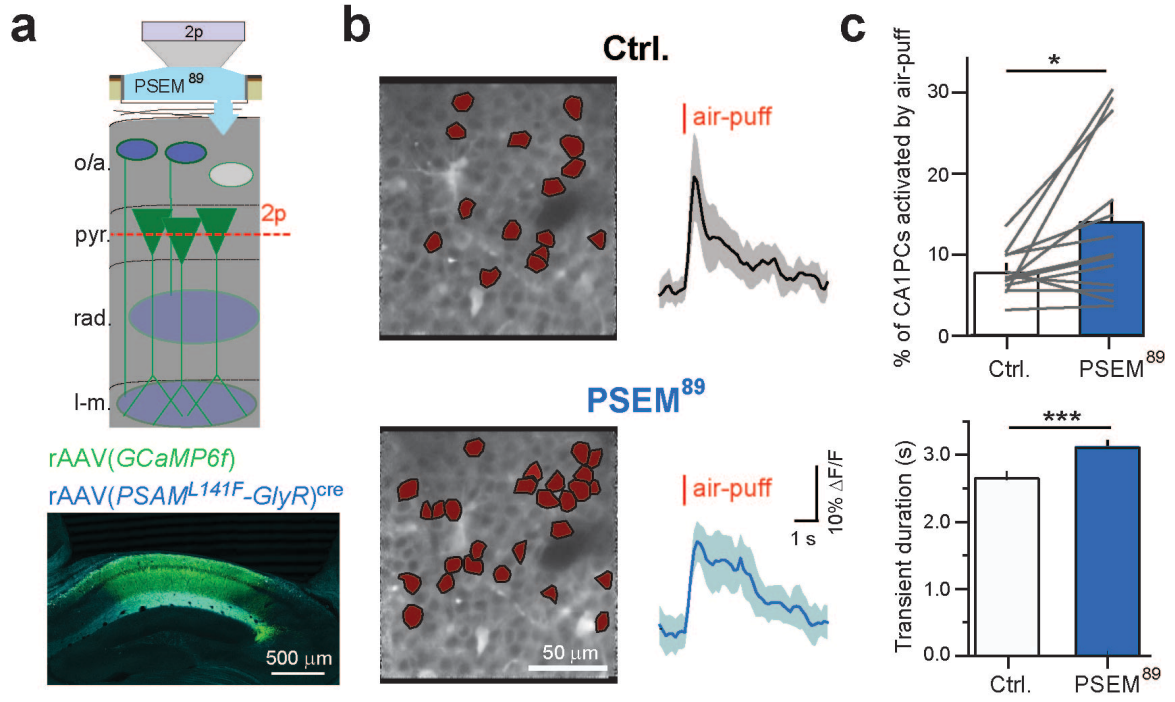

Figure 3.20 - Effects of inactivating CA1 Som+ interneurons on US-evoked PC population activity. **a)** Top: Schematic of recording configuration, with 2-photon imaging from CA1 PC populations in the *pyramidale* layer of CA1 *in vivo*, and local pharmacologenetic manipulation of PSAM^{L141F}-GlyR-expressing Som+ interneurons through an aperture in the imaging window. Bottom: confocal image of coronal CA1 sections, with GCaMP6f expression in all neurons (green) and PSAM^{L141F}-GlyR expression in Som+ interneurons, revealed by α-BTX immunostaining (blue). **b)** Left: corrected time average images of example recordings in *pyr.* of a mouse expressing PSAM^{L141F}-GlyR in Som+ interneurons, with PCs showing significant US responses marked in red. Right: mean ΔF/F responses of cells active in both control and PSEM^{89} conditions from left (shading is standard deviation). Top: pre-drug. Bottom: drug. **c)** Summary data for mulitple FOVs between drug conditions. Top: mean % of signficantly active CA1 PCs (Ctrl: 7.6 ± 0.7%, PSEM^{89}: 13.7 ± 2.5%, n=13 FOVs; paired t-test). Bottom: mean duration of significant transients in cells active in both drug conditions (ctrl: 2.64 ± 0.09 s, PSEM^{89}: 3.09 ± 0.09 s, n = 96 cells; paired t-test). Bars represent mean ± s.e.m., *p < 0.05, ***p < 0.001.

inactivating Som+ interneurons for US-evoked PC population activity, we simultaneously imaged air-puff responses of ~150-200 PCs while inactivating Som+ interneurons. We injected rAAV(*Synapsin-PSAM^{L141F}-GlyR*)^{cre} and rAAV(*Synapsin-GCaMP6f*) into CA1 of *Som-Cre* mice, and imaged air-puff-evoked responses of PC populations in *pyramidale* before and during Som+ interneuron inactivation with local application of PSEM^{89} through the hippocampal imaging window (**Fig 3.20a**). Although systemic PSEM^{89} reduced air-puff-evoked Ca^{2+} activity in Som+/PSAM^{L141F}GlyR+ interneurons (**Fig 3.9**), we applied PSEM^{89} locally to the imaging window to extend the duration of neuronal inactivation. We imaged PC populations during control conditions and PSEM^{89} application, identifying neurons with significant air-puff-evoked Ca^{2+} transients (Dombeck et al., 2007, and Experimental Procedures). This analysis revealed two main effects of inactivating Som+ interneurons on PC population activity. We found that inactivating Som+ interneurons significantly increased the number of PCs activated by the air-puff within a field of view (**Fig 3.20b,c**), and significantly increased the duration of Ca^{2+} transients in PCs that responded to the US in both control and PSEM^{89} conditions (**Fig 3.20b,c**). Extended transient duration likely corresponds to the longer spike bursts previously reported from electrophysiological measurements of CA1 PCs upon inactivating Som+ interneurons (Lovett-Barron et al., 2012; Royer et al., 2012). These effects were not observed in control mice that did not express PSAM^{L141F}-GlyR (**Fig 3.21**). Non-specific reduction in inhibition with $GABA_AR$ blocker bicuculine drastically increased the number of PCs responding to the air-puff and their duration (**Fig 3.22**), suggesting that other inhibitory synapses in CA1 also contribute to the control of PC population activity during aversive sensory events.

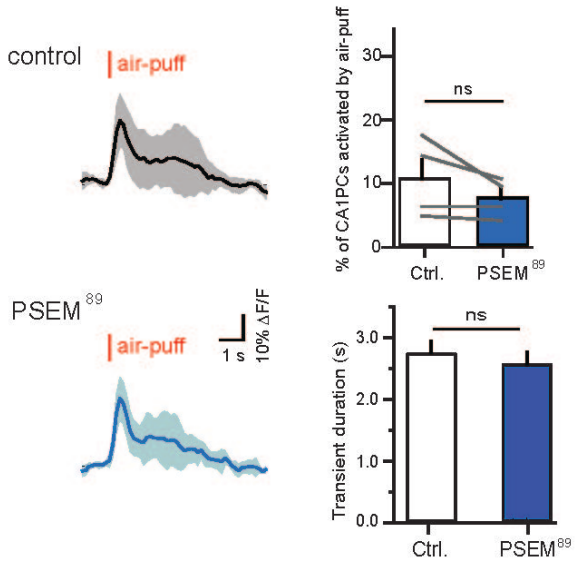

Figure 3.21 - Effects of local PSEM on PC populations in control mice. PSEM^{89} does not alter the mean % of active cells during air-puffs (ctrl: 10.1 ± 2.6%, PSEM^{89}: 7.1 ± 1.3%, n=4 FOVs; paired t-test) or the duration of air-puff-evoked transients in cells active in both drug conditions (ctrl: 2.73 ± 0.2s, PSEM^{89}: 2.56 ± 0.2s, n = 21 cells; paired t-test) in mice that do not express PSAM^{L141F}-GlyR. Bars represent mean ± s.e.m , ns = non-significant

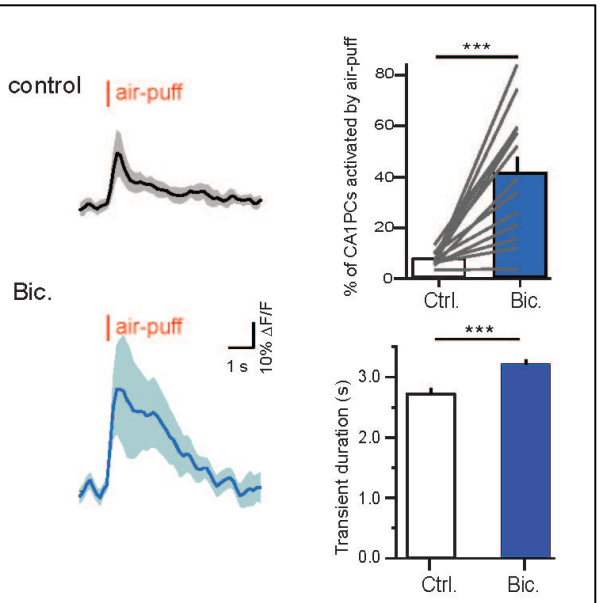

Figure 3.22 - Effects of local bicuculine on PC populations. 20 μM Bicuculine increases the mean % of active cells during air-puffs (ctrl: 7.6 ± 0.7%, Bic.: 41.3 ± 6.7%, n=13 FOVs; paired t-test) and the duration of air-puff-evoked transients in cells active in both drug conditions (ctrl: 2.72 ± 0.09 s, Bic: 3.21 ± 0.09 s, n = 114 cells; paired t-test). Bars represent mean ± s.e.m., ***p < 0.001.

US-driven dendritic inhibition in CA1 is required for CFC

Our imaging data suggest that Som+ interneurons are required for CFC because of their activation during the US. To test this hypothesis directly in a conventional CFC task, we used optogenetic methods in freely moving mice to inactivate Som+ interneurons selectively during the footshock US. We expressed the light-gated Cl^- pump halorhodopsin (*eNphR*; Zhang et al., 2007) in Som+ interneurons by injecting rAAV(*Synapsin-eNpHR3.0-eGFP*)^{cre} bilaterally into dorsal CA1 of *Som-cre* mice and implanting optic fibers over the injection sites (**Fig 3.23a**). Illumination of

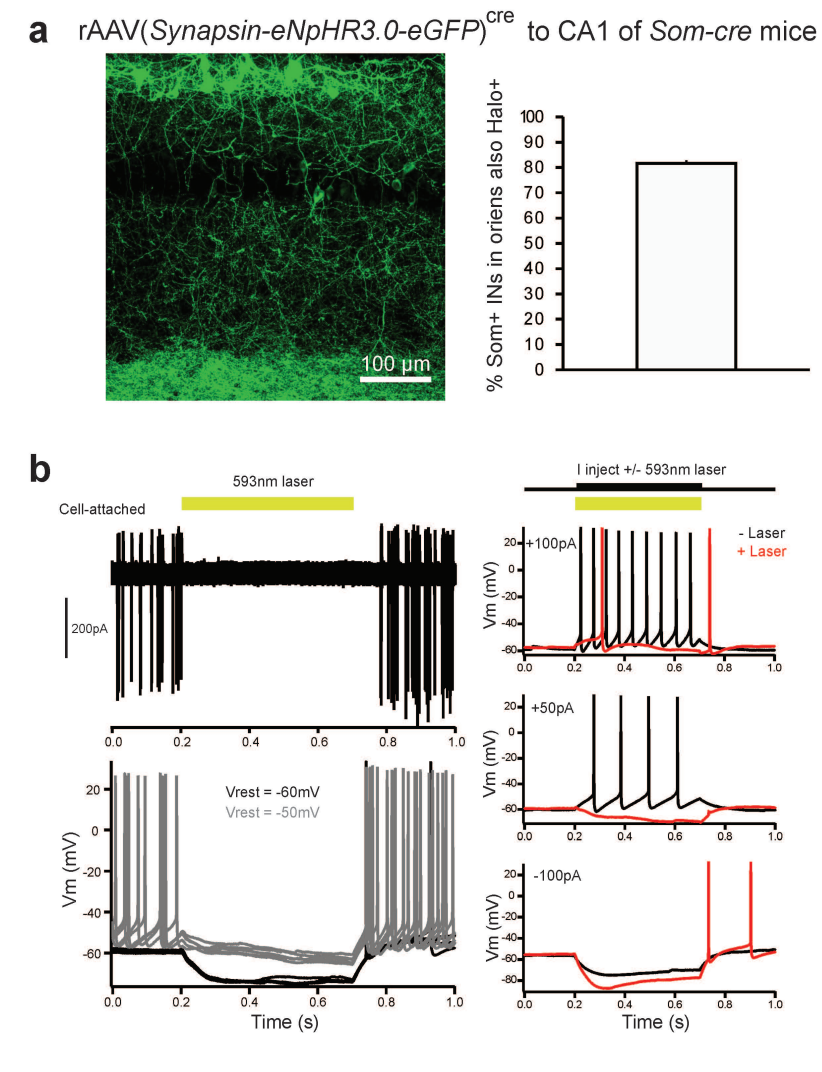

Figure 3.23 - Expression of eNpHR3.0-eGFP in CA1 Som+ interneurons. a) Left: example confocal image of eNpHR3.0-eGFP expression in dorsal CA1 of injected *Som-cre* mice. Right: Mean % of cre/tdTomato+ cells in *oriens* that are also eNpHR3.0-eGFP+. **b)** Top left: Example cell-attached recording from Som+/eNpHR3.0-eGFP+ neuron *ex vivo*, showing suppression of spontaneous spiking with 593 nm light (5 sweeps overlayed). Bottom left: Example whole-cell current clamp recording from Som+/eNpHR3.0-eGFP+ neuron *ex vivo*, showing hyperpolarization with 593 nm laser light at two resting voltages (5 sweeps overlayed). Right: example whole-cell current clamp recordings from Som+/eNpHR3.0-eGFP+ neuron *ex vivo*, with overlapping laser light and current injection.

Som+/eNpHR3.0+ neurons *in vitro* with 593nm light effectively suppressed spiking (**Fig 3.23b**). In bilaterally infected and implanted mice, we used a CFC paradigm with two footshocks, which were each accompanied by coincident illumination of dorsal CA1 with 593 nm light (**Fig 3.24a,b**). Inactivating Som+ interneurons during the US significantly reduced conditioned freezing 24 hours later compared to controls injected with rAAV(*Synapsin-eGFP*)^{cre} (**Fig 3.24c**). Importantly, shifting the optical suppression

ofSom+ interneurons to 30 s before each US did not reduce freezing (**Fig 3.24b,c**). This result indicates that suppression of inhibition from CA1 Som+ interneurons during the US is sufficient to prevent learning.

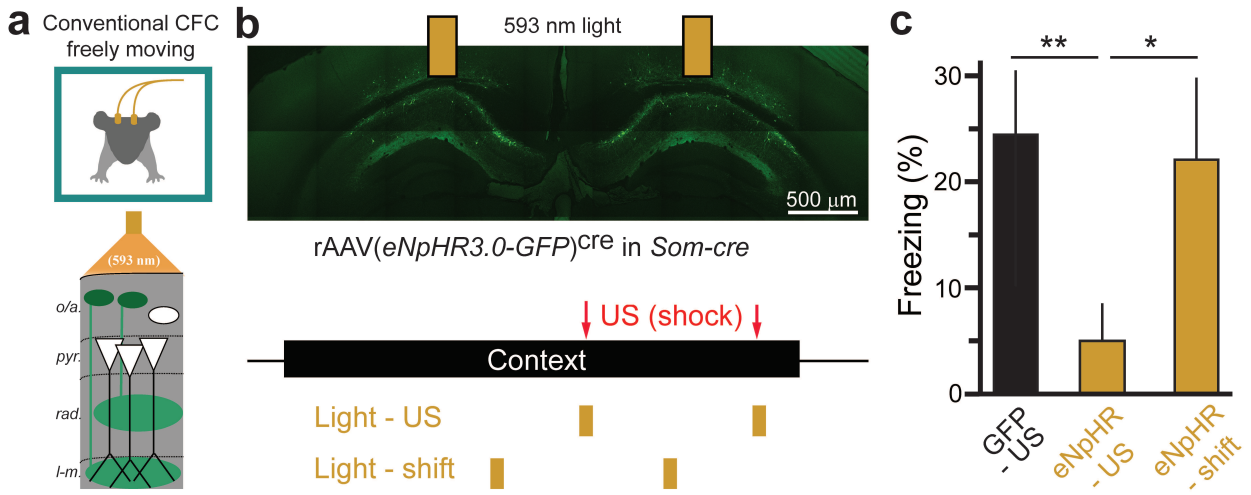

Figure 3.24 - Inactivating CA1 Som+ interneurons during the US alone is sufficient to prevent CFC. **a)** Schematic of optogenetic experiments in freely-moving mice. Bilateral optic fibers deliver 593 nm light to inhibit eNpHR3.0-eGFP-expressing Som+ interneurons in CA1 during CFC in freely-moving mice. **b)** Top: confocal image of eNpHR3.0-eGFP-expressing Som+ interneurons in dorsal CA1, and indication of optic fiber implants. Bottom: experimental protocol. Mice are exposed to a context for 3 min, with two footshocks (2 s, 1 mA) 118 s and 178 s into the context. Two pulses of 593 nm light (6 s) were delivered through bilateral optical fibers starting at 116 s and 176 s (Light-US group) or 86 s and 146 s (Light-shift group). **c)** Summary data for optogenetic stimulation experiments (*GFP-US,* n=6 mice; *eNpHR-US,* n=8 mice; *eNpHR-shift,* n=6 mice; 1-way ANOVA, $F_{(2,19)} = 3.87$, $p<0.05$; comparisons are unpaired t-tests). Bars represent mean ± s.e.m., *p < 0.05, **p < 0.01.

Discussion

An alternative model for hippocampal sensory processing in CFC

Classical fear conditioning implies a separation of CS and US prior to their association in the amygdala (LeDoux, 2000; Maren, 2001; Fanselow & Poulos, 2005). In the case of cued fear conditioning (e.g. tone & shock), the brain achieves CS-US segregation by separate anatomical pathways for auditory and aversive somatosensory inputs (Romanski & LeDoux, 1993; Shi & Davis, 1999; Lanuza et al., 2004). Standard models of CFC also assume the hippocampus does not receive information about the US; rather, the hippocampus encodes the CS alone, whose outputs to the amygdala can be paired with the US for associative conditioning (**Fig 3.25a**). However, here we observe a direct cortical excitatory input to CA1 during the US via the EC, indicating an anatomical overlap between sensory information for CS and US prior to the amygdala (Brankack & Buzsáki, 1986; Burwell & Amaral, 1998). This US input may impede conditioning (Fanselow et al., 1993). We suggest an alternative conceptual model to understand hippocampal sensory processing during CFC. We propose that subcortical neuromodulatory input drives CA1 Som+ interneurons to selectively inhibit the excitatory input pathway carrying US information to CA1. Compartmentalized inhibition suppresses dendritic integration of excitatory input to PC distal dendrites to reduce US-evoked CA1 PC activity, which may limit interference of the US with CS encoding. This circuit ensures hippocampal output reliably encodes the CS during learning, so that memories stored downstream in the amygdala can be re-activated by exposure to the CS alone (**Fig 3.25b**).

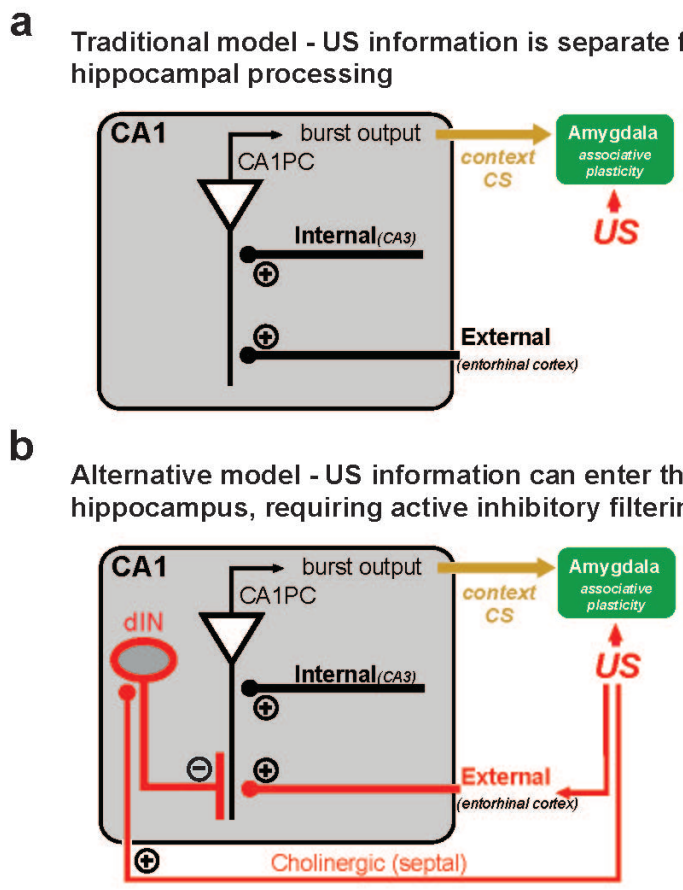

Figure 3.25 - Alternative model for hippocampal sensory processing during CFC. **a)** Traditional view of CFC. The hippocampus processes the context CS independent of the sensory features of the US. **b)** Alternative model of CFC. Sensory information about the US can reach CA1 through direct inputs from the entorhinal cortex, requiring active filtering. The US also sends parallel signals to the medial septum cholinergic system, which excites CA1 dendrite-targeting interneurons to prevent US signals from influencing hippocampal CS processing.

Inactivating Som+ interneurons both increases CA1 PC activity and prevents learning. Impairments in memory storage could result from a disruption of the hippocampal ensemble identity, or in the sparsity of contextual representations (Gdalyahu et al., 2012). The downstream mechanisms by which associative fear memories are impaired by CA1 Som+ interneuron inactivation can be addressed by study of CS-US convergence and plasticity in the amygdala. Alternatively, Som+ interneurons may also exert their effects through their long-range disinhibitory influences over the septum or EC (Toth et al., 1993; Gulyas et al., 2003; Melzer et al., 2012). Furthermore, it remains to be determined how this circuit mechanism contributes

to long-term changes in CA1 PC activity following fear conditioning, such as place-cell remapping (Moita et al., 2004).

Achieving segregated neural processing in anatomically overlapping circuits with dendritic inhibition of input pathways

Our data suggests that inhibitory circuits can inhibit selected dendritic compartments to favor integration of the proximal excitatory input pathway over the distal pathway. GABA release localized to *lacunosum-moleculare* could accomplish this input segregation by inhibiting localized dendritic electrogenesis, which is required for propagating distal EC excitatory inputs to drive output spikes and for inducing synaptic and intrinsic plasticity (Golding et al., 2002; Jarsky et al., 2005; Dudman et al., 2007; Losonczy et al., 2008; Takahashi & Magee, 2009). This mechanism may also be present in sensory neocortex, where aversive footshocks activate cholinergic input to drive layer I interneurons in primary auditory and visual cortex (Letzkus et al, 2011). Layer I interneurons inhibit the apical tuft dendrites of layer V PCs, the primary output cell of the neocortex, at the site of multimodal association in layer I (Palmer et al., 2012a). Therefore the same mechanism we describe in CA1 could protect layer V PCs in primary sensory cortex from interference by the US, so that their outputs to the amygdala are driven by inputs to their basal dendrites reflecting local sensory processing (Constantinople & Bruno, 2013), rather than inputs to tuft dendrites reflecting cross-modal influences.

In conclusion, out results suggest that dendrite-targeting Som+ interneurons provide US-evoked inhibition to CA1 PC distal dendrites that is required for successful

contextual fear learning. These interneurons are central to a mechanism by which the hippocampus processes contextual sensory inputs as a CS while excluding the sensory features of the US. Selective inhibitory control over integration of excitatory input pathways could be a general strategy for nervous systems to achieve separate processing channels in anatomically overlapping circuits, a process that could be flexibly controlled by a multitude of inhibitory cell types (Freund & Buzsáki, 1996; Klausberger & Somogyi, 2008) and neuromodulatory systems (Bargmann, 2012; Marder, 2012).

Experimental Procedures

All experiments were conducted in accordance with the US National Institutes of Health guidelines and with the approval of the Columbia University (to A. Losonczy) and New York State Psychiatry Institute (NYSPI, to R. Hen and M. Kheirbek) Institutional Animal Care and Use Committees.

Mice and virus details

In all experiments we used adult mice of either sex, that were either wild-type C57/Bl6 mice, ChAT-cre mice (Jackson, #006410), or the hemizygous offspring of Som-cre or Pvalb-cre mice with the Ai9 reporter line (loxP-STOP-loxP-tdTomato Cre reporter strain B6;129S6-Gt(ROSA)26Sortm9(CAG-tdTomato)Hze/J (Jackson Laboratory)) on a C57/Bl6 background, have previously reported (Lovett-Barron et al., 2012).

We used the following viruses: rAAV2/1(*Synapsin-PSAM*^{L141F}*-GlyR*), rAAV2/7(*Synapsin-PSAM*^{L141F}*-GlyR*)^{cre} (*21,26*), rAAV2/1(*Synapsin-GCaMP5G*) (*25,30*), rAAV2/7(*Synapsin-GCaMP5G*)^{cre}, rAAV2/1(*Synapsin-GCaMP6f*), rAAV2/7(*Synapsin-GCaMP6f*)^{cre} (*51*; Penn vector core), rAAV2/7(*Synapsin-eNpHR3.0-eGFP*)^{cre}, rAAV2/7(*Synapsin-tdTomato*)^{cre}, or rAAV2/7(*Synapsin-eGFP*)^{cre}. For targeting ChAT+ neurons in the medial septum, rAAV2/1(*ef1α-DIO-GCaMP6f*)^{cre} was created by cloning the GCaMP6f gene (Addgene 40755) into the Cre-conditional vector, rAAV-*ef1α*-DIO-hChR2(H134R)-EYFP-WPRE-pA (Addgene 20298), replacing the existing hChR2-EYFP insert. Restriction sites 5' NheI and 3' AscI were used, and only the core of GCaMP6f was maintained after removing the 5' 6xHis tag. A chimeric serotype 1+2 of AAV was prepared (McClure et al., 2011) for stereotaxic injection. This specific serotype and viral promoter were required to gain reliable expression in ChAT-positive cells, as

synapsin (serotypes 2/1 & 2/7) and *CAG* (serotype 5) viruses were ineffective for labeling these neurons. Stereotaxic viral injections were performed using a Nanoject syringe, as described previously (Lovett-Barron et al., 2012; Kaifosh et al., 2013). Recordings from eNpHR3.0-GFP/Som+ interneurons in CA1 were performed as described previously (Lovett-Barron et al., 2012), and cells were stimulated using the same 593 nm laser used for *in vivo* experiments.

Surgery

Hippocampal imaging window

Hippocampal window implant surgeries were performed as described previously (Dombeck et al., 2010; Kaifosh et al., 2013). Briefly, we anesthetized mice with isofluorane and treated them with buprenorphine (0.1 mg/kg, subcutaneous) to minimize post-operative discomfort. We exposed the skull and drilled a 3-mm diameter circle centered over left dorsal CA1, matching the size of the cannula window to be implanted. We removed the bone and dura, and then slowly aspirated cortex covering the hippocampus while constantly irrigating with chilled cortex buffer until the external capsule was exposed. If the alveus (anterior-posterior fibers) became exposed, surgery was terminated. Otherwise, we implanted the sterilized window implant by wedging it into place, and secured the top of the cannula to the skull and stainless steel headpost with grip cement (Dentsply), leaving it to dry for 15–20 min before returning mice to the home cage (awake and mobile in 5–20 min). We monitored mice every 12 hours for three days after surgery, administering buprenorphine to minimize any signs of discomfort.

Optical fibers

We used published techniques for the construction of chronically dwelling optical fibers and patch cables for optogenetic behavioral procedures (Kheirbek et al., 2013). For all experiments, a 200 μm core, 0.37 numerical aperture (NA) multimode fiber (ThorLabs) was used for optical stimulation via a patch cable connected to either a 100 mw 593.5 or 473 nm laser diode (OEM laser systems). Adult mice were surgically implanted with fiber optic cannulas using published protocols (Khierbek et al., 2013).

Head-fixed stimulus presentation and behavioral readout

We developed a flexible system for combining two-photon imaging with microcontroller-driven (Arduino) stimulus presentation and behavioral read-out, as previously described (Kaifosh et al., 2013). Briefly, tones were presented with speakers near each of the mouse's ears, light flashes lasting 200 ms were delivered with a red LED, and odor stimuli and air-puffs were delivered via separate solenoid valves (NVZ110-6H-M5, SMC) to gate airflow from a compressed air tank to a tube ending in a pipette tip facing the mouse's snout. Odor was delivered with lower pressure air, and passed through a filter covered in a 50:50 mixture of odorant with mineral oil (50 μL). We tracked locomotion by measuring treadmill wheel rotation, recorded as changes in voltage across an infrared photo-transistor as wheel spokes blocked light from an infrared LED. Electrical signals encoding mouse behavior and stimulus presentation were collected with an analog to digital converter (NI USB-6229 DAQPAD, National

Instruments), which was synchronized with two-photon imaging by a common trigger pulse.

We used headpost-implanted adult mice for all experiments. In the case of hf-CFC experiment, starting 3–7 days after implantation we water-restricted mice (>85% pre-deprivation weight) and habituated them to handling and head-fixation. Within 3 or 4 sessions, mice could undergo extended head-fixation while appearing calm, but alert, and periodically running while freely licking for small-volume (~0.5 µl/lick) water rewards during imaging sessions. During the hf-CFC task, mice could lick for water for 4.5 min – 1 min pre context, 3 min context, and 30 s post-context. This protocol was repeated twice a day for three days, with 1-3 hours between each context.

For discrete stimulus presentation, we habituated mice to handling and head-fixation, but did not water-restrict them. We used a variable inter-stimulus interval of 20–40 s between stimuli, which were repeated 5–10 times for each modality in a pseudorandom order. To characterize responses to air-puffs of varying durations, we repeated stimulation with durations from 10 ms to 500 ms; each level was presented 3 times, interspersed with 200 ms tones.

Freely-moving behavior

Fear Conditioning – PSAM^{L141F}-GlyR experiments

Fear conditioning took place in fear-conditioning boxes (Coulbourn Instruments) that contained one clear plexiglass wall, three aluminum walls, and a stainless steel grid as a floor. All mice were injected with PSEM^{89} (60 mg/kg i.p. in saline) 15 min prior to conditioning. The training session began with the onset of the houselight and fan, and

anise scent was placed under the grid floor. In this one-trial contextual fear conditioning protocol, 180 s after placement of the mouse in the training context and onset of houselight and fan, mice received a single 2 s footshock of 1 mA. All freezing was measured before the single footshock. The mouse was taken out 15 s after termination of the footshock and returned to its home cage. The grid and the waste tray were cleaned with Sanicloths between runs. The recall session occurred 24 hours later in the same chamber, but without PSEM^{89} injection or footshocks. Mice were recorded by video cameras mounted above the conditioning chamber and were scored for freezing by an investigator blind to the experimental condition of the animal.

Fear Conditioning – Tone conditioning

All mice were injected with PSEM^{89} (60 mg/kg i.p. in saline) 15 min prior to conditioning. For cued fear conditioning, mice were trained in the same context as in CFC, except that a 20 s, 80 dB, 2 kHz pure tone was provided as the discrete cue CS, and a 2 s footshock (1 mA) that co-terminated with the tone was provided. This was repeated four times. Twenty-four hours later, mice were tested for cued fear in a novel context, in which the conditioning chamber was altered, the stainless steel grid floor was covered with a plastic panel and novel cage bedding, the chamber walls were covered and made circular using colored plastic inserts, the house fan and lights were turned off, and a lemon was used. The tone was presented four times (20 s each), and an investigator blind to condition scored freezing before during each tone presentation as a measure of cued fear.

Fear Conditioning – Optogenetic experiments

In the case of optogenetic manipulations during conditioning, mice were quickly attached to the fiber optic patch cables (bilaterally) via a zirconia sleeve, then placed in a novel cage bottom for five minutes prior to being placed in the testing apparatus. The patch cables were interfaced to an FC/PC rotary joint (Doric lenses), which was attached on the other end to a 593 nm laser diode that was controlled by a Master-8 stimulator (AMPI), as previously described (Khierbek et al., 2013). In these experiments, mice were exposed to two 2 s shocks (1 mA) separated by one minute; shocks were paired with 6 s optogenetic stimulation (593 nm) centered over the shock (Light-US condition) or shifted 30 s before each shock (Light-shift condition). All mice were processed for histology, and subjects were excluded from the study if the implant entered the hippocampus, if viral infection was not complete, or if the viral infection was not limited to CA1 Som+ interneurons.

Delayed non-match to sample

Mice were food-restricted for 1 day prior to experiments. Mice pursued sweetened condensed milk rewards (50% dilution, 30 µL; Deacon & Rawlins, 2006). Mice were injected with 60 mg/kg PSEM^{89} i.p., and tested in a delayed non-match to sample task in a y-maze from 10-35 min post-injection. Mice performed 10 trials, in which the mouse began in the start box, and consisting of a sample phase (shuffling of location across trials), a 30 s delay phase in the start box, and a sample phase, where the correct response is to go to the arm not yet visited. Between trials mice were moved to a clean cage for 60 s, and the location of the sample arm was shuffled.

Animals were scored as the % correct trials, and trials were omitted if mice took >90 s on the sample phase, or >120 s on the choice phase.

Two-photon imaging

We use an *in vivo* X-Y galvanometer-mounted mirror-based multi-photon microscopy system (Ultima, Prairie Technologies) and an ultra-fast pulsed laser beam (920-nm wavelength; Chameleon Ultra II, Coherent, 20–40 mW average power at the back focal plane of the objective) controlled with an electro-optical modulator (Model 302 RM, Conoptics) to excite GCaMP and tdTomato through a 40X objective (Nikon NIR Apo, 0.8 NA, 3.5 mm WD). Distilled water or warmed cortex buffer (in the case of acute pharmacology experiments) served to connect the water immersion objective with the cannula. Green and red fluorescence were separated with an emission filter cube set (green, HQ525/70m-2p; red, HQ607/45m-2p; 575dcxr, Chroma Technology). Fluorescent light was detected with photomultiplier tubes (green GCaMP fluorescence, GaAsP PMT, Hamamatsu Model 7422P-40; red tdTomato fluorescence, multi-alkali PMT, Hamamatsu R3896) operated with PrairieView software (Prairie). Once mice were head-fixed, we used goniometers (Edmund Optics) to adjust the angle of the mouse's head up to 10 degrees to make the imaging window parallel to the objective. Time Two series were collected in red (tdTomato signal) and green (GCaMP signal) channels at 256 × 128 pixels covering 150 × 150 μm at 7.63 Hz (cell bodies, interneuron axons), or 256 × 256 pixels covering 75 × 75 μm at 4.02 Hz (CA3, EC, and ChAT+ axons). Time-series were motion-corrected as described in Kaifosh et al. (2013), adapted from methods established in Dombeck et al. (2007). Regions of interest (ROIs) were

manually drawn over corrected time-series in Image J (NIH), to isolate the somas or axons of cells of interest. Trials with running were excluded from summary analyses of sensory responses in interneurons and excitatory axons.

Local pharmacology during two-photon imaging

For local pharmacology experiments, we replaced the glass coverslip with a plastic coverslip with a punctured hole (~200 μm diameter) (Kaifosh et al., 2013). This hole was plugged by a plastic bar or Kwik-Sil (World Precision Instruments). Instead of waiting several days to perform experiments, mice were habituated and tested 1–5 days after implants. Before imaging, we removed the plastic plug and filled the cannula with warmed (~32 °C) cortex buffer (125 mM NaCl, 5 mM KCl, 10 mM glucose, 10 mM HEPES, 2 mM $CaCl_2$ and 2 mM $MgCl_2$). After control imaging, we filled the cannula and fluid well for the objective with cortex buffer containing dissolved scopolamine (Sigma, 1 mM), pirenzepine (Tocris, 0.01-1 mM), mecamylamine (Tocris, 1 mM), NBQX (Tocris, 20 μM), PSEM^{89} (500 μM), or bicuculine (Sigma, 20 μM) and allowed 30-90 min for drug diffusion before imaging. The imaging window hole could be re-plugged with Kwik-sil so that mice could be used for up to three consecutive days.

Identification of significantly responding PCs

Approximately 150-200 ROIs were drawn over putative PCs for each field of view. Statistically significant calcium transients were identified automatically using an approach similar to that described by Dombeck *et al*. (2007). Briefly, negative deflections in the $\Delta F/F$ trace are assumed to be due to motion out of the z-plane.

Because cells should move into the imaging plane with the same frequency they leave this plane, positive and negative deflections in the $\Delta F/F$ curve that are attributable to motion should occur at the same frequency. Therefore we calculate a false positive event detection rate by dividing the number of negative deflections for a given amplitude and duration by the number of positive deflections at the same magnitude and duration. As signal-to-noise ratio can vary on a per-cell basis, event amplitudes are calculated in terms of the standard-deviation (σ) of the $\Delta F/F$ trace, which provides an estimate of noise for the cell. Transient onsets are defined as the times when the $\Delta F/F$ exceeds 2 σ, and offset is defined as the time at which $\Delta F/F$ falls below 0.5 σ. A decaying exponential was least-squares fitted to the false positive rate values, allowing for the determination of a minimum transient duration at each σ level at different confidence levels.

We analyzed sensory responses in PCs using peri-stimulus-time-histograms (PSTHs). To calculate PSTHs, a binary activity function of time was computed for each cell, indicating whether it was in a significant calcium transient (95% confidence). Time series were aligned by stimulus time, and the binary-activity functions across stimulus presentations were averaged at each time point in a window +/- 20 frames from the stimulus, yielding a PSTH of the binary activity function for each cell and stimulus. The response-value was defined as the mean of the 20 post frames minus the mean of the 20 pre frames. To assess confidence, alignment times were shuffled 10,000 times, yielding a distribution of response-values. A cell was deemed significantly responsive if the true response-value exceeded the 99^{th} percentile of the shuffle distribution. For significantly-responsive cells, PSTHs of the $\Delta F/F$ traces were computed similarly. For

the analysis of PSEM and bicuculine effects on PC population (**Figs 3.20, 3.21,** and **3.22**, fields of view containing fewer than 3% responsive cells were omitted.

Immunohistochemistry and confocal imaging

After imaging experiments, virally-injected mice were deeply anesthetized with isofluorane and perfused with 4% paraformaldehyde dissolved in 0.1 M phosphate-buffered saline (pH = 7.4). Brains were removed, sectioned at 50-60 μm and either mounted for confocal microscopy or processed for immunofluorescence staining. In mice expressing PSAM^{L141F}-GlyR, we performed immunostaining of the hybrid PSAM^{L141F}-GlyR channel as detailed previously (*21,25*), using Alexa 647–conjugated α-bungarotoxin (α-BTX, 1:3000, Invitrogen), selective for the mutated α7-nAChR receptor binding site of PSAM^{L141F}-GlyR. Confocal stack images (40–50 slices, 1-2 μm optical thickness) were collected from dorsal CA1 region with a 20X objective. Stacks were collapsed into one z-plane, and cell bodies that were labeled for tdTomato and/or α-BTX Alexa 647 were counted in the *oriens/alveus* and/or *pyramidale* layers of CA1 (ImageJ, US National Institutes of Health), allowing for quantification of the density and overlap of neuronal expression. In mice expressing GCaMP6f in ChAT+ cells of the medial septum, slices were immunostained with ChAT antibodies (AB144P; Millipore; 1:500 dilution) and detected with 1:500 concentration of anti-goat DyLight 649 (Jackson ImmunoResearch). Confocal tile-stack images (2,535 slices, 1 μm optical thickness) from the medial septum were acquired using a (20X objective), and counted for GCaMP6f and ChAT co-localization as described above.

Data analysis

hf-CFC was scored by automated measurement of the rate of licks in each context (capacitive transients measured from metal water port), as described previously (Kaifosh et al., 2013). Freely-moving conditioning was assessed by freezing scored by a trained observer blind to the experimental condition. Head-fixed contextual fear conditioning behavioral data, delayed non-match to sample behavioral data, and responses by stimulus and cell type were analyzed with two-way ANOVA, with repeated measures in cases that the same subject was used across multiple conditions. Pair-wise comparisons were performed with sign tests for paired data and Mann-Whitney U tests for unpaired data. Sign tests were used to assess pharmacological effects on calcium responses, and Mann-Whitney U tests were used to assess pharmacogenetic effects on head-fixed contextual fear conditioning and differences in running-related activity across cell types. PC population imaging data was analyzed with paired or unpaired t-tests in the cases of % active cells and transient durations, respectively. Statistical tests on imaging data were performed treating each field-of-view as an independent observation by averaging the responses from all simultaneously imaged ROIs. Statistical comparisons were 1-way or 2-way ANOVAs, with pairwise sign tests or unpaired Mann-Whitney U tests, or paired and unpaired t-tests. All tests were two-sided, and the type of statistical test is noted in each case. All summary data are presented as mean ± s.e.m. *$p<0.05$, **$p<0.01$, ***$p<0.001$.

Experiments described in Chapter 3 are in press:

Lovett-Barron M, Kaifosh P, Khierbek MA, Danielson N, Zaremba JM, Turi GF, Reardon TR, Hen R, Zemelman BV, and Losonczy A. (2014) Dendritic Inhibition in the Hippocampus Supports Fear Learning. *Science*, **in press**.

Data from Figs 3.16 and 3.17b have been published in:

Kaifosh P, Lovett-Barron M, Turi GT, Reardon TR, and Losonczy A. (2013). Septo-hippocampal GABAergic Signaling across Multiple Modalities in Awake Mice. *Nature Neuroscience,* **16**, 1182-1184.

Chapter 4 - Conclusions and Discussion

Control of Dendritic Spikes and Burst Output with Dendritic Inhibition

Behavior requires the cooperative interaction of multiple regions of the brain. Determining how different brain regions receive, process, and send information is critical to understanding what brains do and how they do it. This problem can be fist addressed by studying how individual brain regions within large-scale networks use their local circuitry to transform inputs into outputs. Hippocampal area CA1 is a convenient circuit to study this problem, as the excitatory inputs are segregated into distinct strata, and the output at the population level is determined by the responses of many PCs acting as relatively independent processing channels, due to negligible recurrent connectivity. In *Chapter 2* of this thesis, we recorded from single CA1 PCs under controlled conditions *in vitro* to determine how PCs transform CA3 SC synaptic input into action potential output, and the relative contribution of perisomatic-targeting Pvalb+ interneurons and dendrite-targeting Som+ interneurons to this transformation. We found that Som+ interneurons play an essential role in controlling the gain of PC i-o transformations, by suppressing high-frequency burst spikes that are generated via dendritic electrogenesis (Lovett-Barron et al., 2012), a finding that was confirmed *in vivo* (Royer et al., 2012). Therefore we found that one aspect of i-o transformations, gain control, is modulated by a particular subtype of local interneuron.

Prior to our publication of the results from *Chapter 2* (Lovett-Barron et al., 2012) and the result of others (Royer et al., 2012; Gentet et al., 2012), the inhibitory regulation of i-o gain had been largely attributed to somatic inhibition (but see Mehaffey et al., 2005; Capaday & van Vreeswilk, 2006). This belief stems from the view that if the site of transformation from graded membrane polarization into binary action potentials is the

axon initial segment, then inhibition to this region should control the slope of the i-o relationship (Vu & Krasne, 1992). This has indeed been observed in several experimental conditions (Pouille et al., 2009; Atallah et al., 2012; Lee et al., 2012; Wilson et al., 2012;). However, not all modes of spiking are necessarily generated through integration at the perisomatic compartment. As we have reviewed above, burst spikes in PCs are generated in the dendrites (Kamondi et al., 1998; Larkum et al., 1999), through local NMDAR and/or Ca^{2+} dependent electrogenesis. Burst spikes and dendritic spikes are not likely to be recruited under the conditions of the experiments described above, which may account for their conclusions that somatic inhibition mediates gain control. For instance, dendritic nonlinearities and burst spikes are often not generated *in vitro* from current injection at the soma or brief synaptic input, or *in vivo* under conditions of anesthesia (Murayama & Larkum, 2009; Xu et al., 2012a).

Therefore, studying the same neural circuits under experimental conditions conducive to dendritic spike generation and bursting may enhance the capacity for experimenters to observe inhibitory regulation of dendritically-generated burst events (Lovett-Barron & Losonczy, 2014). In hippocampal and neocortical PCs, these conditions include active behavioral engagement *in vivo* (Royer et al., 2012; Gentet et al., 2012; Xu et al., 2012a) or strong dendritic depolarization *in vitro* (Miles et al., 1996; Kamondi et al., 1998; Larkum et al., 1999; Losonczy et al., 2006; Lovett-Barron et al., 2012). These factors may account for discrepancies amongst studies investigating the inhibitory interneurons that control spiking activity. If the preparation (*in vitro* or *in vivo*) is not conducive to the generation of dendritic spikes, then the experimenters are more likely to find that somatic inhibition controls the gain, because spikes will be exclusively

generated at the axosomatic spike generation zone. If the preparation allows for the generation of dendritic spikes, then experimenters may be more likely to find that dendritic inhibition plays a role in controlling burst spike initiation in the dendrites.

In morphologically complex neurons such as PCs, distinct forms of spiking can be modulated by synaptic and intrinsic conductance at distinct subcellular compartments (eg. precise spike timing is mediated by fast integration of excitation and inhibition at the perisomatic compartment; burst spiking is mediated by slow integration of excitation and inhibition at the dendritic compartment via dendritic spikes). While the stimulating parameters used in our study may be particularly suited to detecting control over burst spiking - due to sustained, distributed dendritic excitation without much temporal modulation - *in vivo* conditions are more likely to require concurrent inhibitory modulation over several types of neural spiking patterns. This is supported by the findings of Royer et al. (2012) in behaving mice, where Som+ interneurons were found to control place cell bursting, and Pvalb+ interneurons were found to control place cell phase precession, but both contributed to the control over firing rate, albeit at different parts of the place field. These findings indicate that the multitude of available inhibitory interneurons types work together to flexibly manage the many neural coding schemes present in the spiking activity of PCs at any given time. Understanding the complex interactions between all these interneuron types will likely be required to fully comprehend the perceptual, cognitive, and behavioral consequences of PC spiking patterns.

Temporally Restricted Dendritic Inhibition Enforces CS-US Segregation in the Hippocampus during Fear Conditioning

Based on our findings that Som+ interneurons control burst spiking in hippocampal CA1 output neurons, we next sought to determine their role in CFC - a classical Pavlovian learning task that depends on hippocampal burst spiking (Xu et al., 2012b). We examined these issues in *Chapter 3*. Like other forms of associative Pavlovian fear conditioning, models of CFC depend on the separation between CS and US prior to their associative pairing.

In mammals, associative pairing occurs in the basal and lateral amygdala, and therefore upstream regions are believed to process each of these stimuli separately, as is the case with classical cued fear conditioning through tone (CS) – shock (US) pairings. Tone information is relayed to the basolateral amygdala via cortical (primary auditory cortex) and/or thalamic afferents (medial geniculate nucleus), and shock information is relayed to the basolateral amygdala through separate cortical (insular cortex) and thalamic (posterior intralaminar nuclei) afferents (Romanski & LeDoux, 1993; Shi & Davis, 1999; LeDoux, 2000; Maren, 2001; Sah et al., 2003; Lanuza et al., 2004). These two segregated inputs - CS and US - then proceed to converge on common amygdala neurons, where the paired depolarization and induced spiking allows for associative synaptic plasticity at the afferent synapses (LeDoux, 2000; Maren 2001; Fanselow & Poulos, 2005). This plasticity therefore permits these engram-bearing amygdala neurons to be re-activated by exposure to the CS alone, whose inputs now evoke larger currents to drive output spikes (Blair et al., 2001) and cause defensive behaviors evoked downstream of the amygdala via the central nucleus.

For a similar circumstance to exist in the case of CFC, the context must be processed separately from the US prior to its association in the amygdala. Instead of being processed by unimodal sensory regions of the thalamus and neocortex, the CS in CFC is processed by the hippocampus. However, when the CS is processed by multimodal processing centers, including the hippocampus and some regions of neocortex, there is evidence for the presence of sensory features of both CS and US (Brankack & Buzsáki, 1986; Khanna 1997; Letzkus et al., 2011; Lipski & Grace, 2013; Pi et al., 2013). In *Chapter 3*, we present evidence that excitatory entorhinal cortex inputs to CA1 PCs are activated by the US, and thus require a spatiotemporally matched inhibitory input to prevent widespread excitation of PCs by the US. We find that this inhibition, from dendrite-targeting Som+ interneurons, is required for hippocampal contributions to CFC, and thus may be required to enforce the segregation of CS and US prior to associative pairing in the amygdala.

The hippocampus assembles the multiple sensory components of the environment into a unitary representation of 'context' or 'place', which is then sent to the amygdala for CS-US pairing (Maren & Fanselow, 1997; Rudy et al., 2004). This representation of context must be relayed to the amygdala, or any other non-hippocampal structure for that matter, via the primary hippocampal output neurons – CA1 PCs, often via the subiculum and/or entorhinal cortex. CA1 PCs can thus be seen as the conduit by which presynaptic regions of the hippocampus transmit signals to the rest of the brain.

In the case of CFC, this information will be the multisensory context - believed to be stored in the recurrent network of the CA3 region (Kesner, 2007), which is stabilized

over experience with the context, potentially through attractor dynamics (Colgin et al., 2008). CA1 PCs convey this contextual CA3 information via numerous synaptic contacts with their proximal dendrites (Megias et al., 2001; Ahmed & Mehta, 2008), while also receiving distal excitation from the entorhinal cortex pertaining to the current sensory environment, which typically matches the stored context under static environmental conditions. Under most circumstances CA1 PCs receive excitatory input from both pathways, and may be implementing a form of comparison through pathway interactions (Jarsky et al., 2005; Takahashi & Magee, 2009) before sending an output to the rest of the brain (either via the subiculum or deep-layer entorhinal cortex). However, at the moment of CS-US pairing, the current sensory environment is dominated by the salient US, and therefore is not a sensory attribute representative of the context CS. We found that at the moment of the US, subcortical cholinergic inputs drive OLM cells to inhibit the distal dendrites that receive entorhinal input, potentially to allow CA1 PCs to continue to be driven by the more proximal CA3 inputs without the influence of the distal entorhinal inputs. In fact, recent evidence suggests that activation of OLM cells increases feed-forward excitation from CA3 to CA1 PCs, by inhibiting *stratum radiatum* interneurons that target CA3-recipient dendrites (Leão et al., 2012). This inhibition could effectively compartmentalize the distal tuft dendrites to prevent the propagation of entorhinal inputs to drive output spikes and influence plasticity at proximal synapses receiving CA3 input (Jarsky et al., 2005; Dudman et al., 2007; Takahashi & Magee, 2009), while simultaneously sparing or augmenting synaptic transmission from CA3. This compartmentalized inhibition scheme may allow CA1 to favor the transmission of stored representations over sensory representations.

To provide more support for the hypothesized circuit model discussed above and schematized in **Fig.3.25**, future studies could focus on performing rescue experiments. Specifically, we hypothesize that the deficit in CFC we observe upon pharmacogenetic inactivation of Som+ interneurons in CA1 is because Som+ OLM cells are no longer able to inhibit the excitatory drive from the entorhinal cortex to CA1 PCs during the US. As a consequence, CA1 PCs are excited by a sensory attribute that is not part of the context CS, and thus the output to the amygdala that is stored through associative plasticity is not representative of the CS that will be encountered during future experience with that CS alone, diminishing the predictive nature of the CS and preventing later successful memory recall. Alternatively, this source of excitation may simply disrupt the sparse population code present in CA1, which may in itself be enough to prevent the accurate propagation of CS information to the amygdala. Therefore, under conditions of Som+ interneuron inactivation, we hypothesize that exogenous inactivation of entorhinal input to CA1 during the US alone should be sufficient to rescue this learning deficit.

Although this experiment would provide convincing support for our proposed model, we believe this particular rescue experiment is not technically feasible using presently available methods. Because entorhinal input to CA1 and the rest of the hippocampus is required for CFC except for the brief moments during the US, we would have to use temporally precise optogenetic methods to inactivate entorhinal inputs to CA1 during the US, rather than pharmacogenetic methods. We found that both the lateral and medial entorhinal cortex send axons to CA1 that are responsive to the US. Therefore any rescue strategy would have to involve optogenetic inactivation of the

entire bilateral entorhinal cortex during the US – which is not possible with the focal nature of light delivery to deep regions of the mouse brain using currently available technology. Even if we could deliver light to the entire bilateral entorhinal cortex, we would aim to inhibit layer III entorhinal inputs to CA1 while sparing layer II. Layer II inputs would have to be spared because its inactivation would severely reduce activity in the entire trisynaptic loop, thus preventing the CA3 input to CA1 PCs that must remain. Therefore selective optogenetic inactivation would require viral expression restricted to excitatory neurons in layer III of both lateral and medial entorhinal cortex, which would require development of a cre-driver mouse line. The appropriate mouse for this rescue experiment would require layer III excitatory neuron entorhinal cortex expression of cre, and also cre expression in Som+ interneurons of CA1 for the expression of PSAM-GlyR (but without cre expression in Som+ GABAergic interneurons of the entorhinal cortex, which project to CA1; Melzer et al., 2012) – an intersectional and region-specific cre-expression pattern that does not presently exist. However, given the rapid progress in molecular tool development for systems neuroscience, such an experiment could be possible in the future.

Alternatively, we could target virally transduced layer III axons by placing the optic fiber in CA1 to silence these axons alone. However, this approach suffers from two complications. First, the entorhinal axons are at the deepest layer of CA1, and thus full optical inhibition of these axons would be unlikely without placing the fiber into CA1 itself, and therefore damaging the entire circuit (which may cause CFC to become hippocampal-independent – for discussion see Fanselow, 2010). Second, even if we were able to illuminate these deep layer III entorhinal axons in CA1, we would also likely

illuminate the layer II entorhinal axons in the dentate gyrus, which are in the most superficial part of the dentate bordering CA1. However, the use of stronger light sources and red-shifted optogenetic probes may permit this experiment to be successfully implemented in the future when combined with the appropriate cre line. In summary, although this rescue experiment could provide support for the conceptual model we propose in *Chapter 3* of this thesis, the methods presently available to us make these experiments prohibitive.

The selective inhibition of external distal entorhinal input to CA1 PCs while sparing the internal proximal input may be a useful mechanism for the hippocampus to use in other circumstances. For instance, some behavioral conditions may benefit from reducing the influence of the current sensory environment on hippocampal output to instead favor internally stored representations. This could be the case in which the oscillatory activity in CA1 is coupled with CA3 more than entorhinal cortex, as in speculated in the case of coherent slow gamma frequency oscillations (~25-50Hz; Colgin et al., 2009). These states may favor the consolidation of previously acquired information over the acquisition of new information (Carr & Frank, 2012) – a functional state that could be flexibly implemented by subcortical activation of distal dendrite-targeting inhibitory interneurons.

This kind of selective integration scheme may also be present on faster timescales, such as during theta oscillations or during ripple events, where differential activity of interneuron subtypes has been reported (Csicsvari et al., 1999; Klausberger & Somogyi, 2008). For instance, PCs tend to fire during the trough of theta oscillations – out of phase with perisomatic-targeting interneurons whose rhythmic activity implements

local theta rhythms (Klausberger et al., 2003), at least under anesthesia. Both Som+ bistratified cells and Som+ OLM cells appear to fire in phase with PCs in anesthetized rats (Klausberger et al., 2003; 2004), potentially leading to balanced excitation and inhibition in PC dendrites during theta oscillations. However, Royer and colleagues (2012) reported different observations in awake navigating mice, where PC spiking was widely distributed across theta phase, and Som+ interneurons fire on the ascending phase of theta, rather than at the trough. This may indicate more variable influences of dendritic inhibition on PC integration in behaving animals, when input to these cells are dynamically modulated by changing environmental influences and neuromodulation. Therefore selective input inhibition during different phases of theta oscillations may occur in specific subsets of cells, rather than on the entire population.

Dendritic inhibition is believed to have differential effects during ripple oscillations as well, when subsets of PCs are known to be active (Csicsvari et al., 1999; Klausberger et al., 2003). In anesthetized rats, OLM cells have been demonstrated to reduce their activity during ripples (Klausberger et al., 2003), whereas bistratified cells increase their activity (Klausberger et al., 2004). This suggests a state where CA3 input is suppressed while EC input is favored for integration. This finding is supported by the observation of bimodal responses in Som+ interneurons in awake behaving mice (Royer et al., 2012), where these Som+ interneurons include both bistratified cells and OLM cells that presumably increase and decrease their activity during ripples, respectively. However, morphologically identified OLM cells were found to be activated by ripples in the awake head-fixed mouse (Varga et al., 2012), although with lower probability than strongly ripple-activated Pvalb+ basket cells. Therefore, the contribution of layer-

specific inhibition of input pathways during ripple events in CA1 is still debated, and will benefit from recording morphologically identified interneurons in behaving animals over a range of behavioral conditions (Lapray et al., 2012; Varga et al., 2012), using electrophysiological measurements that do not suffer from the poor temporal resolution of the Ca^{2+} imaging methods used in *Chapter 3*.

Dissociable Functional Roles for Inhibitory Interneuron Types

Based on concepts and predictions outlined in reviews of GABAergic interneuron structure (Freund & Buzsáki, 1996; Klausberger & Somogyi, 2008; Klausberger, 2009), our studies and the work of many other groups have begun to show how distinct types of inhibitory interneurons can have unique functional impacts on local circuit computation and behaviors that require these circuits (Lovett-Barron & Losonczy, 2014). These new insights into inhibitory interneurons, facilitated by a variety of technical developments for studying the rodent nervous system, promise to allow for further classification of interneurons according to their functional and behavioral roles, in addition to their well-known anatomical, molecular, structural, and electrophysiological signatures (Ascoli et al., 2008; DeFilipe et al., 2013).

The findings we have presented make use of knock-in mice that express cre recombinase in interneuron subtypes defined by the expression of a single gene: Gad65 (*Gad65-cre* mice), parvalbumin (*Pvalb-cre* mice) or somatostatin (*Som-cre* mice). However, these cre driver lines do not allow for access to single cell types, and are much less refined than the classification of cell types based on multiple morphological,

electrophysiological, and molecular criteria (Ascoli et al., 2008; DeFilipe et al., 2013). The *Pvalb-cre* line labels both basket cells and axo-axonic cells, which target the soma and proximal dendritic segments of PCs or the axon initial segment of PCs, respectively. Similarly, the *Som-cre* line labels both bistratified cells and OLM cells, which target CA3-recipient dendrites or entorhinal-recipient dendrites of PCs, respectively. Finer analysis of interneuron contributions to neural circuits and behavior will demand a more refined approach to target single cell types, as has been recently demonstrated for OLM cells in CA1 (Leão et al., 2012) and axo-axonic cells in the neocortex (Taniguchi et al., 2013). Identifying novel molecular markers for single cell classes or using intersectional genetic approaches (Taniguchi et al., 2011) may allow for the generation of more specific cre-driver mouse lines, allowing for the flexible expression of exogenous proteins to facilitate recording and manipulation of their activity. By developing and applying these tools to the hippocampus and neocortex, future studies will be able to refine our understanding of how each subtype of inhibitory interneuron contributes to network function and behavior.

By defining links between molecularly defined cell types, circuit computation and behavior, these research efforts may provide a useful means to integrate structural features of neurons and networks with nervous system function. In addition to the invaluable insights into basic neuroscience research, this approach may ultimately lead to the discovery of diagnostic criteria and potential therapeutic targets for neurological and psychiatric diseases characterized by disrupted circuit function and dynamics.

Concluding Remarks

The experiments detailed in this thesis have demonstrated the relationship between Som+ dendrite-targeting interneurons in hippocampal area CA1 and their influences on PC input-output processing and contextual fear conditioning. However, there are many more cell types, circuit functions, and hippocampal-dependent behaviors to investigate. As such, this work is just a small step towards a more detailed and comprehensive investigating of the cellular basis of our higher cognitive functions, including learning and memory.

Future studies could focus on investigating the contributions of interneurons to other forms of hippocampal-dependent memories, including trace conditioning, novel object recognition, and forms of spatial memory. By adapting these tasks to suit the head-fixed behaving mouse, future studies can take advantage of the 2-photon Ca^{2+} imaging methods we employ in *Chapter 3*, which have allowed us to record from GCaMP-expressing inhibitory neurons, excitatory neurons, and axonal projections from excitatory, inhibitory, and neuromodulatory sources across all layers of CA1. As neural activity imaging methods continue to improve, and surgical techniques allow access to all subfields of the hippocampus and associated regions, the use of head-fixed behaving mice will allow for a deeper understanding of the neural circuit elements that implement learning and memory functions.

In conclusion, the work presented in this thesis has established links between cell type (Som+ interneurons), circuit function (control of burst spiking), and memory (contextual fear learning). As technological advancements continue to provide

neuroscientists with tools to ask more refined questions about nervous system structure and function, we will gain more insight into how our brains accomplish the task of learning and remembering events in our lives, which will provide opportunities for repairing or augmenting these functions in patients suffering from diseases of memory.

Literature Cited

Adrian, E.D. and Zotterman, Y. (1926). The impulses produced by sensory nerve endings: Part II: The response of a single end organ. *Journal of Physiology (Lond.),* **61**, 151–171.

Aggleton, J.P., Hunt, P.R., and Rawlins, J.N.P. (1986). The effects of hippocampal lesions upon spatial and non-spatial tests of working memory. *Behavioral Brain Research,* **19**, 133-146.

Ahmed, O.J. and Mehta, M.R. (2009). The hippocampal rate code: anatomy, physiology, and theory. *Trends in Neurosciences* **32**, 329-338.

Akerboom, J., et al. (2012). Optimization of a GCaMP calcium indicator for neural activity imaging. *The Journal of Neuroscience*, **32**, 13819-13840.

Alger, B.E. and Nicoll, R.A. (1982). Feed-forward dendritic inhibition in rat hippocampal pyramidal cells studied in vitro. *The Journal of Physiology,* **328**, 105-123.

Amaral, D.G. (1999). What is Where in the medial temporal lobe? *Hippocampus,* **9**, 1-6.

Amaral, D.G. and Witter, M.P. (1989). The three-dimensional organization of the hippocampal formation: a review of anatomical data. *Neuroscience,* **31**, 571-591.

Anagnostaras, S.G., Gale, G.D., and Fanselow, M.S. (2001). Hippocampus and contextual fear conditioning: recent controversies and advances. *Hippocampus*, **11**, 8-17.

Andersen, P., Morris, R., Amaral, D., Bliss, T., and O'Keefe, J., Eds. (2007). *The Hippocampus Book.* Oxford University Press.

Ascoli, G.A., et al (2008). Petilla terminology: Nomenclature of features of GABAergic interneurons of the cerebral cortex. *Nature Reviews Neuroscience*, **9**, 557-568.

Atallah, B.V., Bruns, W., Carandini, M., and Scanziani, M. (2012). Parvalbumin-expressing interneurons linearly transform cortical responses to visual stimuli. *Neuron*, **73**, 159-170.

Atasoy, D., Aponte, Y., Su, H.H., and Sternson, S.M. (2008). A FLEX switch targets Channelrhodopsin-2 to multiple cell types for imaging and long-range circuit mapping. *The Journal of Neuroscience* **28**, 7025-7030.

Bargmann, C.I. (2012). Beyond the connectome: how neuromodulators shape neural circuits. *Bioessays*, **34**, 458-65.

Berger, T.W., Alger, B., and Thompson, R.F. (1976). Neuronal substrate of classical conditioning in the hippocampus. *Science,* **192**, 483-485.

Blair, H.T., Schafe, G.E., Bauer, E.P., Rodrigues, S.M., and LeDoux, J.E. (2001). Synaptic plasticity in the lateral amygdala: A cellular hypothesis of fear conditioning. *Learning & Memory,* **8**, 229-242.

Bliss, T.V. and Lomo, T. (1973). Long-lasting potentiation of synaptic transmission in the dentate area of the anaesthetized rabbit following stimulation of the perforant path. *The Journal of Physiology, London,* **232**, 331-356.

Bliss, T.V.P. and Collingridge, G.L. (1993). A synaptic model of memory: long-term potentiation in the hippocampus. *Nature,* **361**, 31-39.

Bouton, M.E., and Bolles, R.C. (1980). Conditioned fear assessed by freezing and by the suppression of three different baselines. *Animal Learning and Behavior*, **8**, 429-434.

Brankack, J., and Buzsáki, G. (1986). Hippocampal responses evoked by tooth pulp and acoustic stimulation: depth profiles and effect of behavior. *Brain Research,* **378**, 303-314.

Broadbent, N.J., Squire, L.R., and Clark, R.E. (2004). Spatial memory, recognition memory, and the hippocampus. *PNAS,* **101***,* 14515-14520.

Buhl, E.H., Halasy, K., and Somogyi, P. (1994). Diverse sources of hippocampal unitary inhibitory postsynaptic potentials and the number of synaptic release sites. *Nature* **368**, 823-828.

Burwell, R.D., and Amaral, D,G (1998). Cortical afferents of the perirhinal, postrhinal, and entorhinal cortices of the rat. *The Journal of Comparative Neurology*, **398**, 179–205.

Buzsáki, G. (1984). Feed-forward inhibition in the hippocampal formation. *Progress in Neurobiology, 22*, 131-153.

Buzsáki, G. (2002). Theta Oscillations in the Hippocampus. *Neuron* **33**, 325-340.

Buzsáki, G. (2010). Neural syntax: cell assemblies, synapsembles, and readers. *Neuron* **68**, 362–385.

Buzsáki, G., and Moser, E.I. (2013). Memory, navigation and theta rhythm in the hippocampal-entorhinal system. *Nature Neuroscience*, **16**, 130-138.

Buzsáki, G., and Wang, X.J. (2012). Mechanisms of gamma oscillations. *Ann Rev Neurosci*, **35**, 203-225.

Buzsáki, G., Csicsvari, J., Dragoi, G., Harris, K., Henze, D., and Hirase, H. (2002). Homeostatic maintenance of neuronal excitability by burst discharges in vivo. *Cerebral Cortex,* **12**, 893-899.

Calandreau, L., Jaffard, R., and Desmet, A. (2007). Dissociated roles for the lateral and medial septum in elemental and contextual fear conditioning. *Learning & Memory,* **14**, 422-429.

Capaday, C., and van Vreeswilk, C. (2006). Direct control of firing rate gain by dendritic shunting inhibition. *Journal of Integrative Neuroscience,* **5**, 199-222.

Carandini, M., and Ferster, D. (2000). Membrane potential and firing rate in cat primary visual cortex. *The Journal of Neuroscience,* **20**, 470–484.

Carlen, M., et al (2012). A critical role for NMDA receptors in parvalbumin interneurons for gamma rhythm induction and behavior. *Molecular Psychiatry*, **17**, 537-548.

Carr, M.F. and Frank, L.M. (2012) A single microcircuit with multiple functions: state dependent information processing in the hippocampus. *Current Opinion in Neurobiology,* **22**, 1-5.

Chen, T-W. *et al*., (2013). Ultrasensitive fluorescent proteins for imaging neuronal activity. *Nature*, **499**, 295-300.

Chevaleyre, V., and Siegelbaum, S.A. (2010). Strong CA2 pyramidal neuron synapses define a powerful disynaptic cortico-hippocampal loop. *Neuron,* **66**, 560-572

Clayton, N.S., and Dickinson. A. (1998). Episodic-like memory during cache recovery by scrub jays. *Nature*, **395**, 272-274.

Cobb, S.R., Buhl, E.H., Halasy, K., Paulsen, O., and Somogyi, P. (1995) Synchronization of neuronal activity in hippocampus by individual GABAergic neurons. *Nature,* **378**, 75-58.

Cobb, S.R., Halasy, K., Vida, I., Nyiri, G., Tamás, G., Buhl, E.H., and Somogyi, P. (1997) Synaptic effects of identified interneurons innervating both interneurons and pyramidal cells in the rat hippocampus. *Neuroscience,* **79**, 629-648.

Colgin, L.L., Denninger, T., Fyhn, M., Hafting, T., Bonnevie, T., Jensen, O., Moser, M-B., and Moser, E.I. (2009). Frequency of gamma oscillations routes flow of information in the hippocampus. *Nature,* **462**, 353-357.

Colgin, L.L., Moser, E.I. and Moser, M-B. (2008). Understanding memory through hippocampal remapping. *Trends in Neurosciences,* **31***,* 469-477.

Collingridge, G.L., Herron, C.E., and Lester, R.A.J. (1988). Synaptic activation of *N*-methyl-D-aspartate receptors in the Schaffer Collateral-commissural pathway of rat hippocampus. *Journal of Physiology,* **399**, 282-300.

Constantinople, C.M., and Bruno, R.M. (2013). Deep cortical layers are activated directly by thalamus. *Science*, **340**, 1591-1594.

Cope, D.W., Maccaferri, G., Marton, L.F., Roberts, J.D.B., Cobden, P.M., and Somogyi, P. (2002). Cholecystokinin-immunopositive basket and schaffer collateral-associated interneurons target different domains of pyramidal cells in the CA1 area of the rat hippocampus. *Neuroscience,* **109**, 63–68.

Csicsvari, J., Hirase, H., Czurko, A., Mamiya, A., and Buzsáki, G. (1999). Oscillatory coupling of hippocampal pyramidal cells and interneurons in the behaving rat. *J. Neurosci*., **19**, 274-287.

Dasari, S., and Gulledge, A.T. (2011). M1 and M4 receptors modulate hippocampal pyramidal cells. *Journal of Neurophysiology,* **105**, 779-792.

Deacon, R.M.J., and Rawlins, J.N.P. (2006). T-maze alternation in the rodent. *Nature Protocols,* **1**, 7-12.

DeFelipe, J., et al (2013). New insights into the classification and nomenclature of cortical gabaergic interneurons. *Nature Reviews Neuroscience*, **14**, 202-216.

Deisseroth, K. (2011). Optogenetics. *Nature Methods*, **8**, 26-29.

Dombeck, D.A., Harvey, C.D., Tian, L., Looger, L.L., and Tank, D.W. (2010). Functional imaging of hippocampal place cells at cellular resolution during virtual navigation. *Nature Neuroscience*, **13**, 1433-1440.

Dombeck, D.A., Khabbaz, A.N., Collman, F., Adelman, T.L., and Tank, D.W. (2007). Imaging large scale neural activity with cellular resolution in awake mobile mice. *Neuron*, **56**, 43-57

Dudman, J.T., Tsay, D., and Siegelbaum, S.A. (2007). A role for synaptic inputs at distal dendrites: instructive signals for hippocampal long-term plasticity. *Neuron*, **56**, 866-879.

Eichenbaum, H., and Fortin, N.J. (2003). Episodic memory and the hippocampus: it's about time. *Current Directions in Psychological Science,* **12**, 53-57.

Eichenbaum, H., Dudchenko, P., Wood, E., Shapiro, M., and Tanila, H. (1999). The Hippocampus, Memory, and Place cells: Is it spatial memory or a memory space? *Neuron,* **23**, 209-226.

Ekstrom, A.D., Kahana, M.J., Capla, J.B., Fields, T.A., Isham, E.A., Newman, E.L., and Fried, I. (2003). Cellular networks underlying human spatial navigation. *Nature,* **425**, 184-188.

Epsztein, J., Brecht, M, and Lee, A.K. Intracellular determinants of hippocampal CA1 place and silence cell activity in a novel environment. *Neuron* **70**, 109-120 (2011).

Epsztein, J., Brecht. M., and Lee. A.K. (2011). Intracellular determinants of hippocampal CA1 place and silent cell activity in a novel environment. *Neuron,* **70**, 109-120.

Fanselow, M.S. (2010). From contextual fear to a dynamic view of memory system. *Trends in Cognitive Sciences*, **14**, 7-15.

Fanselow, M.S., DeCola, J.P., and Young, S.L. (1993). Mechanisms responsible for reduced conditioning with massed unsignaled unconditional stimuli. *Journal of Experimental Psychology: Animal Behavior Processes*, **19**, 121 – 137.

Fanselow, M.S. (1986). Associative vs. topographical accounts of the immediate shock freezing deficit in rats: implications for the response selection rules governing species specific defensive reactions. *Learning & Motivation*, **17**, 16-39.

Fanselow, M.S. (1990). Factors governing one-trial contextual conditioning. *Animal Learning & Behavior*, **18**, 264-270.

Fanselow, M.S., and Dong, H.W. (2010). Are the dorsal and ventral hippocampus functionally distinct structures? *Neuron*, **65**, 7-19.

Fanselow, M.S., and Poulos, A.M. (2005). The neuroscience of mammalian associative learning. *Annual Review in Psychology*, **56**, 207-234.

Felix-Ortiz, A.C., Beyeler, A., Seo, C., Leppa, C.A., Wildes, C.P., and Tye, K.M. (2013). BLA to vHPC inputs modulate anxiety-related behaviors. *Neuron*, **79**, 658-664.

Fenno, L., Yizhar, O., and Deisseroth, K. (2011). The development and application of optogenetics. *Annual Review of Neuroscience*, **34**, 389-412.

Frankland, P.W., Cestari, V., Filipkowski, R.K., McDonald, R.J., and Silva, A.J. (1998). The dorsal hippocampus is essential for context discrimination but not for contextual conditioning. *Behavioral Neuroscience,* **112**, 863-874.

Frankland, P.W., Josselyn, S.A., Anagnostaras, S.G., Kogan, J.H., Takahashi, E., and Silva, A.J. (2004). Consolidation of CS and US representations in associative fear conditioning. *Hippocampus*, **14**, 557-569.

Freund, T.F., and Antal, M. (1988). GABA-containing neurons in the septum control inhibitory interneurons in the hippocampus. *Nature*, **336**, 170-173.

Freund, T.F., and Buzsáki, G. (1996). Interneurons of the Hippocampus. *Hippocampus* **6**, 347-470.

Fuchs, E.C. et al. (2007). Recruitment of parvalbumin-positive interneurons determines hippocampal function and associated behavior. *Neuron*, **53**, 591-604.

Fuentealba, P., *et al.* (2008). Ivy cells: a population of nitric-oxide-producing, slow-spiking GABAergic neurons and their involvement in hippocampal network activity. *Neuron* **57**, 917-929.

Funahashi, M., He, Y.F., Sugimoto, T., and Matsuo, R. (1999). Noxious tooth pulp stimulation suppresses c-fos expression in the rat hippocampal formation. *Brain Research,* **827**, 215-220.

Gale, G.D., Anagnostaras, S.G., Fanselow, M.S. (2001). Cholinergic modulation of Pavlovian fear conditioning: Effects of intrahippocampal scopolamine infusion. *Hippocampus*, **11**, 371-376.

Garner, A.R., Rowland, D.C., Hwang, S.Y., Baumgaertel, K., Roth, B.L., Kentros, C., and Mayford, M. (2012). Generation of a synthetic memory trace. *Science*, **335**, 1513-1516.

Gasparini, S., and Magee, J.C. (2006) State-dependent dendritic computation in hippocampal CA1 pyramidal neurons. *The Journal of Neuroscience* **26**, 2088-2100.

Gdalyahu, A., Tring, E., Polack, P.O., Gruver, R., Golshani, P., Fanselow, M.S., Silva, A.J., and Trachtenberg, J.T. (2012). Associative fear learning enhances sparse network coding in primary sensory cortex. *Neuron*, **75**, 121-32.

Gentet, L.J., Kremer, Y., Taniguchi, H., Huang, Z.J., Staiger, J.F., and Petersen, C.C.H. (2012). Unique functional properties of somatostatin-expressing gabaergic neurons in mouse barrel cortex. *Nature Neuroscience*, **15**, 607-612.,

Golding, N.L., Jung, H.Y., Mickus, T., and Spruston, N. (1999). Dendritic calcium spike initiation and repolarization are controlled by distinct potassium channel subtypes in CA1 pyramidal neurons. *The Journal of Neuroscience* **19**, 8789-8798.

Golding, N.L., Staff, N.P., and Spruston, N. (2002). Dendritic spikes as a mechanism for cooperative long-term potentiation. *Nature*, **418**, 326-331.

Goshen, I., Brodsky, M., Prakash, R., Wallace, J., Gradinaru, V., Ramakrishnan, C., and Deisseroth, K. (2011). Dynamics of retrieval strategies for remote memories. *Cell*, **28**, 678-689.

Gulyas, A.I., Hajos, N., Katona, I., and Freund, T.F. (2003). Interneurons are the local targets of hippocampal inhibitory cells which project to the medial septum. The *European Journal of Neuroscience*, **17**, 861-1872.

Hampton, R.R, and Schwartz, B.L. (2004). Episodic memory in nonhumans: what, and where, is when? *Current Opinion in Neurobiology,* **14**, 192-197.

Hampton, R.R. (2001). Rhesus monkeys know when they remember. *PNAS*, **98**, 5359-5362.

Hargreaves, E.L., Rao, G., Lee, I., and Knierim, J.J. (2005). Major dissociation between medial and lateral entorhinal input to dorsal hippocampus. *Science,* **308**, 1792-1794.

Harris , K.D, Csicsvari, J., Hirase, H., Daroi, G., and Buzsáki, G. (2003). Organization of cell assemblies in the hippocampus. *Nature,* **424**, 552-556.

Harris, K.D., Hirase, H., Leinekugel, X., Henze, D.A., and Buzsáki, G. (2001). Temporal interaction between single spikes and complex spike bursts in hippocampal pyramidal cells. *Neuron*, **32**, 141-149.

Harvey, C.D., Collman, F., Dombeck, D.A., and Tank, D.W. Intracellular dynamics of hippocampal place cells during virtual navigation. *Nature* **461**, 941-946 (2009).

Hasselmo, M.E. (2006). The role of acetylcholine in learning and memory. *Current Opinion in Neurobiology*, **16**, 710-715.

Hebb, D. O. (1949). *The Organization of Behaviour.* Wiley, New York.

Herreras, O., Solís, J.M., Herranz, A.S., Martín del Río, R., and Lerma, J. (1988b). Sensory modulation of hippocampal transmission. II. Evidence for a cholinergic locus of inhibition in the Schaffer-CA1 synapse. *Brain Research*, **461**, 303-313.

Herreras, O., Solís, J.M., Muñoz, M.D., Martín del Río R., and Lerma J. (1988a). Sensory modulation of hippocampal transmission. I. Opposite effects on CA1 and dentate gyrus synapsis. *Brain Research*, **461**, 290-302.

Hock, B.J. and Bunsey, M.D. (1998) Differential effects of dorsal and ventral hippocampal lesions. *J Neurosci,* **18**, 7027-7032.

Holland, P.C., and Bouton, M.E. (1999).Hippocampus and context in classical conditioning. *Curr Opin Neurobiol,* **9**, 195-202.

Holtmaat, A., and Svoboda, K. (2009). Experience-dependent structural synaptic plasticity in the mammalian brain. *Nature Reviews Neuroscience,* **10**, 647-658.

Huxter, J., Burgess, N., and O'Keefe, J. (2003). Independent rate and temporal coding in hippocampal pyramidal cells. *Nature*, **425**, 828-832.

Isaacson, J.S., and Scanziani, M. (2011). How inhibition shapes cortical activity. *Neuron* **72**, 231-243.

Jadhav, S.P., Kemere, C., German, P.W., and Frank, L.M. (2012). Awake hippocampal sharp-wave ripples support spatial memory. *Science,* **336**, 1454-1458.

Jarsky, T., Roxin, A., Kath, W.L., and Spruston, N. (2005). Conditional dendritic spike propagation following distal synaptic activation of hippocampal CA1 pyramidal neurons. *Nature Neuroscience* **8***,* 1667-1676.

Jones, M.W., and Wilson, M.A. (2005). Theta rhythms coordinate hippocampal-prefrontal interactions in a spatial memory task. *PLoS Biology,* **3**, e402.

Kaifosh, P., Lovett-Barron, M., Turi, G., Reardon., T.R., and Losonczy, A**.**, Septo-hippocampal GABAergic signaling across multiple modalities in awake mouse. *Nature Neuroscience,* **16**, 1182-1184.

Kamondi, A., Acsady, L., and Buzsáki, G. (1998) Dendritic spikes are enhanced by cooperative network activity in the intact hippocampus. *J Neurosci,* **18**, 3919–3928.

Kandel, E.R., and Spencer, W.A (1961) Electrophysiology of hippocampal neurons. II. Afterpotentials and repetitive firing. *J Neurophysiol* **24**, 243–259.

Katona, I., Sperlágh, B., Sík, A., Kofalvi, A., Vizi, E.S., Mackie, K. and Freund, T.F. (1999). Presynaptically located CB1 cannabinoid receptors regulate GABA release from axon terminals of specific hippocampal interneurons. *The Journal of Neuroscience* **19**, 4544-4558.

Kepecs, A., and Lisman, J. (2004). How to read a burst duration code. *Neurocomputing,* **58-60**, 1-6.

Kerlin, A.M., Andermann, M.L., Berezovskii, V.K., and Reid, R.C. (2010). Broadly tuned response properties of diverse inhibitory neuron subtypes in mouse visual cortex. *Neuron*, **67**, 858-871.

Kesner, R.P. (2007). Behavioral functions of the CA3 subregion of the hippocampus. *Learning & Memory,* **14**, 771-781.

Khanna, S. (1997). Dorsal hippocampus field CA1 pyramidal cell responses to a persistent versus an acute nociceptive stimulus and their septal modulation. *Neuroscience,* **77**, 713-721.

Kheirbek, M.A., *et al.* (2013). Differential control of learning and anxiety along the dorsoventral axis of the dentate gyrus. *Neuron,* **77**, 955-968.

Kim, J.J., and Fanselow, M.S. (1992). Modality-specific retrograde amnesia of fear following hippocampal lesions. *Science*, **256**, 675-677.

Kim, J.J., Clark, R.E., and Thompson, R.F. (1995). Hippocampectomy impairs the memory of recently, but not remotely, acquired trace eyeblink conditioned responses. *Behavioral Neuroscience,* **109**, 195-203.

Kjelstrup, K.B., et al. (2008). Finite scale of spatial representation in the hippocampus. *Science*, **321**, 140-143.

Klausberger, T. (2009). GABAergic interneurons targeting dendrites of pyramidal cells in the CA1 area of the hippocampus. *European Journal of Neuroscience* **30**, 947-957.

Klausberger, T. Magill, P.J., Marton, L.F., Roberts, J.D., Cobden, P.M., Buzsáki, G., and Somogyi, P. (2003). Brain-state- and cell-type-specific firing of hippocampal interneurons *in vivo*. *Nature* **421**, 844-848.

Klausberger, T., and Somogyi, P. Neuronal diversity and temporal dynamics: The unity of hippocampal circuit operations. *Science* **321**, 53-57 (2008).

Klausberger, T., Márton, L.F., Baude, A., Roberts, J.D.B., Magill, P.J., and Somogyi, P. (2004). Spike timing of dendrite-targeting bistratified cells during hippocampal network oscillations *in vivo*. *Nature Neuroscience* **7**, 41-47.

Knierim, J.J., Lee, I., and Hargreaves, E.L. (2006). Hippocampal place cells: parallel input streams, subregional processing, and implications for episodic memory. *Hippocampus*, **16**, 755-64.

Knowles, W.D., and Schwartzkroin, P.S. Axonal ramifications of hippocampal CA1 pyramidal cells, *The Journal of Neuroscience* **1**, 1236–1241 (1981).

Korotkova, T., Fuchs, E.C., Ponomarenko, A., von Engelhardt, J., and Monyer, H. (2010). NMDA receptor ablation on parvalbumin-positive interneurons impairs hippocampal synchrony, spatial representations, and working memory. *Neuron*, **68**, 557-569.

Kuhlman, S.J., Olivas, N.D., Tring, E., Ikrar, T., Xu, X., and Trachtenberg, J.T. (2013). A disinhibitory microcircuit initiates critical-period plasticity in the visual cortex. *Nature*, **501**, 543-546.

Lanuza, E., Nader, K., Ledoux, J.E. (2004). Unconditioned stimulus pathways to the amygdala: effects of posterior thalamic and cortical lesions on fear conditioning. *Neuroscience*, **125**, 305-315.

Lapray, D., et al. (2012). Behavior-dependent specialization of identified hippocampal interneurons. *Nature Neuroscience*, **15**, 1265-1271.

Larkum, M.E., Nevian, T., Sandler, M., Polsky, A., and Schiller, J. (2009). Synaptic integration in tuft dendrites of layer 5 pyramidal neurons: a new unifying principle. *Science* **325**, 756-760.

Larkum, M.E., Zhu, J.J., and Sakmann, B. (1999) .A new cellular mechanism for coupling inputs arriving at different cortical layers. *Nature* **398**, 338-341.

Lawrence, J.J., Ststland, J.M., Grinspan, Z.M., and McBain, C.J. (2006). Cell type-specific dependence of muscarinic signaling in mouse hippocampal stratum oriens interneurons. *Journal of Physiology*, **570**, 595-610.

Leão, R.N. et al., (2012). OLM interneurons differentially modulate CA3 and entorhinal inputs to hippocampal CA1 neurons. *Nature Neuroscience*, **15**, 1524-1530.

LeDoux, J.E. (2000). Emotion circuits in the brain. *Annual Review in Neuroscience*, **23**, 155-184.

Lee, D., Lin, B.J., and Lee, A.K.. (2012a). Hippocampal place fields emerge upon single-cell manipulation of excitability during behavior. *Science,* **337**, 849-853.

Lee, S.H., et al (2012b). Activation of specific interneurons improves v1 feature selectivity and visual perception. *Nature*, **488**, 379-383.

Letzkus, J.J., Wolff, S.B., Meyer, E.M., Tovote, P., Courtin, J., Herry, C., Lüthi, A. (2011). A disinhibitory microcircuit for associative fear learning in the auditory cortex. *Nature*, **480**, 331-335.

Leutgeb, S., Leutgeb, J.K., Barnes, C.A., Moser, E.I., McNaughton, B.L., and Moser, M-B. (2005). Independent codes for spatial and episodic memory in hippocampal neuronal ensembles. *Science*, **309**, 619-623.

Lima, S.Q., Hromadka, T., Znamenskiy, P., and Zador, A.M. (2009). Pinp: A new method of tagging neuronal populations for identification during in vivo electrophysiological recording. *PloS one*, **4**, e6099.

Lipski, W.J., and Grace, A.A. (2013). Footshock-induced responses in ventral subiculum neurons are mediated by locus coeruleus noradrenergic afferents. *European Journal of Neuropsychopharmacology,* **23**, 1320-1328.

Lisman, J.E. (1997). Bursts as a unit of neural information: Making unreliable synapses reliable. *Trends in Neurosciences*, **20**, 38-43.

Lisman, J.E. and Idiart, M.A. (1995) Storage of 7 +/− 2 short-term memories in oscillatory subcycles. *Science,* **267**, 1512–1515.

Liu, X., Ramirez, S., Pang, P.T., Puryear, C.B., Govindarajan, A., Deisseroth, K., and Tonegawa, S. (2012). Optogenetic stimulation of a hippocampal engram activates fear memory recall. *Nature*, **484**, 381-385.

London, M., Roth, A., Beeren, L., Häusser, M., and Latham, P.E. (2010). Sensitivity to perturbations in vivo implies high noise and suggests rate coding in cortex. *Nature,* **466**, 123-127

Losonczy, A., and Magee, J.C. (2006). Integrative properties of radial oblique dendrites in hippocampal CA1 pyramidal neurons. *Neuron* **50**, 291-307.

Losonczy, A., Makara, J.K., and Magee, J.C. (2008) Compartmentalized dendritic plasticity and input feature storage in neurons. *Nature*, **452**, 436-441.

Losonczy, A., Zemelman, B.V., Vaziri, A., and Magee, J.C. (2010). Network mechanisms of theta related neuronal activity in hippocampal CA1 pyramidal neurons. *Nature Neuroscience* **13**, 967-972.

Losonczy, A., Zhang, L., Shigemoto, R., Somogyi, P., and Nusser, Z. (2002). Cell type dependence and variability in the short-term plasticity of EPSCs in identified mouse hippocampal interneurons. *Journal of Physiology* **542**, 193-210.

Loughlin, S.E., Foote, S.L., and Grzanna, R. (1986). Efferent projections of nucleus locus coeruleus: morphologic subpopulations have different efferent targets. *Neuroscience*, **18**, 307-19.

Lovett-Barron M, Kaifosh P, Khierbek MA, Danielson N, Zaremba JM, Turi GF, Reardon TR, Hen R, Zemelman BV, and Losonczy A. (Under review) Dendritic Inhibition in the Hippocampus Supports Fear Learning.

Lovett-Barron, M., and Losonczy, A. (2014). Behavioral consequences of GABAergic neuronal diversity. *Curr Opn Neurobiol*, **26**, 27-33.

Lovett-Barron, M., Turi, G.F., Kaifosh, P., Lee, P.H., Bolze, F., Sun, X.H., Nicoud, J.F., Zemelman, B.V., Sternson, S.M., and Losonczy, A. (2012). Regulation of neuronal input transformations by tunable dendritic inhibition. *Nature Neuroscience*, **15**, 423-430.

Luo, L., Callaway, E.M., and Svoboda, K. (2008). Genetic dissection of neural circuits. *Neuron*, **57**, 634-660.

Ma, W.P., Liu, B.H., Li, Y.T., Huang, Z.J., Zhang, L.I., and Tao, H.W. (2010). Visual representations by cortical somatostatin inhibitory neurons--selective but with weak and delayed responses. *The Journal of Neuroscience*, **30**, 4371-14379.

Maccaferri, G., Roberts, J.D., Szucs, P., Cottingham, C.A., and Somogyi, P. (2000) Cell surface domain specific postsynaptic currents evoked by identified GABAergic neurones in rat hippocampus in vitro. *The Journal of Physiology* **524**, 91–116.

MacDonald, C.J., Lepage, K.Q., Eden, U.T. and Eichenbaum, H. (2011). Hippocampal “time cells” bridge the gap in memory for discontiguous events. *Neuron,* **71**, 737–749.

Magee, J.C. (2000). Dendritic integration of excitatory synaptic input. *Nature Reviews Neuroscience,* **1**, 181-190.

Magee, J.C. and Carruth, M. (1999). Dendritic voltage-gated ion channels regulate the action potential firing mode of hippocampal CA1 pyramidal neurons. *Journal of Neurophysiology* **82**, 1895-1901.

Magnus, C.J., Lee, P.H., Atasoy, D., Su, H.H., Looger, L.L., and Sternson, S.M. (2011). Chemical and genetic engineering of selective ion channel-ligand interactions. *Science*, **333**, 1292-1296.

Mahoney, W.J. and Ayres, J.J.B. (1976). One-trial simultaneous and backward fear conditioning as reflected in conditioned suppression of licking in rats. *Animal Learning and Behavior*, **4**, 357-362.

Makara, J.K., Losonczy, A., Wen, Q. and Magee, J.C. (2009) Experience-dependent compartmentalized dendritic plasticity in rat hippocampal CA1 pyramidal neurons. *Nature Neuroscience,* **12**, 1485-1487.

Malenka, R.C., and Nicoll, R.A. (1999). Long-term potentiation – a decade of progress? *Science,* **285**, 1870-1874.

Marder, E. (2012). Neuromodulation of neuronal circuits: back to the future. *Neuron*, **76**, 1-11.

Maren, S. (2001). Neurobiology of Pavlovian fear conditioning. *Annual Review in Neuroscience*, **24**, 897-931.

Maren, S., and Fanselow, M.S. (1995). Synaptic plasticity in the basolateral amygdala induced by hippocampal formation stimulation in vivo. *The Journal of Neuroscience,* **15**, 7548-7564.

Maren, S., and Fanselow, M.S. (1997). Electrolytic lesions of the fimbria/fornix, dorsal hippocampus, or entorhinal cortex produce anterograde deficits in contextual fear conditioning in rats. *Neurobiology of Learning and Memory*, **67**, 142-149.

Maren, S., Phan, K. L., and Liberzon, I. (2013). The contextual brain: Implications for fear conditioning, extinction and psychopathology. *Nature Reviews Neuroscience,* **14**, 417-428.

Markram, H., Toledo-Rodriguez, M., Wang, Y., Gupta, A., Silberberg, G., and Wu, C. (2004). Interneurons of the neocortical inhibitory system. *Nature Reviews Neuroscience*, **5**, 793-807.

Marr, D. (1971). Simple memory: A theory for archicortex. *Philosophical Transactions of the Royal Society of London. Series B, Biological Sciences,* **262**, 23-81.

McClure, C., Cole, K.L., Wulff, P., Klugmann, M., and Murray, A.J. (2011). Production and titering of recombinant adeno-associated viral vectors. *J Vis Exp*, **57**, e3348, doi:10.3791/3348

McEchron, M.D. and Disterhoft, J.F. (1999). Hippocampal encoding of non-spatial trace conditioning. *Hippocampus,* **9**, 385-396.

McEchron, M.D. and Disterhoft. J.F. (1997). Sequence of single neuron changes in CA1 hippocampus of rabbits during acquisition of trace eyeblink conditioned responses. *Journal of Neurophysiology,* **78**, 1030-1044.

Megias, M., Emri, Z., Freund, T.F., and Gulyas, A.I. (2001). Total number and distribution of inhibitory and excitatory synapses on hippocampal CA1 pyramidal cells. *Neuroscience* **102**, 527-540.

Mehaffey, W.H., Boiron, B., Maler, L., and Turner, R.W. (2005). Deterministic multiplicative gain control with active dendrites. *The Journal of Neuroscience,* **25**, 9968-9977.

Mehta, M.R., Lee, A.K., and Wilson, M.A. (2002). Role of experience and oscillations in transforming a rate code into a temporal code. *Nature,* **417**, 741-746.

Melzer, S., Michael, M., Caputi, A., Eliava, M., Fuchs, E.C., Whittington, M.A., and Monyer, H. (2012). Long-range-projecting gabaergic neurons modulate inhibition in hippocampus and entorhinal cortex. *Science*, **335**, 1506-1510.

Miles, R., Tóthe, K, Gulyás, A.I., Hájos, N., and Freund, T.F. (1996) Differences between somatic and dendritic inhibition in the hippocampus. *Neuron* **16**, 815-823.

Miller, S.W., and Groves, P.M. (1977). Sensory evoked neuronal activity in the hippocampus before and after lesions of the medial septal nuclei. *Physiology and Behvaior,* **18**, 141-146.

Mizrahi, A., Crowley, J.C., Shtoyerman, E., and Katz, L.C. (2004). High-resolution in vivo imaging of hippocampal dendrites and spines. *The Journal of Neuroscience*, **24**, 3147-3151.

Mizuseki, K., Diba, K., Pastalkova, E., and Buzsáki, G. (2011). Hippocampal CA1 pyramidal cells form functionally distinct sublayers. *Nature Neuroscience,* **14**, 1174-1181.

Moita, M.A., Rosis, S., Zhou, Y., LeDoux, J.E., and Blair, H.T. (2004). Putting fear in its place: remapping of hippocampal place cells during fear conditioning. *The Journal of Neuroscience*, **24**, 7015-7023.

Moser, E, Moser, M-B, and Andersen P. (1993). Spatial learning impairment parallels the magnitude of dorsal hippocampal lesions, but is hardly present following ventral lesions. *J Neurosci,* **13**, 3916-3925.

Moser, M-B., and Moser, E.I. (1998). Functional differentiation in the hippocampus. *Hippocampus*, **8**, 608-619.

Moser, M-B., Moser, E., Forrest, E., Andersen, P., and Morris, R.G.M. (1995). Spatial learning with a minislab in the dorsal hippocampus. *PNAS,* **92**, 9697-9701.

Mulligan, K.A., and Törk, I. (1988). Serotoninergic innervation of the cat cerebral cortex. *Journal of Comparative Neurology* **270**, 86-110.

Murayama, M., and Larkum, M.E. (2009). Enhanced dendritic activity in awake rats. *PNAS*, **106**, 20482-20486.

Murayama, M., Perez-Garci, E., Nevian, T., Bock, T., Senn, W., and Larkum, M.E. (2009). Dendritic encoding of sensory stimuli controlled by deep cortical interneurons. *Nature*, **457**, 1137-1141.

Murray, A.J., et al. (2011). Parvalbumin-positive CA1 interneurons are required for spatial working memory but not for reference memory. *Nature Neuroscience*, **14**, 297-299.

Nadel, L., Ryan, L., Hayes, S.M., Gilboa, A., and Moscovitch, M. (2003). The role of the hippocampal complex in long-term episodic memory. *International Congress Series*, **1250**, 215-234.

Naloor, R., Bunting, K.M., and Vazdarjanova, A. (2012). Encoding of emotion-paired spatial stimuli in the rodent hippocampus. *Frontiers in Behavioral Neuroscience,* doi: 10.3389/fnbeh.2012.00027

Neves, G., Cooke, S.F., and Bliss, T.V.P. (2008). Synaptic plasticity, memory, and the hippocampus: a neural network approach to causality. *Nature Reviews Neuroscience,* **9**, 65-75.

Nevian, T., Larkum, M.E., Polsky, A., and Schiller, J. (2007). Properties of basal dendrites of layer 5 pyramidal neurons: a direct patch-clamp recording study. *Nature Neuroscience* **10**, 206-214.

O'Keefe, J. and Dostrovsky, J. (1971). The hippocampus as a spatial map. Preliminary evidence from unit activity in the freely-moving rat. *Brain Research* **34**, 171–175.

O'Keefe, J. and Nadel, L. (1978). *The Hippocampus as a Cognitive Map.* Oxford Univ. Press.

O'Keefe, J., and Conway, D.H. (1978). Hippocampal place units in the freely moving rat: why they fire where they fire. *Exp Brain Res*, **31**, 573-590.

O'Keefe, J., and Recce, M.L. (1993). Phase relationship between hippocampal place units and the EEG theta rhythm. *Hippocampus*, **3**, 317-330.

Olshausen, B.A., and Field, D.J. (2004). Sparse coding of sensory inputs. *Curr Opn Neurobiol.,* **14**, 481-487.

Palmer, L., Murayama, M. Larkum, M. (2012b). Inhibitory regulation of dendritic activity in vivo. *Frontiers in Neural Circuits*, **6:26**. doi: 10.3389/fncir.2012.00026.

Palmer, L.M., Schulz, J.M., Murphy, S.C., Ledergerber, D., Murayama, M., and Larkum, M.E. (2012a) The cellular basis of GABAb-mediated interhemispheric inhibition. *Science*, **335**, 989-993.

Pasquier, D.A. and Reinoso-Suarez, F. (1978). The topographic organization of hypothalamic and brain stem projections to the hippocampus. *Brain Res Bull*, **3**, 373-389

Pastalkova, E., Itskov, V., Amarasingham, A. and Buzsáki, G. (2008). Internally generated cell assembly sequences in the rat hippocampus. *Science* **321**, 1322–1327

Paulsen, O., and Moser, E.I. (1998). A model of hippocampal memory encoding and retrieval: GABAergic control of synaptic plasticity. *Trends in Neuroscience*, **21**, 273-278.

Pavlov, I.P. (1927). *Conditional Reflexes*. Oxford University Press.

Phillips, R.G., and LeDoux, J.E. (1992). Differential contribution of amygdala and hippocampus to cued and contextual fear conditioning. *Behavioral Neuroscience*, **106**, 274-285.

Pi, H-J., Hangya, B., Kvitsiani, D., Sanders, J.I., Huang., Z.J., and Kepecs, A. (2013). Cortical interneurons that specialize in disinhibitory control. *Nature,* doi10.1038/nature12676

Potvin, O., Allen, K., Thibaudeau, G., Dore, F.Y., and Goulet. S. (2006). Performance on spatial working memory tasks after dorsal or ventral hippocampal lesions and adjacent damage to the subiculum. *Behavioral Neuroscience,* **120**, 413-422.

Pouille, F. and Scanziani, M. (2001). Enforcement of temporal fidelity in pyramidal cells by somatic feed-forward inhibition. *Science* **293**, 1159-1163.

Pouille, F. and Scanziani, M. (2004). Routing of spike series by dynamic circuits in the hippocampus. *Nature,* **429**, 717-723.

Pouille, F., Marin-Burgin, A., Adesnik, H., Atallah, B.V., and Scanziani, M. (2009). Input normalization by global feedforward inhibition expands cortical dynamic range. *Nature Neuroscience,* **12**, 1577-1585.

Quinn, J.J., Loya, F., Ma, Q.D., and Fanselow, M.S. (2005). Dorsal hippocampus NMDA receptors differentially mediate trace and contextual fear conditioning. *Hippocampus*, **15**, 665-674.

Ramirez, S., Liu, X., Lin, P.A., Suh, J., Pignatelli, M., Redondo, R.L., Ryan, T.J., and Tonegawa, S. (2013). Creating a false memory in the hippocampus. *Science,* **341**, 387-391.

Risold, P.Y. and Swanson, L.W. (1996). Structural evidence for functional domains in the rat hippocampus. *Science,* **272**, 1484-1486.

Rogan, S.C., and Roth, B.L. (2011). Remote control of neuronal signaling. *Pharmacological reviews*, **63**, 291-315.

Romanski, L.M., and LeDoux, J.E. (1993). Information cascade from primary auditory cortex to the amygdala: corticocortical and corticoamygdaloid projections of temporal cortex in the rat. *Cerebral Cortex*, **6**, 515-532.

Rovira, C., Ben-Ari, Y., and Cherubini, E. (1983). Dual cholinergic modulation of hippocampal somatic and dendritic field potentials by the septo-hippocampal pathway. *Experimental Brain Research,* **49**, 151-155.

Royer, S. Zemelman, B.V., Losonczy, A., Kim, J., Chance, F., Magee, J.C., and Buzsáki, G. (2012). Control of timing, rate and bursts of hippocampal place cells by dendritic and somatic inhibition. *Nature Neuroscience*, **15**, 769-775.

Royer, S., Sirota, A., Patel, J., and Buzsáki, G. (2010). Distinct representations and theta dynamics in dorsal and ventral hippocampus. *J Neurosci,* **30**, 1777-1787.

Rudy, J.W., Huff, N.C., and Matus-Amat, P. (2004). Understanding contextual fear conditioning: insights from a two-process model. *Neuroscience and Biobehavioral Reviews,* **28**, 675-685.

Runyan, C.A., and Sur, M. (2013). Response selectivity is correlated to dendritic structure in parvalbumin-expressing inhibitory neurons in visual cortex. *J. Neurosci*, **33**, 11724-11733.

Runyan, C.A., Schummers, J., Van Wart, A., Kuhlman, S.J., Wilson, N.R., Huang, Z.J., and Sur, M. (2010). Response features of parvalbumin-expressing interneurons suggest precise roles for subtypes of inhibition in visual cortex. *Neuron*, **67**, 847-857.

Sachidhanandam, S., Sreenivasan, V., Kyriakatos, A., Kremer, Y., and Petersen, C.C. (2013) Membrane potential correlates of sensory perception in mouse barrel cortex. *Nature Neuroscience*, **16**, 1671-1677.

Sah, P., Faber, E.S., Lopez De Armentia, M., and Power, J. (2003). The amygdaloid complex: anatomy and physiology. *Physiology Review*, **83**, 803-834.

Sakagushi, T., Ishikawa, D., Nomura, H., Matsuki, N., and Ikegaya, Y. (2012). Normal learning ability of mice with a surgically exposed hippocampus. *NeuroReport,* **23**, 457-461.

Schwartz, B.L., and Evans, S. (2001). Episodic memory in primates. *Am J Primatol*, **55**, 71-85

Scoville, W.B., and Milner, B. (1957). Loss of recent memory after bilateral hippocmpal lesions. *J Neurol Neurosurg Psychiatry,* **20**, 11-21.

Shadlen, M.N. and Newsome, W.T. (1998). The variable discharge of cortical neurons: Implications for connectivity, computation, and information coding. *The Journal of Neuroscience,* **18**, 3870-3896.

Sheth, A., Berretta, A. Lange, N., and Eichenbaum, H. (2008) The amygdala modulates neuronal activation in the hippocampus in response to spatial novelty. *Hippocampus*, **18**, 169.

Shi, C., and Davis, M. (1999). Pain pathways involved in fear conditioning measured with fear-potentiated startle: lesion studies. *The Journal of Neuroscience*, **19**, 420-430.

Siapas, A.G., Lubenov, E.V., and Wilson, M.A. (2005). Prefrontal phase locking to hippocampal theta oscillations. *Neuron*, **46**, 141–151.

Sigurdsson, T., Stark, K.L. Karayiorgou, M. Gogos, J.A. and Gordon, J.A.. (2010) Impaired hippocampal-prefrontal synchrony in a genetic mouse model of schizophrenia. *Nature*, **464**, 763-767.

Silva, A. J., Zhou, Y., Rogerson, T., Shobe, J., and Balaji, J. (2009). Molecular and cellular approaches to memory allocation in neural circuits. *Science*, **326**, 391-395.

Silver, R.A. (2010). Neuronal arithmetic. *Nature Reviews Neuroscience*, **11**, 474-489.

Sjostrom, P.J., Rancz, E.A., Roth, A., and Hausser, M. (2008). Dendritic excitability and synaptic plasticity. *Physiol Rev*, **88**, 769-840.

Sloviter, R.S. (1991). Feedforward and feedback inhibition of hippocampal principal cell activity evoked by perforant path stimulation: GABA-mediated mechanisms that regulate excitability in vivo. *Hippocampus,* **1**, 31-40.

Spruston, N. (2008). Pyramidal neurons: dendritic structure and synaptic integration. *Nature Reviews Neuroscience*, **9**, 206-221.

Squire, LR, and Zola, S.M. (1998) Episodic memory, semantic memory, and amnesia. *Hippocampus*, **8**, 205-211

Squire, LR. (1992). Memory and the hippocampus: a synthesis from findings with rats, monkeys, and humans. *Psychological Review,* **99**, 195-231.

Stevens, R. and Cowey, A. (1973) Effects of dorsal and ventral hippocampal lesions on spontaneous alternation, learned alternation, and probability learning in rats. *Brain Research,* **52**, 203-224.

Swanson, L.W. (2003). *Brain Architechture: Understanding the Basic Plan.* Oxford University Press.

Swanson, L.W. and Cowan, W.M. (1975). Hippocampo-hypothalamic connections: origin in subicular cortex, not ammon's horn. *Science,* **189**, 303-304.

Swanson, L.W., and Cowan, W.M. (1979). The connections of the septal region in the rat. *J Comp Neurol,* **186**, 621-55.

Takahashi, H., and Magee, J.C. Pathway interactions and synaptic plasticity in the dendritic tuft regions of CA1 pyramidal neurons. *Neuron* **62**, 102-111 (2009).

Taniguchi, H., He, M., Wu, P., Kim, S., Paik, R., Sugino, K., Kvitsiani, D., Fu, Y., Lu, J., Lin, Y., Miyoshi. G. et al. (2011). A resource of cre driver lines for genetic targeting of gabaergic neurons in cerebral cortex. *Neuron*, **71**, 995-1013.

Taniguchi, H., Lu, K., and Huang, Z.J. (2013). The spatial and temporal origin of chandelier cells in mouse neocortex. *Science,* **339**, 70-74.

Thompson RF, and Kim, JJ. (1996). Memory systems in the brain and localization of a memory. *Proc. Natl. Acad. Sci USA,* **93**, 13438-13444.

Thompson, L.T., and Best, P.J (1989). Place cells and silent cells in the hippocampus of freely-behaving rats. *The Journal of Neuroscience* **9**, 2382-2390.

Toth, K., Borhegyi, Z., and Freund, T.F. (1993). Postsynaptic targets of GABAergic hippocampal neurons in the medial septum-diagonal band of broca complex. *The Journal of Neuroscience*, **13**, 3712-3724.

Toth, K., Freund, T.F., and Miles, R. (1997). Disinhibition of rat hippocampal pyramidal cells by gabaergic afferents from the septum. *The Journal of Physiology*, **500**, 463-474.

Tulving, E. (1972). Episodic and semantic memory. In Tulving, E., and Donaldson, W., Eds. *Organization of Memory*. New York Academic Press.

Tulving, E., and Markowitsch, H.J. (1998). Episodic and declarative memory: role of the hippocampus. *Hippocampus,* **8**, 198-204.

Varga, C., Golshani, P., and Soltesz, I. (2012). Frequency-invariant temporal ordering of interneuronal discharges during hippocampal oscillations in awake mice. *PNAS*, **109**, 2726-2734.

Varga, V., *et al.* Fast synaptic subcortical control of hippocampal circuits. *Science* **326**, 449–453 (2009).

Vargha-Khadem, F., Gadian, D.G., Watkins, K.E., Connely, A., Van Paesschen, W., and Mishkin, M. (1997). Differential effects of early hippocampal pathology on episodic and semantic memory. *Science*, **277**, 376–380.

Vazdarjanova, A. and Guzowski, J.F. (2004) Differences in hippocampal neuronal population responses to modifications of an environmental context: evidence for distinct, yet complementary, functions of CA3 and CA1 ensembles. *J. Neurosci*. **24**, 6489.

Vertes, R.P., Hoover, W.B., Szigeti-Buck, K., and Leranth, C. (2007). Nucleus reunions of the midline thalamus: link between the medial prefrontal cortex and the hippocampus. *Brain Res Bull*, **71**, 601-609.

Vinogradova, O.S. (2001). Hippocampus as comparator: role of the two input and two output systems of the hippocampus in selection and registration of information. *Hippocampus*, **11**, 578-598.

Vu, E.T., and Krasne, F.B. (1992). Evidence for a computational distinction between proximal and distal neuronal inhibition. *Science*, **255**, 1710-1712.

Wang, M.E., Wann, E.G., Yuan, R.K., Ramos Álvarez, M.M., Stead, S.M., and Muzzio, I.A. (2012). Long-term stabilization of place cell remapping produced by a fearful experience. *J Neurosci*, 32, 15802-14.

Weiss C, Kronforst-Collins MA, and Disterhoft JF. (1996). Activity of hippocampal pyramidal neurons during trace eyeblink conditioning. *Hippocampus, 6*, 192-209.

Weiss, C., Bouwmeester. H,, Power, J.M., and Disterhoft, J.F. (1999). Hippocampal lesions prevent trace eyeblink conditioning in the freely moving rat. *Behavioral Brain Research,* **99**, 123-132.

Whitlock JR, Heynen AJ, Shuler MG, and Bear MF. (2006). Learning induces long-term potentiation in the hippocampus. *Science,* **313***,* 1093-1097.

Widmer, H., Ferrigan, L., Davies, C.H., and Cobb, S.R. (2006). Evoked slow muscarinic acetylcholine synaptic potentials in rat hippocampal interneurons. *Hippocampus*, **16**, 617-628.

Wilson, M.A., and McNaughton, B.L. (1993). Dynamics of the hippocampal ensemble code for space. *Science*, **261**, 1055-1058.

Wilson, N.R., Runyan, C.A., Wang, F.L., and Sur, M. (2012). Division and subtraction by distinct cortical inhibitory networks in vivo. *Nature*, **488**, 343-348.

Wyss, J.M., Swanson, L.W., and Cowan, W.M. (1979). A study of subcortical afferents to the hippocampal formation in the rat. *Neuroscience*, **4**, 463-76.

Xu, N.L., Harnett, M.T., Williams, S.R., Huber, D., O'Connor, D.H., Svoboda, K., and Magee, J.C. (2012a). Nonlinear dendritic integration of sensory and motor input during an active sensing task. *Nature, 492*, 247-251.

Xu, W., Morishita, W., Buckmaster, P.S., Pang, Z.P., Malenka, R.C., Südhof T.C. (2012b). Distinct neuronal coding schemes in memory revealed by selective erasure of fast synchronous synaptic transmission. *Neuron*, **73**, 990-1001.

Young, S.L., Bohenek, D.L., and Fanselow, M.S. (1994). NMDA processes mediate anterograde amnesia of contextual fear conditioning induced by hippocampal damage: Immunization against amnesia by context preexposure. *Behavioral Neuroscience*, **108**, 19-29.

Zhang, F., et al. (2007). Multimodal fast optical interrogation of neural circuitry. *Nature*, **446**, 633-639

Zhang, S-J., Ye, J., Miao, C., Tsao, A., Cerniauskas, I., Ledergerber, D., oser, M-B, and Moser, E.I. (2013). Optogenetic dissection of entorhinal-hippocampal functional connectivity. *Science, 340*, 1232627.

Zhang, W. and Linden, D.J. (2003). The other side of the engram: experience-driven changes in neuronal intrinsic excitability. *Nature Reviews Neuroscience,* **4**, 885-900.

Zheng, F., and Khanna, S. (2001). Selective destruction of medial septal cholinergic neurons attenuates pyramidal cell suppression, but not excitation in dorsal hippocampus field CA1 induced by subcutaneous injection of formalin. *Neuroscience,* **103**, 985-998.

Ziv, Y., Burns, L.D., Cocker, E.D., Hamel, E.O., Ghosh, K.K., Kitch, L.J., El Gamal, A., and Schnitzer, M.J. (2013). Long-term dynamics of CA1 hippocampal place codes. *Nature Neuroscience,* **16**, 264-266.